Multi-scale constitutive modelling of nanoparticle/epoxy nanocomposites: Molecular simulation-based methods and experimental validation

Von der Fakultät für Bauingenieurwesen und Geodäsie

der Gottfried Wilhelm Leibniz Universität Hannover

zur Erlangung des Grades

Doktor der Ingenieurwissenschaften
Dr.-Ing

genehmigte Dissertation von

Robin Unger, M.Sc.

Erscheinungsjahr 2020

Referent:	Prof. Dr.-Ing. habil. Raimund Rolfes Gottfried Wilhelm Leibniz Universität Hannover
Korreferent:	Univ.-Prof. Dr.-Ing. Bernd Markert RWTH Aachen University
Tag der Promotion	02. Juli 2020

Abstract

Innovative material systems such as nanocomposites, composed of thermosetting polymers reinforced by nano-scale additives, are of great interest in the field of lightweight engineering applications due to their remarkable thermo-chemo-mechanical properties. Accurate and comprehensive knowledge of the material characteristics is a key factor in their successful application and only if the underlying physical mechanisms are understood, a reliable description of the material behaviour is possible. The present thesis contributes to this challenge by providing molecular simulation-based methods with the potential to predict the material behaviour and get insights into nano-scale effects.

Firstly, a methodology for molecular simulations of the curing process of an epoxy resin is presented that is developed with respect to accuracy and efficiency. For the first time, not only the final network topology is analysed but also the evolution of reactive groups during the curing process is predicted, both are in good agreement with experimental near-infrared spectroscopy data. With the developed simulation routine, deeper insights into the curing mechanism of epoxy systems can be obtained and reliable input data for molecular simulation-based analysis of cured epoxy systems can be provided.

Secondly, the temperature-dependent non-linear viscoelastic material behaviour of the epoxy system is studied by providing a consistent comparison and assessment of three viscoelastic theories (i.e., the Eyring, Argon and Cooperative model). The distinctive innovation of this study is to propose a simulation-based framework for the identification of viscoelastic properties. The method allows bridging the inherently different timescales of molecular dynamics (femtoseconds to nanoseconds) and experiments (seconds to hours). The study shows that molecular simulations are powerful tools for characterising physical phenomena on the molecular level and thus can replace extensive experimental testing for the description of the viscoelastic material behaviour of polymers.

Finally, a multi-scale constitutive model for the viscoelastic damage behaviour of nanoparticle/epoxy nanocomposites is extended to finite temperatures in the glassy regime. The general predictive capabilities of the constitutive model are studied and found to be in good agreement with experimental results. Furthermore, a multi-scale framework is proposed that incorporates molecular simulation-based methods to replace extensive experimental testing required for the parameter identification. An experimental validation underlines that the number of experimental tests required for the identification of material parameters can significantly be reduced, without a significant loss of accuracy in the material response prediction.

The present thesis contributes to a better understanding of the thermo-viscoelastic behaviour of nanoparticle/epoxy nanocomposites and provides approaches for the associated challenges of modelling these materials. The

methods developed are intended for the characterisation of material properties concerning physically-based constitutive modelling and multi-scale approaches with a focus on a significant reduction in the number of experimental tests required. The framework, in principle, is not limited to the studied epoxy system and can easily be extended towards a more comprehensive material description, for which an outlook is provided.

Keywords: Nanoparticle/epoxy nanocomposites; Non-linear viscoelasticity; Multi-scale constitutive modelling; Molecular simulations;

Zusammenfassung

Neuartige Materialsysteme wie Nanokomposite, hergestellt durch die Zugabe von nanoskaligen Additiven zu herkömmlichen Duroplasten, sind im Bereich der Leichtbautechnik von großem Interesse aufgrund ihrer bemerkenswerten thermo-chemisch-mechanischen Eigenschaften. Umfassende Kenntnisse der Materialeigenschaften sind ein Schlüsselfaktor für ihre erfolgreiche Anwendung. Nur wenn die zugrundeliegenden physikalischen Mechanismen verstanden werden, ist eine zuverlässige Beschreibung des Materialverhaltens möglich. Die vorliegende Arbeit trägt zu dieser Herausforderung bei, indem Methoden auf Basis molekularer Simulationen vorgestellt werden, welche das Potenzial besitzen, das Materialverhalten vorherzusagen und Einblicke in Phänomene auf der Nanoskala zu gewähren.

Zunächst wird eine, im Hinblick auf Genauigkeit und Effizienz entwickelte, Methodik für molekulare Simulationen des Aushärtungsprozesses eines Epoxidharzes vorgestellt. Zum ersten Mal wird nicht nur die endgültige Netzwerktopologie analysiert, sondern auch die Evolution reaktiver Gruppen während der Aushärtung vorhergesagt, beides in guter Übereinstimmung mit experimentellen Ergebnissen aus Nahinfrarotspektroskopie-Messungen. Die entwickelte Simulationsroutine ermöglicht tiefere Einblicke in den Aushärtungsmechanismus von Epoxidharzsystemen und die Bereitstellung zuverlässiger Eingangsdaten für die Analyse ausgehärteter Epoxidharzsysteme anhand von molekularen Simulationen.

Anschließend wird das temperaturabhängige nichtlineare viskoelastische Materialverhalten des Epoxidsystems untersucht, indem ein Vergleich und eine Bewertung von drei viskoelastischen Theorien (Eyring, Argon und Cooperative Model) durchgeführt wird. Die besondere Innovation dieser Studie besteht darin, einen simulationsbasierten Ansatz für die Identifizierung viskoelastischer Eigenschaften zu präsentieren. Die dargestellte Methodik ermöglicht die Überbrückung der von Natur aus unterschiedlichen Zeitskalen der Molekulardynamik (Femtosekunden bis Nanosekunden) und der Experimente (Sekunden bis Stunden). Die Studie zeigt, dass molekulare Simulationen leistungsfähige Werkzeuge zur Charakterisierung physikalischer Phänomene auf der molekularen Ebene sind und somit umfangreiche experimentelle Tests zur Beschreibung des viskoelastischen Materialverhaltens von Polymeren ersetzen können.

Schließlich wird ein Multiskalen-Konstitutivgesetz für das viskoelastische Schädigungsverhalten von Nanopartikel/Epoxid-Nanokompositen hinsichtlich des Einflusses der Temperatur, für Temperaturen unterhalb der Glasübergangstemperatur, erweitert. Die allgemeinen Vorhersagefähigkeiten des konstitutiven Modells werden untersucht und zeigen eine gute Übereinstimmung mit experimentellen Ergebnissen. Darüber hinaus wird ein Multiskalen-Rahmenkonzept vorgeschlagen, das auf molekularen Simulationen basierende Methoden umfasst,

um umfangreiche experimentelle Tests zu ersetzen, die für die Parameteridentifizierung erforderlich sind. Eine experimentelle Validierung unterstreicht, dass die Anzahl der für die Identifizierung von Materialparametern erforderlichen experimentellen Tests erheblich reduziert werden kann, ohne dass es zu einem signifikanten Verlust an Genauigkeit bei der Vorhersage der Materialantwort kommt.
Die vorliegende Arbeit trägt zu einem besseren Verständnis des thermoviskoelastischen Verhaltens von Nanopartikel/Epoxid-Nanokompositen bei und liefert Ansätze für die damit verbundenen Herausforderungen bei der Modellierung dieser Materialien. Die entwickelten Methoden dienen der Charakterisierung von Materialeigenschaften im Hinblick auf physikalisch basierte Konstitutivgesetze und Multiskalenansätze mit dem Ziel, die Anzahl der erforderlichen experimentellen Tests deutlich zu reduzieren. Die entwickelten Methoden und das dargestellte Konstitutivgesetz sind prinzipiell nicht auf das untersuchte Epoxidsystem beschränkt und können leicht hinsichtlich weiterer Materialeigenschaften erweitert werden, für welche ein Ausblick gegeben wird.

Stichwörter: Nanopartikel/Epoxid-Nanokomposite; Nichtlineare Viskoelastizität; Multiskalen Konstitutivgesetz; Molekulare Simulationen;

Contents

List of Figures

Chapter 1

Introduction

1.1 Introduction and motivation

The superior motivation of the present thesis is to contribute to the fundamental research on material science with the development and validation of computational methods to analyse and improve polymers and nanoparticle reinforced polymers (nanocomposites). A strong focus is put on an accurate and reliable prediction of the material characteristics and behaviour through an understanding of underlying mechanisms concerning engineering applications.
Generally, a world without polymers is only hardly imaginable nowadays. Due to the huge variety of different monomers, an uncountable number of polymers was developed, each tailored for a specific application - from a mono-material plastic bottle to advanced polymer blends for high-performance applications such as wind energy rotor blades or aircraft structures. In this thesis, the focus is put on epoxy resins, which are thermosetting polymers, typically used in the infusion process of composite components.
Thermosetting polymers are solids that are irreversibly hardened due to the curing process, in which a highly cross-linked network is formed by covalent bonds between the epoxy monomers and the hardener molecules. These two-component polymers have a low viscosity in the liquid state, which is beneficial for infusion of endless fibre-reinforced parts, and they show a high heat resistance after curing. In contrast, thermoplastics do not form covalent bonds during the curing process and can be remelted or reshaped in the presence of heat without a negative effect on the material's physical properties. This makes thermoplastics highly recyclable and crystallinity has a strong effect on the mechanical properties (i.e., the higher the degree of crystallinity the stronger the material).
The combination of epoxy resins with endless fibres leads to fibre-reinforced plastics (FRP) with an orthotropic material response due to the fibre direction. These materials, in which commonly either glass or carbon fibres are used, lead to a new generation in the design of high-performance lightweight structures. In contrast to isotropic materials, for example, metals, ceramics or pure polymers, these composites can be used in a structural design tailored according to the expected load cases. This has made glass fibre-reinforced plastics (GFRP) and carbon fibre-reinforced plastics (CFRP) nowadays standard in lightweight structural design in the aerospace or wind energy industry.
An impressive example of today's achievements in exploiting the advantages of

composite materials is the Airbus A350 XWB (extra wide body), shown in Figure 1.1 (a). The aeroplane, that had its first commercial flight in 2014, is made of 53 % composites and the wing cover was one of the biggest CFRP components (with dimensions of 32 m x 7 m) built by the aeronautical industry by that time [48, 49]. With the use of FRP, Siemens Gamesa was able to push the boundaries of wind energy turbines towards a 10 MW wind energy turbine (SG 10.0-193 DD), whose imposing dimensions are schematically shown in 1.1 (b). The wind turbine, of which serial production is scheduled to start in 2022, has a rotor blade diameter of 193 m with a blade length of 94 m [78].

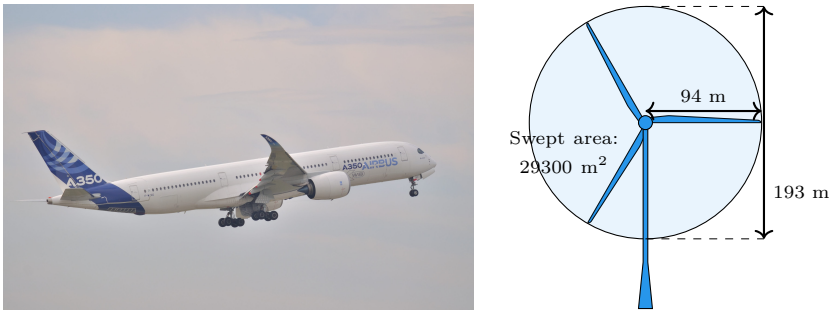

(a) **(b)**

Figure 1.1: Examples for today's achievements in exploiting the advantages of composite materials: (a) Airbus A350 XWB [1] made of 53 % composite materials and (b) dimensions of a Siemens Gamesa 10 MW wind turbine [78].

However, some material properties of these composites, such as the tensile strength perpendicular to the fibre direction, the shear strength, and the compressive strength, are still limited by the matrix material. In the last decades, a lot of research was carried out, giving strong evidence that nano-scale additives can increase the mechanical resistance of the matrix material, without losing its positive attributes [37]. Under the requirement that the generally stiffer nanoparticles are well dispersed, they act as a strong filler material enhancing several matrix dominated properties in fibre-reinforced composites. Figure 1.2 exemplary shows the increase of matrix dominated material properties that were experimentally investigated by Arlt et al. [8]. The relative increase for a CFRP with 15 weight per cent boehmite nanoparticles in the matrix material is compared to the reference without any nanoparticle reinforcement. The boehmite particles, which were coated with a taurine modification, lead to an improvement in the range of 10% to 20%.

[1] Airbus A350 XWB (https://commons.wikimedia.org/wiki/File:AIB_A350_F-WZGG_3nov14_LFBO-2.jpg), photo (unmodified) taken by Gyrostat (https://commons.wikimedia.org/wiki/User:Gyrostat), Wikimedia Commons, licensed under CC-BY-SA 4 (https://creativecommons.org/licenses/by-sa/4.0/legalcode).

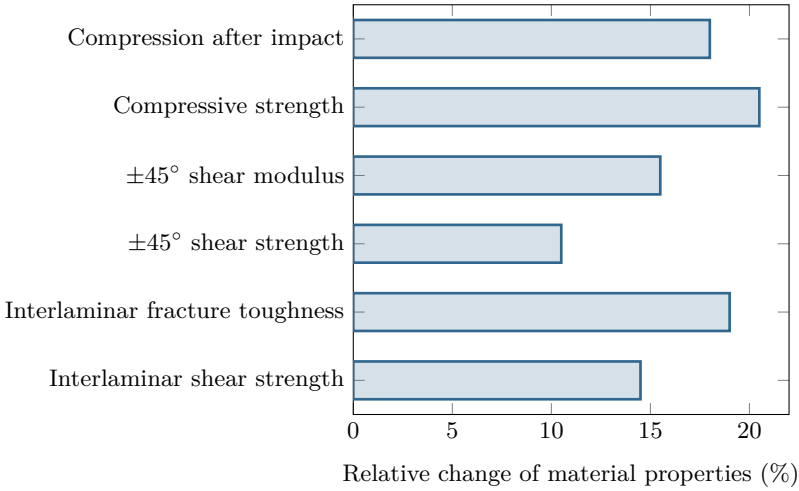

Figure 1.2: Improvement of matrix dominated material properties of a CFRP due to addition of 15 weight per cent taurine modified boehmite nanoparticles compared to the reference value [8].

The need for these kinds of innovative lightweight materials with outstanding mechanical properties is enormous, especially with regard to nowadays challenges in the energy sector. The German federal government explicitly stated that new materials for weight reduction or reliability increase are to be researched for wind energy applications [35]. Innovative lightweight technologies are one focus in the 7th Energy Research Programme of the German Federal Ministry for Economic Affairs and Energy [29], which is the guideline for the national energy research in the coming years. A long-term perspective on the challenges in wind energy is addressed by the research agenda of the European Academy of Wind Energy (EAWE) [41]. Innovations in the field of material science are mentioned as one contribution to an improved performance/cost ratio, with the reinforcement due to the addition of nanoparticles explicitly stated as one possibility.
To meet these requirements in the field of material science, the development and application of computational methods are unavoidable. A large variety of polymers and nanoparticles lead to a huge number of possible nanocomposites that need to be taken into account. However, already the comprehensive experimental study of one specific nanocomposite becomes very time consuming and costly once the effect of time and temperature is included. Not to mention the complex manufacturing of nanocomposite test specimen, in which the accurate dispersion of nanoparticles is a crucial but time-consuming aspect.
Basically, advanced computational methods come with two major arguments.

Firstly, computational tools can replace experiments and lead to a faster but still reasonable material development procedure. After careful development, calibration and validation, these tools allow efficient analysis of polymers and nanocomposites without labour intensive tasks. Secondly, computational methods can be used to study phenomena that are only hardly examinable using experiments. This is especially interesting for effects arising from nano-scale physics that can be invested with molecular simulation at the atomistic length scale, such as the viscoelasticity governed by the inter- and intramolecular polymer chain interaction (i.e. molecular chain sliding and rearrangement). Furthermore, the combination of computational methods acting on different length scales allows to analyse the material behaviour from the nano-scale to the component level. These multi-scale analyses are desirable as the accumulation of different length scale effects, which may affect the final material response significantly, can be captured. Especially for nanoparticle reinforced polymers, molecular simulations are highly reasonable as they cover the mechanisms occurring at the interface of nanoparticle and matrix.
Nevertheless, to make the undeniable benefits of computational methods available, namely the reduction of development time and costs, a lot of research was done in the past and is still needed in the future. This thesis contributes with the development of methods, corresponding experimental validation and their combination to a multi-scale constitutive model to answer some of the currently open questions. A clear picture of the objective and outline of the present thesis is given in Section 1.3.

1.2 State of the art

This section will provide an overview of nowadays approaches and open questions in the three main topics that are part of the present thesis. In Section 1.2.1 the state of the art of the atomistic model generation for polymers with molecular curing simulations is presented. The challenges and current approaches regarding the prediction of non-linear viscoelasticity of polymers using molecular simulations are discussed in Section 5.1. Finally, an overview of molecular simulation-based methods that are used in the context of multi-scale constitutive modelling is given in Section 1.2.3.

1.2.1 Molecular curing simulation for polymer cross-linking

In general, a uncured epoxy system comes as two individual components, the resin (i.e., the epoxy monomers) and the hardener (i.e., the curing agents). When combined and mixed properly the exothermic curing reaction is initiated, forming the strong three-dimensional network topology. Depending on the epoxy system a specific ambient temperature may be required to stimulate the curing mechanism, whereas for other systems the exothermic reaction may need to be controlled to avoid a thermal degradation. It is well known that the physical

properties of the cured epoxy system depend on the underlying network structure [34, 66] and the process parameters of the curing [42, 75]. Generally an increased temperature close to the glass transition temperature is required to achieve a high degree of polymerisation, which is desired to obtain maximum material properties. Therefore, a typical curing process starts with a gradual heating of the liquid epoxy system to the curing temperature. After keeping the temperature constant for several hours to ensure a fully cured system, a gradual cool down to the room temperature is applied.
The established state of the art in molecular modelling of cured polymers is to use a simulative approach, i.e., a simulation to mimic the above-mentioned curing process to generate an atomistic representation of a real-world polymer network. Although a variety of different algorithms can be found, a common procedure is generally followed by most of them. First, an unlinked model, representing the liquid mixture of all components, is generated. With this model, the molecular simulation is initialised, which includes a relaxation of the system at the desired curing temperature. The actual cross-linking is imitated by the formation of a certain number of chemical bonds in a cross-linking step, followed by a short relaxation of the system to account for the changes in the network topology. Typically, a maximum allowed bond distance, the cut-off radius, is predefined so that the initial bond length can not exceed this value. The number of allowed chemical bonds can also be predefined or all possible bonds within the cut-off radius are allowed to be formed. Finally, the completely cured simulation model is subjected to a sufficiently long equilibrium simulation to ensure a minimised internal energy state. The accuracy and efficiency are mainly dominated by these two aspects, the cut-off radius and the number of possible bonds that are allowed to be formed within one cross-linking step.
As it is generally desired to reduce the simulation time required to obtain a cured but well-relaxed simulation box, the trade-off between accuracy and efficiency was intensely discussed in recent studies [23, 45]. Approaches that allow only one individual bond with the shortest reaction distance to be formed [19, 82, 83] typically need a larger cut-off radius to achieve realistic degrees of curing. Following this approach, the system is steadily cured, but large values for the cut-off may come with the drawback of a high artificial internal energy that is suddenly added. Approaches that follow the concept that all possible bonds within the cut-off distance are formed [33, 80, 85] generally use a smaller cut-off distance to assure only a limited number of bonds are formed in each cross-linking step. A too fast cross-linking may lead to unstable simulations and to a higher internal energy that needs to be reduced in a final relaxation.
Besides the trade-off between accuracy and efficiency, the second main challenge is to capture the complex curing mechanism that may consist of various chemical reactions during the complete curing. The complexity is mainly caused by the fact that most industrial applied epoxy systems are an advanced blend of a number of epoxy monomers and hardener curing agents. Therefore, the curing mechanism is not limited to only one chemical reaction, but different chemical

reactions are possible within the system and are affecting each other. This challenge leads to the question in the ongoing research if predefined probabilities for individual chemical reactions are needed to capture the complex curing path, or if this effect is indirectly included due to steric hindrance and physical interactions. This aspect is crucial especially for an amine cured epoxy system in which the reactive amine groups can react with two epoxy groups.
Noteworthy approaches in this field were published by Wu et al. [82, 83] and Bandyopadhyay et al. [11] in which an equal reactivity of primary and secondary amines was assumed. Varshney et al. [80] followed up on these methods by developing a more efficient method that also leads to better-equilibrated systems (i.e., systems with lower internal energy). An important study was presented by Estridge [23] in which the effect of different reaction probabilities for the curing agents of an amine-cured epoxy system was investigated. It was clearly shown that the reaction probability had a significant influence on the final network topology of the cured epoxy system. But as no experimental data were available, an assessment or validation was out of the scope of the study and no conclusion regarding a realistic choice of reaction probability was drawn. The molecular weight of the largest and second largest molecular cluster as a function of the degree of curing was investigated by Varshney et al. [80], Estridge [23], and Yang et al. [84]. A prediction of the theoretical gel point was possible and their results indicate that the network structure has a significant effect on the physical properties. These studies underline that realistic molecular modelling of the curing mechanism is crucial for a realistic material behaviour characterisation.
Unfortunately, in most of the present studies, experimental validation of the complete curing mechanism is missing, due to the difficulty in obtaining experimental insights. A promising study was presented by Okabe et al. [59, 60] in which the curing of different mixtures of epoxy resin and amine curing agents were analysed with MD simulations and experimental differential scanning calorimetry (DSC). The simulative evolution of epoxy conversion was in good agreement with experimentally obtained data. However, due to the method of DSC, involving the measurement of the heat of the exothermic reactions, the differentiation of curing agent reactions is impossible.
Experimental validation of a molecular curing simulation that not only takes the reaction of epoxy groups but also the reaction of all hardener curing agents into account was still pending in the literature. A comparison to experimentally obtained insights into the curing mechanism also allows answering the question if specific reaction probabilities need to be predefined to capture the realistic evolution of chemical reactions. The publication on the molecular modelling of epoxy cross-linking (see Chapter 3) is concerned with these two main aspects. For the first time, experimental validation of the complete curing process is provided, based on near-infrared spectroscopy data. It was shown that the developed method leads to well-equilibrated systems while being efficient and thus reducing the computational time needed.

1.2.2 Prediction of non-linear viscoelasticity of polymers using molecular simulation

The characterisation and prediction of fundamental thermo-mechanical properties (glass transition temperature, coefficient of thermal expansion) and mechanical properties (Young's modulus, yield stress and viscoelasticity) are of great interest in the field of material science for polymer applications. With molecular simulations, a powerful tool is given that can be used to obtain insights into nano-scale effects and generate an understanding of the underlying mechanisms of action. However, the prediction of mechanical behaviour is challenging as polymers exhibit a complex material response affected by the temperature and strain rate as shown in Figure 1.3. Generally, the material behaviour shows different characteristic stages until failure. Firstly, the stress response is dominated by the initial linear elastic stiffness, followed by a non-linear elastic stage due to a combination of non-linear viscoelasticity and hyperelasticity. After reaching the yield point, a combination of softening behaviour and viscose flow is identifiable with increasing strain.

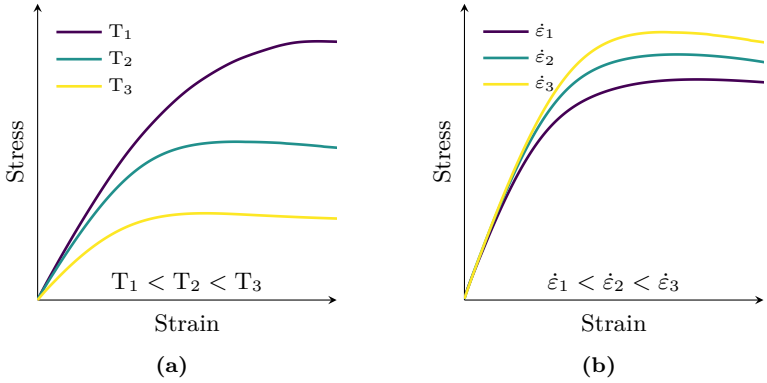

Figure 1.3: Exemplary stress strain response of thermosetting polymers in the glassy regime: (a) Effect of temperature at a constant strain rate and (b) effect of strain rate at a constant temperature.

The effect of temperature is presented in Figure 1.3 (a) and shows that the stiffness and yield stress decrease with increasing temperature. For temperatures above the glass transition temperature, both material characteristics are decreased significantly by several decades. Figure 1.3 (b) shows the effect of the strain rate. The yield stress increases with increasing strain rate, but generally, no significant effect on the initial stiffness is observable.
Regarding the rate-dependent material behaviour of cured thermosetting polymers, the yield stress and viscoelasticity cannot be determined directly from molecular simulations due to the limitation of timescale. The length and

timescales that are typically examinable by molecular dynamics simulations are illustrated in Figure 1.4. Although a large-scale MD simulation may be able to include a hundred thousands of atoms and span several nanoseconds, the difference to the continuum-scale is still significant and need to be bridged. The application of coarse-grained (CG) methods can help to increase both, the length and timescales. But with nowadays computational resources, still, no direct transition between CG and continuum simulations is possible.

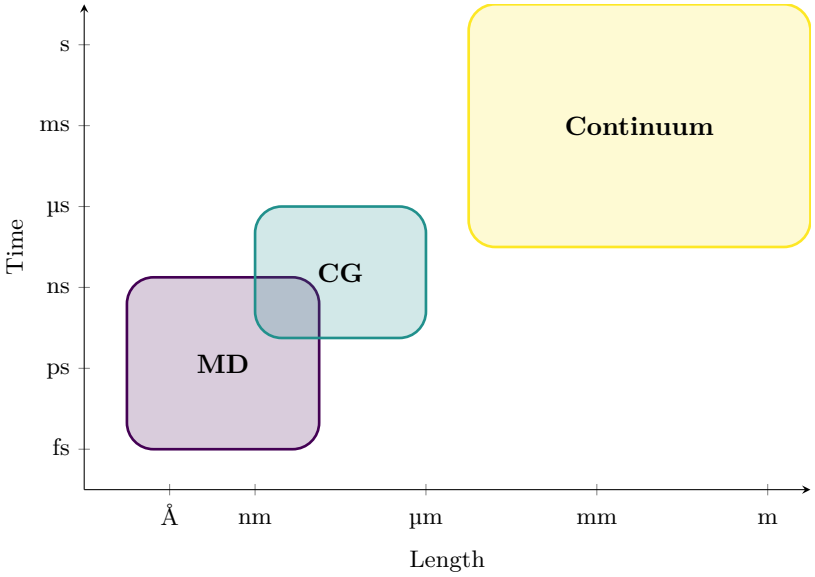

Figure 1.4: Visualisation of typical length and timescales of molecular dynamics (MD), coarse-grained (CG) methods and continuum simulation.

Concerning polymer viscoelasticity, this major challenge of bridging the huge gap between molecular and continuum length and timescale can be achieved by utilising viscoelastic theories. Existing viscoelastic models describe the stress as a function of the strain rate, temperature and material parameters that are related to physical quantities or mechanisms.
Noteworthy models to describe the viscoelasticitiy were presented by Eyring [24, 25], Ree and Eyring [67–69], Argon [5–7], Robertson [72] and Forthering [30, 31]. Their models share the general idea that the macroscopic yielding is the result of the viscous flow of polymer chains at the molecular level. Under externally applied stress, the polymer chains are moving in the direction of minimum potential energy between adjacent equilibrium states. The individual models mainly differ in their interpretation and description of the underlying polymer

chain interaction. The Eyring model is motivated by the concept of viscoelasticity being a thermally activated rate process and is based on the transition state theory for the description of elementary chemical reaction rates [24, 25]. Ree and Eyring enhanced this model by considering two rate processes, individually taking the stress-dominated and the temperature-dominated material response into account [67–69]. The application of these models was presented by Bauwens-Crowet et al. [13, 14] and Bauwens et al. [15] and showed that these models, generally, lead to a reasonable description of the viscoelasticity of polymers. Fotheringham et al. [30, 31] developed the Cooperative model by introducing a parameter that depicts the number of parallel elementary transitions, based on the Ree-Eyring formulation with two rate processes. Similar theories were presented by Argon et al. [5–7] and Robertson [72], which differ in their assumption of polymer chain interaction. It is generally agreed that these models describe the viscoelasticity of various polymers fairly well in the typical ranges of experimental length and timescales and for temperatures in the glassy regime [18, 51].

Furthermore, evidence can be found that these theories can also be applied to molecular simulation data. Assuming that the general nano-scale physics, governing the viscoelasticity, are covered by the simulations, identification of the model parameters is possible in order to extrapolate to experimental length and timescales. Promising results in this direction were published by Arash et al. [3, 4], Park et al. [62] and Vu-Bac et al. [10]. The Eyring model was incorporated into a multi-scale viscoelastic damage model for nanoparticle/epoxy nanocomposites by Arash et al. [3, 4]. The model parameters were identified using purely molecular simulation data. The validation of numerical results with experimental data shows that the constitutive model is able to predict the material response in good agreement with experimental results for a tensile test and a four-point bending test. A similar approach was presented by Vu-Bac et al. [10], with a multi-scale model for the quasi-static thermo-plastic behaviour of cross-linked polymers. Here, the Argon model was implemented to predict the yield stress after calibration using molecular simulation data. The presented results indicate that the Argon model is able to describe the effect of temperature on the elasto-plastic behaviour and the yielding phenomena, activated by the polymer chain interaction at the nano-scale, fairly well. The capabilities of the Ree-Eyring model to predict the quasi-static yield stress was investigated by Park et al. [62]. In this study, the Ree-Eyring model was calibrated using purely MD simulation data obtained at different temperatures and was able to extrapolate to experimental timescales with an acceptable agreement to experimental results.

Unfortunately, a consistent analysis with a comparison and assessment of existing theories and their capabilities to predict the viscoelastic material behaviour over a broad range of temperatures and strain rates was still pending in current literature. The second publication of the present thesis (see Chapter 4) is concerned with this open question. For the first time, three viscoelastic theories are compared and assessed on their predictive capabilities after a parameter

identification in which purely molecular simulation data was used. Experimental validation is provided based on tensile tests results obtained at different strain rates and temperatures.

1.2.3 Molecular simulation-based multi-scale constitutive modelling

Multi-scale approaches are well-established nowadays and specifically favourable for material combinations that are composed of individual materials of significantly different sizes. Typical applications in engineering science are the analysis and prediction of material behaviour of composites composed of a polymer matrix and either nanoparticles (nanocomposites), fibres (fibre-reinforced plastics (FRP)) or a combination of both. In a hierarchical multi-scale analysis, simulations on different scales are performed sequentially with an information transfer up the scales. Generally, an analysis on a lower scale is performed to homogenise the material behaviour for the next higher scale.
By taking molecular simulations into account, a multi-scale analysis can be extended to smaller length scales that cannot be meaningfully investigated by continuum formulations. Starting on the atomistic length scale, the effect of nano-scale physics can be covered, providing a more comprehensive material analysis and leading to the development of physically-based constitutive models. With regard to polymers, the effect of the degree of curing, polymer composition and chemical shrinkage on the final material response at the component level can be included [2, 40, 44, 85]. Furthermore, the effect of nano-scale matrix additives that interact with the polymer molecules can be considered directly at the length scale of acting mechanisms [26, 87].
An exemplary hierarchical multi-scale analysis is shown in Figure 1.5, illustrating the procedure from the nano- to the macro-scale for a unidirectional fibre-reinforced composite component. Initially, an atomistic simulation model is used at the nano-scale to derive material properties of the bulk epoxy material. In case a nanocomposite is considered, the nanoparticle may be explicitly represented in the atomistic simulation model. The homogenised material properties are used for the constitutive model of the polymer matrix at the next higher micro-scale. Here, individual material models for the matrix and the fibres are used and the homogenised material behaviour in each direction is derived. This homogenised material behaviour is used for the constitutive model at the macro-scale, at which the orthotropic material behaviour is modelled by only one material model. For woven fibre laminates, an additional meso-scale may be added between the micro- and the macro-scale to take the effect of the woven fibre arrangement into account. This multi-scale procedure allows transferring information on the material behaviour up the scales. Finally, the complex material behaviour with phenomena, arising from different length scales, is well represented at the final macro-scale, which is of interest for the design of composite structures.

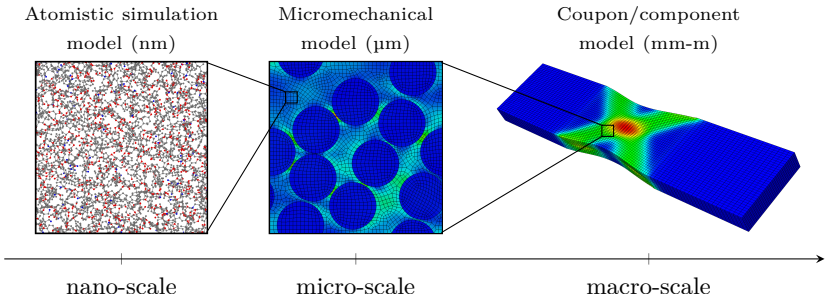

Figure 1.5: Schematic illustration of a multi-scale analysis consisting of of three scales: An atomistic simulation model at the nano-scale, a micromechanical model of unidirectional continuous filaments at the micro-scale and a coupon/component model at the macro-scale.

One of the current challenges in the field of multi-scale constitutive modelling is the reliable derivation of input for continuum formulations using molecular simulations (i.e., the transfer from the nano- to the micro-scale). The application of molecular simulations is limited, since material behaviour that is strongly affected by phenomena at larger scales, such as damage or fracture mechanism, can not be characterised. In the past, noteworthy approaches with promising results pushing the boundaries of the capabilities of atomistic simulations were published [3, 4, 10, 26, 46, 87].
Molecular simulations of nanocomposites made of an epoxy matrix and various sized alumina (Al_2O_3) nanoparticles were performed by Yu et al. [87]. A sequential bridging method was used to estimate the effect of particle size and epoxy network on the particle-matrix interphase which was explicitly modelled as a characteristic phase in a micro-mechanical finite element model. A more comprehensive analysis focusing on the particle-matrix interaction in nanocomposites using molecular simulations was presented by Fankhänel et al. [26], although it was limited to only elastic properties. The proposed simulative framework was used to derive interphase properties on the atomistic length scale which were utilised to model an interphase region in a micromechanical model. The results show that analysis on the nano-scale can reveal phenomena, such as the stiffness profile at the interface, that have a significant effect on the material behaviour at larger scales. Li et al. [46] presented a predictive multi-scale framework for viscoelastic properties of linear polymers. The gap between the nano- and meso-scale was bridged by molecular simulations that were used to identify the parameters of a coarse-grained model (meso-scale). This coarse-grained model was used to identify the required parameters for a proposed constitutive model on the micro-scale that is based on the tube model of primitive paths [20]. The authors

emphasise that the viscoelastic properties of entangled polymers can be directly predicted from the molecular level. A multi-scale model for the prediction of the thermo-plastic behaviour of polymers was proposed by Vu-Bac et al. [10] that incorporates molecular simulations. The Argon model was used in combination with MD results to define the yield surface taking the strain rate effect into account. The nano-scale model was also used to upscale the effect of temperature on the elasto-plastic response. Arash et al. [3] recently proposed a more general viscoelastic damage model for nanocomposites, composed of boehmite nanoparticles and an epoxy matrix. It was shown that molecular simulations are able to replace some experiments required for the parameter identification. The effect of temperature was not considered, but an extension to take the effect short-fibre reinforcement into account was presented [4]. An extensive review from a critical point of view on multi-scale molecular simulations of nanocomposites was published by Vogiatzis et al. [81].

In summary, strong evidence can be found that molecular simulations are a powerful tool for the parameter identification of constitutive models by replacing some experiments. A consistent multi-scale constitutive model in which the abilities of molecular simulations are taken advantage of is highly desirable. This aspect is especially interesting for constitutive models that take the effect of temperatures into account. Here, molecular simulations can help to reduce the extensive experimental tests at various temperatures, which are otherwise required for the parameter identification. The previous section (Section 5.1) already motivated the necessity of an accurate representation of the temperature-dependent material behaviour as the effect can be significant (see Figure 1.3 (a)). The previous section also points out that the temperature-dependent viscoelasticity can be described using a viscoelastic model, as it was shown in the second publication of this thesis (see Chapter 4).

However, no physical-based theories are available to describe the temperature-dependent elastic properties. A common approach is to use a power law to scale the elastic properties based on a reference value at a reference temperature and a scaling parameter. The model proposed by Kitagawa [38] is one kind of such a phenomenological model, which was implemented in constitutive models with a fair agreement to experimental results [10, 65]. Due to the rather simple formulation, the material model can only be represented in the glassy regime and no glass transition is considered. Richeton et al. [71] proposed a more complex model that describes the Young's modulus over a wide range of temperatures from the glassy to the rubbery regime. The model consist of a summation of exponential terms and each term describes the effect of temperature in a certain temperature range. Due to its complexity, the model comes with the drawback of a significantly larger number of parameters that need to be identified.

The present publication on the multi-scale constitutive modelling (see Chapter 5) is concerned with both previously discussed major aspects: (1) the consistent implementation of molecular simulation in a multi-scale constitutive model and (2) capturing the effect of temperature on the material response. Therefore, the

constitutive model proposed by Arash et al. [3] is extended to finite temperatures and the molecular simulations are consistently implemented in the multi-scale framework. It is shown that simulation at the atomistic length scale can reduce the number of experiments required for the parameter identification considerably without a significant loss in accuracy. A comprehensive experimental validation confirms the predictive capability and underlines that MD simulations enhance multi-scale analysis towards a virtual material development.

1.3 Objectives and outline

This thesis includes three substantial scientific contributions in the form of three journal publications. The work done extends the state of the art not only by presenting and discussing innovative methods for specific open questions but also by providing a consistent experimental validation throughout all publication. The publications build upon each other and finally lead to an extension of a multi-scale constitutive model towards the effect of temperature. The constitutive model (see Chapter 5) integrates the developments of both first publications (see Chapter 3 and 4) and was extended to take the effect of temperature on the material behaviour of nanoparticle/epoxy nanocomposites into account. In summary, a comprehensive framework is presented that covers the key factors that arise from the atomistic model generation to the homogenised material response on a continuum level. The present work is limited to nanoparticle/epoxy nanocomposites, although it generally can be extended to other polymers or nanocomposites.

This thesis is divided into six chapters. This first introductory chapter provides the fundamental motivation and the state of the art on which the following chapters are based. It is followed by Chapter 2 that outlines the basic concept of molecular simulations with regard to polymers. This methodical chapter is limited to the fundamentals of molecular simulations that are used in the present thesis in order to provide a clear and comprehensible picture.

In Chapter 3 the essential aspect of a realistic model generation is discussed. A curing simulation for the cross-linking of epoxy systems is presented that was developed concerning accuracy and efficiency. A simulation of the realistic curing mechanism is crucial to obtain a realistic representation of the final network topology. To assure this, the proposed approach was validated with experimental near-infrared spectroscopy. For the first time, it is shown that the simulated evolution of reactive groups during the whole curing process is predicted in good agreement with experimental measurements.

Starting from a realistic simulation model, the characterisation and prediction of the viscoelasticity are studied in Chapter 4. The challenge of bringing the scales between molecular simulation and experiments is accomplished by using viscoelastic models for the extrapolation. It is shown that the parameters of the viscoelastic Argon model can be obtained purely from molecular simulations. The calibrated model allows an extrapolation not only for a broad range of tem-

peratures in the glassy regime but also across the huge difference in time scales and leads to a good agreement with experimental data. This study underlines the abilities of molecular simulations for the prediction of macroscopic material behaviour as the underlying mechanism of viscoelasticity are captured.
The third publication is presented in Chapter 5 and fundamentally builds upon both previous publications. Both, the curing simulation and the calibrated Argon model are integrated into a constitutive model, which is extended to finite temperatures in the glassy regime. Firstly, the theoretical foundation for the extension to temperatures in the glassy regime is clearly stated. Secondly, it is shown that the constitutive model is generally able to represent the material behaviour of nanoparticle/epoxy nanocomposites over a broad range of strain rates, temperatures and nanoparticle weight fractions. Finally, molecular simulation-based methods are presented that allow reducing the required number of experimental data considerably without a significant loss in accuracy of the material behaviour. Validation with experimental results underlines that experiments can be replaced by molecular simulations.
Finally, in Chapter 6 the present work is summarised and the main contributions are highlighted. Based on the drawn conclusions, the current limitations are stated and an outlook of open questions for future research is provided.

Chapter 2

Fundamentals of molecular simulations

2.1 Introduction to molecular dynamics

Computer simulations on the atomistic length scale are conducted with the aim of predicting material properties, revealing physical phenomena and studying the underlying mechanism of action. They need to be understood as a complement to conventional experimental testing and, after careful calibration and validation, may be able to replace some experiments. But only the combination of both, experimental and numerical analysis, will lead to a comprehensive understanding of the material behaviour.
Of course, both approaches come with their individual benefits and drawbacks. Experimental testing is, generally, closer to the engineering application and the material behaviour of interest can often be directly examined and assessed. The disadvantage of experimental testing is that it can become very time- and cost-intensive if complex effects of temperature, rate-dependency and damage need to be characterised. In contrast, molecular simulations are limited by the computational resources and are favourable for the analysis of nano-scale physics that are only hardly examinable in experiments. The analysis of extreme temperatures and pressure or even chemical reactions is possible, but not all material properties can be derived directly due to the huge difference in time and length scale. Molecular simulations can only be as exact as the provided input, which means that a realistic simulation model and reliable parameters for the atomic interactions (i.e., the force field) need to be assured. Under this assumption, molecular simulations are a bridge between physical theory and experiments by linking the atomic interactions to the macroscopic continuum material behaviour.
This chapter will recall the fundamentals of molecular simulations for the application to macromolecular systems of polymers. Generally, two major simulation techniques can be distinguished: deterministic molecular dynamics (MD) and stochastic Monte Carlo (MC) simulations. Since only MD simulations were used and MC simulations are not part of the present thesis, the following fundamentals are limited to the theory of MD. Furthermore, this section is limited to the important details to understand the main developments and repeat the simulations of the thesis. Further information and a comprehensive mathematical description is provided by the excellent work of Allen et al. [1], Tadmor et al. [77] and Attig et al. [9].

2.2 Governing equations

Molecular dynamics simulations are based on solving the classical equations of motion step-wise with time integration. For a system consisting of N discrete atoms, the equations can be written as

$$m_i \ddot{\boldsymbol{r}}_i = \boldsymbol{f}_i, \tag{2.1}$$

$$\boldsymbol{f}_i = -\frac{\partial \mathcal{U}(\boldsymbol{r})}{\partial \boldsymbol{r}_i}. \tag{2.2}$$

Here, m_i is the mass of an atom i and $\boldsymbol{f}_i$ is the force vector applied to the mass. The coordinates of the atom i are represented by a vector $\boldsymbol{r}_i$, which is a subset of the vector $\boldsymbol{r} = (\boldsymbol{r}_1, \boldsymbol{r}_2, ..., \boldsymbol{r}_N)$ that contains all $3N$ atom coordinates for a three-dimensional case. The force acting on an atom can be described as the negative derivation of the potential energy $\mathcal{U}(\boldsymbol{r})$ with respect to the atom position. For molecular simulations, the total potential energy of the system is a function of all atom coordinates and need to cover all atom interactions. The mathematical description for each kind of atom interaction is provided by the applied force field and is summed up for the overall potential energy.
The atomic momentum $\boldsymbol{p}_i$ is defined as

$$\boldsymbol{p}_i = \dot{\boldsymbol{r}}_i m_i, \tag{2.3}$$

$$\dot{\boldsymbol{p}}_i = \boldsymbol{f}_i. \tag{2.4}$$

The overall kinetic energy $\mathcal{K}$ is a function of all atom momenta $\boldsymbol{p}$ and can be written as the sum of the kinetic energies of all atoms

$$\mathcal{K}(\boldsymbol{p}) = \sum_i^N \frac{1}{2} \dot{\boldsymbol{r}}_i^2 m_i = \sum_i^N \frac{1}{2} \frac{\boldsymbol{p}_i^2}{m_i}. \tag{2.5}$$

Finally, the Hamiltonian function $\mathcal{H}$, describing the total energy of the system, is the sum of potential and kinetic energy

$$\mathcal{H}(\boldsymbol{r}, \boldsymbol{p}) = \mathcal{U}(\boldsymbol{r}) + \mathcal{K}(\boldsymbol{p}). \tag{2.6}$$

2.3 Force fields

From an engineering point of view, force fields can be understood as the underlying material law for a system of discrete atoms at the atomistic length scale. A force field is the point of intersection between quantum mechanics and continuum formulations by providing a formulation of the atom interactions. In contrast to the high degree of details of quantum mechanics, the movement of electrons is not considered but the general physical mechanism needs to be captured. An accurate force field allows simulating complex material phenomena if a sufficiently large system (i.e., a representative large number of atoms) is

modelled.
A huge variety of different force fields can be found in the literature that can be distinguished by the class of materials (i.e., the atom types) that are covered and the capability of describing the underlying mechanism for the phenomena of interest. For polymers, several atom types (i.e., hydrogen, carbon, oxygen, nitrogen) need to be covered and for a nanocomposite, even more atoms need to be included, which reduces the number of available force fields significantly.
One common force field that accounts for a large number of different atoms is the Dreiding force field by Mayo et al. [50]. The generic force field was developed based on the DREIDING Stereomodels developed by Andre S. Dreiding. Strong evidence can be found in the literature that the DREIDING force field is an accurate choice for the simulation of polymers [12, 36, 82, 83] and nanocomposites [3, 4, 26–28]. The following overview of atom interactions follows the DREIDING force field and presents the potential functions used in the present thesis.
Generally, the atom interaction is divided in non-bonded (physical) interactions and bonded (chemical) interactions

$$\mathcal{U}(\boldsymbol{r}) = \mathcal{U}_{\text{non-bonded}}(\boldsymbol{r}) + \mathcal{U}_{\text{bonded}}(\boldsymbol{r}). \tag{2.7}$$

The bonded interaction involve terms that account for the bond stretch ($\mathcal{U}_B$, two-body), angle bend ($\mathcal{U}_A$, three-body) and dihedral angle torsion ($\mathcal{U}_D$, four-body)

$$\mathcal{U}_{\text{bonded}}(\boldsymbol{r}) = \mathcal{U}_B(\boldsymbol{r}) + \mathcal{U}_A(\boldsymbol{r}) + \mathcal{U}_D(\boldsymbol{r}). \tag{2.8}$$

For a better understanding, Figure 2.1 illustrates the distances and angles used in the potential functions for a simple polymer atom chain. Figure 2.2 shows the different bond, angle and dihedral potential functions based on DREIDING force field parameters for carbon (C3) atoms.
The bond stretch energy can be described by the simple harmonic potential

$$\mathcal{U}_B^{\text{harmonic}}(\boldsymbol{r}) = \frac{1}{2} \sum_{\text{bonds}} k_{ij} \left(r_{ij}^0 - r_{ij}\right)^2, \tag{2.9}$$

with the parameter k_{ij} being the bond stiffness and r_{ij}^0 being the equilibrium distance between two atoms i and j. A more accurate description is given with the non-linear Morse potential

$$\mathcal{U}_B^{\text{Morse}}(\boldsymbol{r}) = \sum_{\text{bonds}} D_{ij} \left[\exp\left(\alpha n \left(r_{ij}^0 - r_{ij}\right)\right) - 1\right]^2, \tag{2.10a}$$

$$\text{with } \alpha = \left(\frac{k_{ij}}{2D_{ij}}\right)^{\frac{1}{2}}. \tag{2.10b}$$

Here n is the bond order and D_{ij} defines an energy barrier for bond breakage (i.e., the bond-dissociation energy). As shown in Figure 2.2 (a), the harmonic

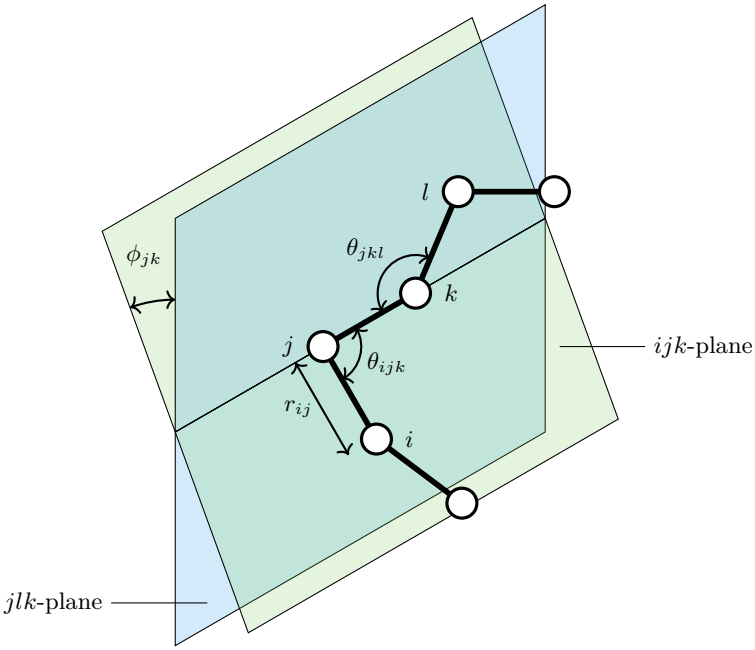

Figure 2.1: Illustration of the relevant distances and angles used in the bonded potential functions for a simple polymer atom chain.

potential is valid if only small deformations from the equilibrium distances occur. For increasing bond length r_{ij} the energy of the harmonic potential increases rapidly towards infinity. In contrast, the Morse potential function increases moderately and converges to the bond-dissociation energy D_{ij} that is required for a bond breakage.
For the angle potential a harmonic cosine form is used

$$\mathcal{U}_A(\boldsymbol{r}) = \frac{1}{2} \sum_{\text{angles}} \frac{k_{ijk}}{\left(\sin\theta^0_{ijk}\right)^2} \left(\cos\theta^0_{ijk} - \cos\theta_{ijk}\right)^2 . \tag{2.11}$$

that depends on the equilibrium angle θ^0_{ijk} and a bending stiffness k_{ijk} of adjacent atoms i, j and k as shown in Figure 2.1. Figure 2.2 (b) shows the potential function that has two minima at θ^0_{ijk} and $360^\circ - \theta^0_{ijk}$ due to the harmonic form. The torsion interaction for two bonds ij and kl that are connected by a bond jk is considered by the dihedral potential

$$\mathcal{U}_D(\boldsymbol{r}) = \frac{1}{2} \sum_{\text{dihedrals}} v_{jk} \left[1 - \cos\left(n_{jk}\left(\phi^0_{jk} - \phi_{jk}\right)\right)\right] \tag{2.12}$$

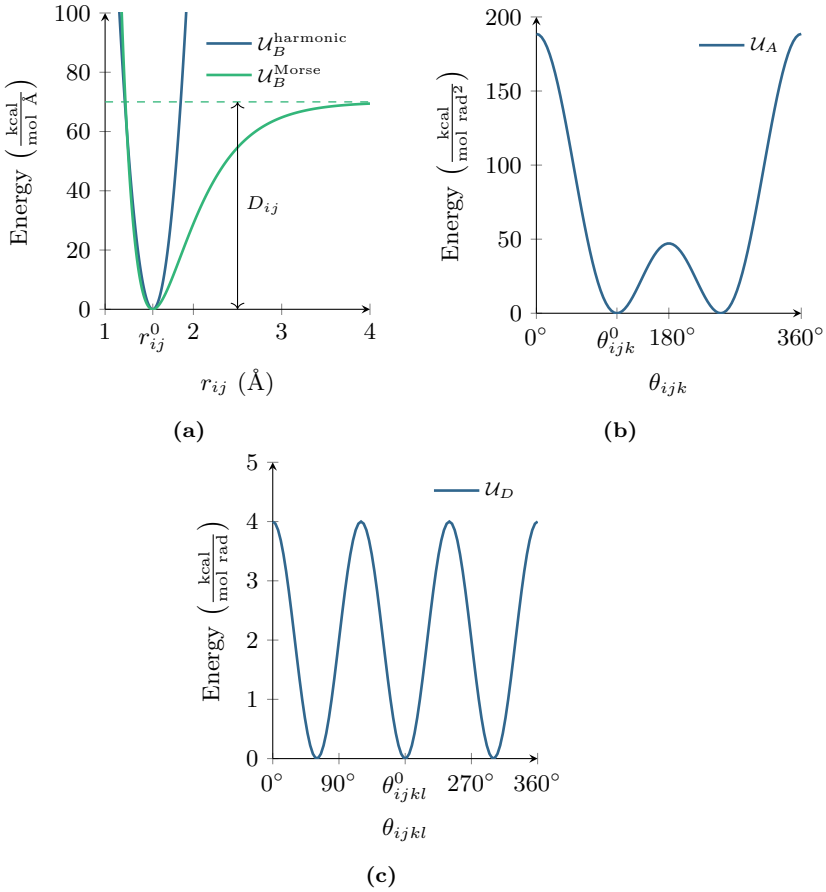

Figure 2.2: Exemplary potential functions of the DREIDING force field, based on the parameter values for carbon (C3) atoms: (a) Harmonic and Morse potential for the bonded interaction, (b) harmonic cosine form for the angle interactions and (c) periodic cosine form for the dihedral interactions.

Here, the periodicity is defined as n_{jk} and the torsional stiffness is given by v_{jk}. The rotational angle between the ijk- and jkl- planes is given with ϕ_{jk}, as shown in Figure 2.1, and ϕ_{jk}^0 is the respective equilibrium angle. The parameters n_{jk}, v_{jk} and ϕ_{jk}^0 only depend on the atom types of j and k and are independent of the first and fourth atom i and l. Figure 2.2 (c) shows the potential function that has three minima due to the periodicity of $n_{jk} = 3$. Since the dihedral interactions

are rather weak, compared to bond and angle interactions, their absolute energy values are also comparably small (compare energy levels of Figures 2.2 (a),(b) and (c)).
The non-bonded interaction typically involves two parts

$$\mathcal{U}_{\text{non-bonded}}(\boldsymbol{r}) = \mathcal{U}_{vdW}(\boldsymbol{r}) + \mathcal{U}_{Q}(\boldsymbol{r}), \tag{2.13}$$

which are the potential due to the van der Waals forces ($\mathcal{U}_{vdW}$) and due to electrostatic forces ($\mathcal{U}_{Q}$). The sum of non-bonded interactions may be extended by an explicit formulation for hydrogen bonding for specific cases. One common description for the van der Waals forces is given by the 12-6 Lennard-Jones potential

$$\mathcal{U}_{vdW}^{\text{LJ}}(\boldsymbol{r}) = \sum_{i}^{N} \sum_{j>i}^{N} D_{ij,vdW} \left[\rho^{-12} - \rho^{-6} \right], \tag{2.14}$$

Here, $\rho = \frac{r_{ij}}{r_{ij}^{0}}$ is the scaled distance and r_{ij}^{0} is the equilibrium distance between two non-bonded atoms i and j. The van der Waals well depth is given by $D_{ij,vdW}$ and can be understood as the stiffness of the physical interaction. It is worth to note that also the Morse potential (Equation 2.10a) can be used to describe the van der Waals force with good approximation of the Lennard-Jones potential [39, 47].
The electrostatic interactions between atoms i and j with respective charges Q_i and Q_j are considered by the Coulomb potential

$$\mathcal{U}_{Q}^{\text{Coulomb}}(\boldsymbol{r}) = \sum_{i}^{N} \sum_{j>i}^{N} \frac{Q_i Q_j}{\epsilon_0 r_{ij}}. \tag{2.15}$$

The parameter ϵ_0 describes the dielectric constant. The electrostatic interactions are not computed for atoms that form a bond (two-body interaction) or are involved in an angle (three-body interaction), as these are assumed to be included in the bond and angle interactions. The respective charges of the atoms can be computed using the Gasteiger model [32] or the electronegativity equalisation method [16, 17, 52, 53].
With these potential functions and provided parameters, the force on each atom can be calculated by the derivative with respect to the atom coordination (Equation 2.2). The long-range physical interactions theoretically contain the interactions between all atoms in form of two sums of all atoms (see Equation 2.14 and 2.15). However, for practical reasons generally, a cut-off is chosen for these long-range interactions in order to keep the computational cost at a reasonable level without a significant loss in accuracy.

2.4 Time integration

The governing equations form a system of coupled ordinary differential equations that generally can be solved by any explicit time integration scheme. One of the most common time integration schemes for molecular simulation is the explicit velocity Verlet algorithm. This method is similar to the leap-frog method, except that the positions and the velocity (in form of atom momenta $\boldsymbol{p}_i$) are directly calculated at each full time steps. This aspect is one of the main advantages, as the atom velocities are required for the calculation of kinetic energy. The time integration from time step t to the next time step $t + \Delta t$ is done by performing the following calculations

$$\boldsymbol{p}_i\left(t + \tfrac{1}{2}\Delta t\right) = \boldsymbol{p}_i\left(t\right) + \tfrac{1}{2}\Delta t \boldsymbol{f}_i\left(t\right), \tag{2.16a}$$

$$\boldsymbol{r}_i\left(t + \Delta t\right) = \boldsymbol{r}_i\left(t\right) + \Delta t \boldsymbol{p}_i\left(t + \tfrac{1}{2}\Delta t\right)/m_i, \tag{2.16b}$$

$$\boldsymbol{p}_i(t + \Delta t) = \boldsymbol{p}_i\left(t + \tfrac{1}{2}\Delta t\right) + \tfrac{1}{2}\Delta t \boldsymbol{f}_i\left(t + \Delta t\right). \tag{2.16c}$$

The forces only need to be evaluated at each full time step and no additional evaluation at intermediate time steps is required. This makes the algorithm efficient, as the computational expensive evaluation of all atom interactions (i.e., evaluation of large sums of all interactions) is reduced to a minimum. The algorithm is exactly time-reversible and energy conserving.

2.5 Periodic boundary conditions

For any reliable derivation of information from an atomistic system, a representative system size must be assured. In order to approximate a large (infinite) system, periodic boundary conditions (PBC) are used to avoid boundary effects. The concept of PBC is shown in Figure 2.3 for the two-dimensional case. The original simulation box (left) is replicated in each direction leading to eight image boxes surrounding the original cell. Each image cell is a copy of the original cell with the identical shape, atom positions and velocities. The number of atoms and the total momentum of each box is preserved since in case an atom leaves the original box the respective image atom will enter on the opposing box boundary. Each atom in the original cell can interact with the image atoms leading to an imaginary infinitive system. To assure that each atom only interacts with its nearest (original or image) neighbour atom, but not with several images of the same original atom, a cut-off must be chosen smaller than half the box size (minimum image convention). For the three-dimensional case, the box is additionally replicated in the third dimension resulting in 26 image cells.

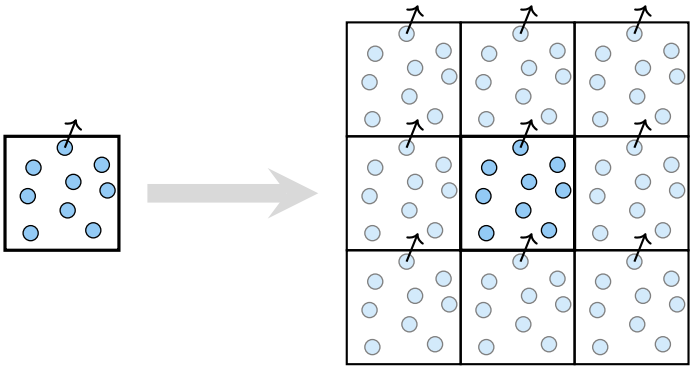

Figure 2.3: Schematic visualisation of periodic boundary conditions for two dimensions. The original system is centred and surrounded by eighth image systems with image atoms that are shifted along the box axis by the respective box size.

2.6 Ensembles

Depending on the aim of a molecular simulation a specific ensemble is used or different ensembles may be sequentially combined in order to perform the desired analysis. Figure 2.4 shows the common ensembles for the simulation of condensed matters, which are the micro-canonical ensemble (NVE), the canonical ensemble (NVT) and the isothermal isobaric ensemble (NPT).
Solving the governing equations using the energy-conserving velocity Verlet time integration leads to a system with constant energy. In this micro-canonical ensemble, called NVE, the number of particles (N), the volume (V) and the energy (E) are constant but the temperature or pressure may change significantly. With the NVE ensemble, an equilibration (i.e., energy dissipation) towards a state of minimal energy is not possible. The NVE ensemble can be understood as a completely isolated system that does not allow for any exchange of energy with the environment, as indicated in Figure 2.4 (left).
To mimic more realistic conditions it is desirable to specify the temperature of the box for which a canonical ensemble (NVT) ensemble can be used. This NVT ensemble, in which the number of particles (N) and the volume (V) are constant, is achieved by adding a thermal bath that keeps the temperature (T) at a specified level, as illustrated in Figure 2.4 (centre). Usually, this thermal bath, called thermostat, modifies the atom velocities and thus scales the kinetic energy, to assure the specified temperature. This leads to changes in the total energy of the system.
In order to perform simulations at experimental conditions, additionally, the pressure needs to be specified (i.e., zero external pressure or atmosphere pres-

sure). This configuration, called isothermal isobaric ensemble (NPT), can be achieved by keeping the thermostat and adding a barostat that keeps the pressure at a specified level. In this case, the number of particles (N) is kept constant and the temperature (T) and pressure (P) are specified. Since the volume is not kept constant, the box can deform and the density may change due to a change in the volume as indicated in Figure 2.4 (right). The total energy of the system can change due to both, the thermostat and barostat, which makes the NPT ensemble also favourable for energy minimisation.
A detailed description and discussion of thermostat and barostat formulations are deliberately omitted and the reader is referred to the overview given by Allen et al. [1] and Tadmor et al. [77].

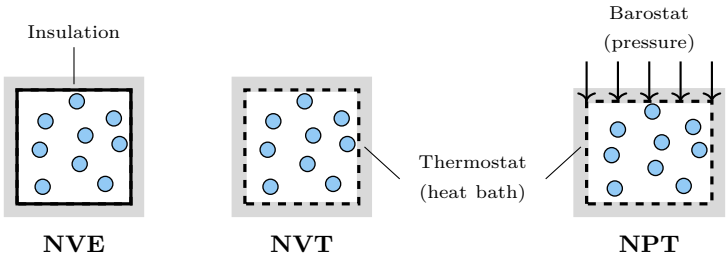

Figure 2.4: Schematic representation of the differences between the micro-canonical (NVE), the canonical (NVT) and isobaric-isothermal (NPT) ensembles.

2.7 Molecular Dynamic Finite Element Method

The molecular curing simulations, presented in the second Chapter, are conducted with the Molecular Dynamic Finite Element Method (MDFEM). This method is an incorporation of molecular dynamics in a Finite Element Method (FEM) framework developed by Nasdala et al. [55, 56]. The atomic interactions (i.e., bonded and non-bonded interactions) are implemented as user-defined finite elements into a FEM framework [54]. For two-body interactions, non-linear beam formulations can be used to describe the different potentials required (harmonic, Morse, Lennard-Jones, etc.). For three- and four-body interactions specific user elements were developed that accurately represent the specific potential functions, i.e., the harmonic cosine form (Equation 2.11) for the angles and the periodic cosine form (Equation 2.12) for the dihedrals. The combination of the quite general applicability of FE frameworks and the MDFEM can be used to couple atomistic and continuum regions. Therefore, the main advantage of the MDFEM is its application with regard to atomistic continuum coupling. Without such a coupling, a MDFEM calculation is equal to a MD simulation.

Chapter 3

Molecular curing simulation for epoxy resin cross-linking

3.1 Research context

To enable a reliable analysis and accurate prediction of material behaviour using molecular simulations, first, a realistic simulation model at the nano-scale is required. Especially for polymers, the underlying network topology and the final degree of curing are important due to their substantial effect on the bulk material behaviour [43, 66]. However, an accurate representation of these characteristics can be challenging for a polymer consisting of several constituent monomers concerning a variety of possible chemical reactions that affect the polymer network topology. Besides this aspect, the efficiency of generating realistic models need to be considered, since the computational cost increases rapidly with increasing model size and simulation time.
As molecular simulations are undeniable a powerful tool for investigations on the nano-scale induced material behaviour, a variety of molecular modelling methods for a variety of polymers have been published. The majority of these approaches follow the common procedure of a dynamic step-wise bond formation during a simulation with relaxation steps in between, followed by a final equilibrium step. Two main aspects are part of the research focus, from which one is the trade-off between efficiency and accuracy [80, 82, 83]. This aspect is affected by the choice of cut-off radius and by the number of bonds that are formed (i.e., all possible bonds within this radius or only the one with the shortest reaction distance). The second aspect is the application of predefined reaction probabilities, to reproduce the realistic curing mechanism and obtain a reasonably cured simulation model [23].
However, in existing studies, experimental validation of the whole curing process, not only the final degree of cross-linking, is pending. This lack of validation is mainly caused by the difficulty of experimentally measuring the curing process and quantifying the development of the network topology. In the best case, the procedures available in existing literature are validated with the evolution of reactive epoxy groups without considering the evolution of curing agents [59, 60]. Other studies only rely on a comparison of material properties, derived from molecular simulations using the cross-linked model with experimental values, which can be seen only as an indirect validation [43, 45, 84].

In this thesis, a molecular modelling method is presented that uses MDFEM simulations to mimic the polymerisation of an epoxy system. Experimental near-infrared spectroscopy measurements are performed to characterise not only the final network topology but also the whole curing mechanism, from a liquid to a solid polymer. For the first time, the predicted evolution of reactive groups during the complete curing process is successfully validated with near-infrared spectroscopy data.

3.2 Methods

The proposed molecular modelling method is implemented in the MDFEM framework [55, 56]. It follows the common methodology to dynamically form chemical cross-links between reactive sites, based on the distance between reactive groups, followed by equilibrium steps. In-situ near-infrared spectroscopy (NIR) is used for the experimental measurement of the entire time evolution of instantaneous concentrations of reactive groups (i.e., epoxy, hydroxy and amine curing groups). The NIR measurements were performed by the Federal Institute for Materials Research and Testing (BAM). The processing of the experimental data, from a time series of absorption bands to the evolution of reactive groups, is presented in detail and the related difficulties are discussed. It has been shown that this method is well suited for analysing the curing process and for characterising the fully hardened epoxy system [21, 22, 61].

3.3 Results and outlook

A good agreement between numerical data and experimental measurement of the whole curing mechanism is presented not only for the default mixing ration of epoxy and hardener component but also for two variations. Numerical studies on the curing process lead to the final choice for the cut-off distance of $r_A = 10$ Å, which is the relevant parameter in terms of efficiency and accuracy. It is shown that the chosen value has a strong effect on the simulation time, which can be significantly reduced for a realistic cross-linking while still maintaining a well-equilibrated system. The present experimental validation underlines the predictive capabilities of the proposed approach and thus, contributes to the computer-aided testing and development of new polymers. With the simulation models generated in the present publication, the fundamentals for all following work is given, since only realistic simulation models allow a reliable study on the material behaviour. The investigations on the viscoelastic behaviour of epoxy polymers (Chapter 4) and finally the incorporation into a multi-scale constitutive model for epoxy/nanoparticle nanocomposites (Chapter 5) strongly rely on the substantial developments provided in this chapter. Furthermore, the curing simulations can easily be extended to study curing related phenomena such as the polymerisation induced chemical shrinkage [2, 79] or the effect of water [73].

3.4 Paper A: Molecular modelling of epoxy resin cross-linking experimentally validated by near-infrared spectroscopy

The following paper is published in Computational Material Science, Volume 161, April 2019, Pages 223-235.

Author contribution

The main work was done by the author of this thesis. Ulrike Braun contributed the near-infrared spectroscopy experiments and the draft for the corresponding paragraphs. Johannes Fankhänel contributed with supporting work, especially software development of the general MDFEM framework, but not on the cross-linking algorithm implementation. Benedikt Daum, Behrouz Arash and Raimund Rolfes contributed with advisory and supporting work.

Graphical Abstract

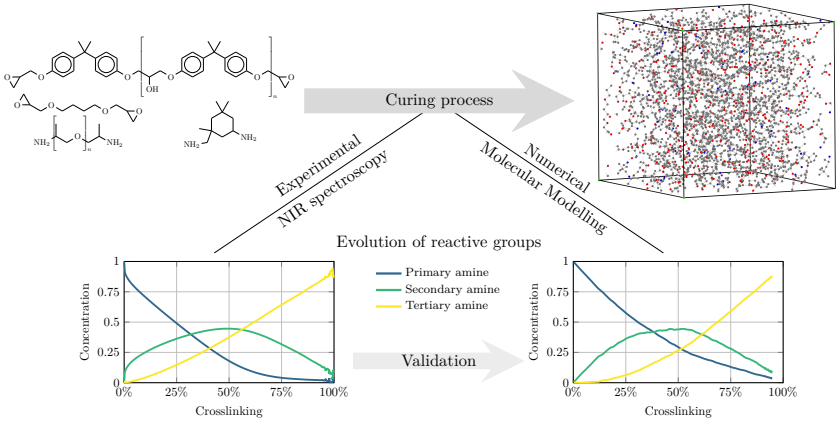

Computational Materials Science 161 (2019) 223–235

Contents lists available at ScienceDirect

Computational Materials Science

journal homepage: www.elsevier.com/locate/commatsci

Molecular modelling of epoxy resin crosslinking experimentally validated by near-infrared spectroscopy

Robin Unger[a,*], Ulrike Braun[b], Johannes Fankhänel[a], Benedikt Daum[a], Behrouz Arash[a], Raimund Rolfes[a]

[a] Institute of Structural Analysis, Leibniz Universität Hannover, Appelstraße 9A, 30167 Hannover, Germany
[b] BAM Federal Institute for Materials Research and Testing, Unter den Eichen 87, 12205 Berlin, Germany

ARTICLE INFO

Keywords:
Epoxy system
Curing process
Molecular dynamics simulation
Near-infrared spectroscopy

ABSTRACT

Reliable simulation of polymers on an atomistic length scale requires a realistic representation of the cured material. A molecular modelling method for the curing of epoxy systems is presented, which is developed with respect to efficiency while maintaining a well equilibrated system. The main criterion for bond formation is the distance between reactive groups and no specific reaction probability is prescribed. The molecular modelling is studied for three different mixing ratios with respect to the curing evolution of reactive groups and the final curing stage. For the first time, the evolution of reactive groups during the curing process predicted by the molecular modelling is validated with near-infrared spectroscopy data, showing a good agreement between simulation results and experimental measurements. With the proposed method, deeper insights into the curing mechanism of epoxy systems can be gained and it allows us to provide reliable input data for molecular dynamics simulations of material properties.

1. Introduction

Thermosetting polymers belong to a class of polymers that are characterised by their irreversible curing process, changing the material consistency from a liquid soluble prepolymer to a solid material. The physical properties of the highly linked network formation depend very much on the underlying molecule network structure, which is primarily influenced by the constituent monomers and the polymerisation reaction [1,2]. As there is a large number of constituent monomers, that allow a huge variety of combinations, computer-aided testing and design of new polymers is desirable in order to reduce the needed time and costs. With molecular dynamics (MD), a suitable method is available for simulating nanoscale effects and predicting material properties, however, it requires the associated simulation model to be an accurate representation of the real material system.

This necessity of an appropriate molecular modelling led to research in this field, resulting in a variety of molecular modelling methods for different polymer materials that can be found in literature. One initial method for a MD crosslinking simulation, focussing on the polymerisation of poly(methacrylate) networks, was presented by Doherty et al. [3]. The crosslinking was realised by forming covalent bonds between reactive groups with the smallest distance (reaction radius) in between, succeeded by a short relaxation to let the system react to the changes of the network structure. Other publications suggested molecular modelling methods for various polymer systems focussing on different aspects of the curing mechanism. However, all of them followed the same fundamental principle of a dynamic covalent bond formation, with the main criterion being the reactive distance between two possible reaction partners.

These molecular modelling methods share the following procedure: (1) generation of the unlinked model, (2) initialisation of the MD simulation, (3) MD crosslinking simulation, (4) final equilibration of the system. The first step involves the initial generation of a random unlinked model from separate monomer and curing agent molecules. An energy optimisation is applied to the initial model to minimise internal energy as a preparation for the following MD simulation. The crosslinking simulation is initialised by heating up the simulation box to the desired curing temperature and an equilibration before the crosslinking is started. In the actual crosslinking procedure, a number of bonds are formed in every crosslinking step, followed by a relaxation time to let the system react to the changes of the network structure. Depending on the specific method, only the bond with the shortest reactive distance [3–5] or all bonds within a certain reaction cut-off are formed [6–8]. The crosslinking is either continued until a desired degree of

* Corresponding author.
E-mail address: r.unger@isd.uni-hannover.de (R. Unger).

https://doi.org/10.1016/j.commatsci.2019.01.054
Received 23 October 2018; Received in revised form 30 January 2019; Accepted 31 January 2019
Available online 11 February 2019
0927-0256/

crosslinking is achieved or until no possible bonds are found any more. The final cured system is equilibrated and charges are updated, if not done dynamically.

Approaches focussing on amine-cured epoxy systems differ especially in their assessment of reactive amine group reactivity. Wu et al. [4,5] and Bandyopadhyay et al. [9] assumed an equal reactivity of primary and secondary amines. Varshney et al. [8] continued on this research by adopting the methodology of Wu et al. [4,5] and comparing it with a newly developed method, which finally leads to better equilibrated structures with lower energies and reduced computational time. Extensive investigations on the influence of different reaction probabilities of curing agents of an amine-cured epoxy system were done by Estridge [10]. The study showed, that significantly changed reactivities of primary and secondary amines lead to different network structures of the cured epoxy system. Furthermore, Varshney et al. [8], Estridge [10] as well as Yang et al. [11] investigated the molecular weight of the largest and second largest molecular cluster as a function of the degree of curing. The authors were able to predict a theoretical gel point and the investigation of the effect of the network structure showed an influence on the physical properties. These results underline the need for an accurate molecular modelling in order to reliably predict material properties. For a general review on the evolution of polymer networks with respect to the structure evolution and the gel point the reader is referred to Li et al. [12].

Okabe et al. [13,14] studied different mixtures of epoxy resin and amine curing agents with MD simulations and experimental differential scanning calorimetry (DSC). The molecular modelling results showed an acceptable agreement to experimental results in the general behaviour of the curing curves and reactivity of the epoxy groups. However, specific characterisation of the different crosslinking reactions during the curing process was not possible with DSC.

Jang et al. [15] presented a relative reactivity volume criterion for the crosslinking of vinyl ester resins that takes the regioselectivity (head-to-tail chain propagation) and the corresponding monomer reactivity ratios into account. Li et al. [16,17] focussed their research on an accurate charge updating using the electronegativity equalisation method (EEM) after each bond formation. As multiple EEM updates are computationally intensive, a parameterised EEM-based charge assignment was developed, that leads to reasonable results with a decrease in computational cost. Demir et al. [18] proposed a related molecular modelling approach, with the difference of using the Charge Equilibration (QEq) method and an increasing reaction cut-off during the crosslinking.

Crosslinking of novolac-type phenolic system was investigated by Monk et al. [19,20] with respect to the chain motif (*ortho–ortho* or *ortho–para*) and the chain length. The results show, that the type of hydrogen bonding (interchain or intrachain) was strongly affected by the chain motif and lead to differing physical properties of the crosslinked system. Shudo et al. [21] followed up on a study of Izumi et al. [22] and constructed and characterised the network structure of phenolic resins by MD simulation. They presented a good agreement with experimental results, obtained by small- and wide-angle X-ray scattering, in terms of the branching structure of the phenolic units and the methylene linkages, the molecular weight distributions and densities for various conversion rates.

The effect of water on the crosslinking of epoxy resins was investigated with MD simulations by Sharp et al. [23]. The obtained results were in agreement to experimental data and showed that water increases the molecular diffusion, which lead to an increase in the cure rate for low degrees of crosslinking. Tam et al. [24] presented a study on the molecular modelling of an epoxy resin with various water concentrations, with results indicating that the bonding behaviour and the resultant network structure is significantly influenced by the moisture concentration.

The methodology of curing nanocomposites, composed of epoxy systems and nano-sized filler materials is also considered in literature [25–29]. Coto et al. [26] focussed on the molecular modelling of epoxy/carbon nanotube nanocomposites and Vo et al. [27] investigated the effect of the atomistic modelling on the morphology and thermo-mechanical properties of thermosetting epoxy/clay nanocomposites. Molecular modelling of an epoxy-POSS (polyhedral oligomeric silsesquioxane) nanocomposite was presented by Song et al. [28] and Neyertz et al. [29].

The discussed molecular modelling procedures follow the common method to use a dynamic step-wise crosslinking algorithm with equilibration steps between the bond formation. A comparison and validation of these molecular modelling methods with experimental results of the curing process is still pending in literature. Because of the difficulty of obtaining experimental insight into the curing process, the procedures presented are validated indirectly by comparing simulated material properties with experimental values.

In this publication, a molecular modelling method for crosslinking epoxy resins is presented that is able to realistically describe the curing mechanism and to generate simulation models that are in good agreement with experimentally analysed cured epoxy resins. In order to reduce simulation time, and with this the computational cost, a parameter study was conducted to increase the efficiency while keeping the crosslinked model well equilibrated. By using the method of in situ near-infrared spectroscopy (NIR), the entire time evolution of instantaneous concentrations of reactive groups, epoxy and either amine or anhydrite curing groups, can be observed, instead of only the concentrations of the final cured polymer. It has been shown that this method is well suited for analysing the curing process and for characterising the fully hardened epoxy system [30–32]. Thus, NIR measurements of the polymerisation reaction of an epoxy system give valuable insights into the curing process that can be used to significantly improve the model generation towards reality. Experimentally obtained measurement data of the curing process is used to compare and validate the presented numerical crosslinking method with respect to the crosslinking procedure and the resulting network structure. The molecular modelling method is incorporated into the Molecular Dynamic Finite Element Method (MDFEM) [33–35] framework that can be used for deriving physical material properties [36,37].

2. Near-infrared spectroscopy

2.1. Material system

A commercially available amine-cured epoxy system from Olin Epoxy was chosen for the study. The epoxy resin was of type AIRSTONE 880E and as a hardener AIRSTONE 886H was chosen, both made for the infusion process of large and thick composite parts, such as wind turbine blades. An overview of the chemical composition of the epoxy system is given in Table 1 and the chemical structures of all molecules are shown in Fig. 1 (all information is taken from material data sheets [38,39]).

Table 1
Overview of the chemical composition of the epoxy system (names, mixing ratios and CAS identification numbers). Corresponding chemical structures are shown in Fig. 1.

	Name	Parts (wt%)	CAS-No.
Resin (AIRSTONE 880E)	Bisphenol A diglycidyl ether	75–100	25068-38-6
	1,4-Butanediol diglycidyl ether	10–25	2425-79-8
	Alkyl (C12-C14) glycidyl ether	1–5	68609-97-2
Hardener (AIRSTONE 886H)	α, ω-poly(oxypropylene) diamine	50–75	9046-10-0
	3-(aminomethyl)-3,5,5-trimethyl-cyclohexanamine	25–50	2855-13-2
	2,4,6-tris[(dimethylamino) methyl]phenol	1–5	90-72-2

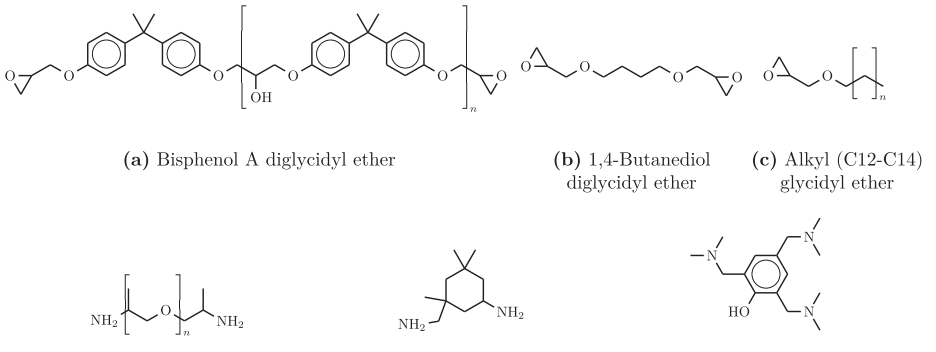

(a) Bisphenol A diglycidyl ether

(b) 1,4-Butanediol diglycidyl ether

(c) Alkyl (C12-C14) glycidyl ether

(d) α,ω-poly(oxypropylene)diamine

(e) 3-(aminomethyl)-3,5,5-trimethyl-cyclohexanamine

(f) 2,4,6-tris[(dimethylamino)methyl]phenol

Fig. 1. Chemical structures of all molecules of the investigated epoxy system: (a)–(c) chemical components of the epoxy resin, (d)–(f) chemical components of the hardener.

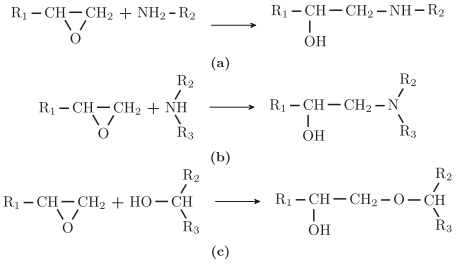

Fig. 2. Principle polymerisation reactions: (a) epoxy group with primary amine, (b) epoxy group with secondary amine, (c) epoxy group with hydroxyl group.

The two main chemical components of the epoxy resin, Bisphenol A diglycidyl ether and 1,4-Butanediol diglycidyl ether, each consist of two epoxy groups as the reactive groups. The reactive groups of the two main hardener molecules, α, ω-poly(oxypropylene) diamine and 3-(aminomethyl)-3,5,5-trimethyl-cyclohexanamine, are the amine groups (NH_2), from which each can form two covalent bonds to an epoxy group. The respective polymerisation reactions, from primary to secondary amine and from secondary to tertiary amine, are shown in Fig. 2(a) & (b). First, the epoxy ring is opened, resulting in an additional hydroxyl group and a reactive methylene group, which then is the reaction partner for the amine group, forming a bond. Beside this dominant reaction of amines and initially epoxy groups, also an etherification reaction between a hydroxy group and an epoxy group is possible. The existing hydroxyl groups as well as the newly created hydroxyl groups, can be a reaction partner for the etherification reaction, shown in Fig. 2(c).

NIR measurements of the curing process were conducted on the standard stoichiometric mixture (100 parts epoxy resin, 31 parts hardener), as well as on mixtures with a shortage of hardener (100:15) and with an excess of hardener (100:60). The near-infrared spectroscopy was conducted during the 5-h isothermal curing process at 80 °C with an additional heat-up process of 50 min prior to the curing. The overall curing and measurement time is 350 min.

2.2. Methodology

Spectroscopy methods allow to identify the chemical composition of a material and by repeated measurements during a chemical reaction, the changes in the molecule structure can be observed. Common spectroscopy methods for polymer characterisation are the near-infrared (NIR), mid-infrared (MIR) and Raman spectroscopy. Specific vibrations and rotations are the consequence of the specific wavelength absorption by covalent bonds, which is measured. Poisson et al. [40] compared NIR and MIR spectroscopy with respect to measurements of the epoxy curing conversion and showed that NIR is very well suited to analyse the curing kinetics. This result was underlined by Lachenal et al. [41], whose results showed a very good agreement of NIR results with differential scanning calorimetry (DSC) and size-exclusion chromatography (SEC) results. They concluded that NIR spectroscopy allows for a valuable real-time analysis of epoxy systems. Pandita et al. [30], Duemichen et al. [31] and Erdmann et al. [32] successfully realised the idea of NIR spectroscopy of in situ curing kinetics of epoxy resin. In the NIR, light with wavelengths between 800 nm and 2500 nm is used, which include mainly the less intensive overtones and combination vibrations compared to the fundamental signals in mid-infrared. As a consequence, the spectra often give unspecific structural information, but due to the lower intensities of these overtones compared to the fundamentals, thicker samples can be measured. Because glass does not absorb in NIR wavelength range, samples can be measured through glass, hence, we can use optical cuvettes, analysing the change of chemical structure during the complete curing process from the liquid up to the fully cured state. The experimental setup as well as the relevant experimental parameters are described in detail in the work of Duemichen et al. [31] and Erdmann et al. [32].

Exemplarily selected spectra of the studied epoxy system during the complete curing process are shown in Fig. 3. The decrease of epoxy and amine absorption band signals during the curing process is illustrated as well as the formation of hydroxyl groups. For the determination of signal evolution rates of each absorption band, integration limits are chosen and a corresponding basis line is defined as a lower boundary. Based on the integration limits and the basis lines, the respective peak area is integrated, quantifying the absorbance of each absorption band over the curing time. An overview about the absorption bands and the corresponding signal assignment as well as the integration limits are given in Table 2. The integrated peak area of the absorption bands can

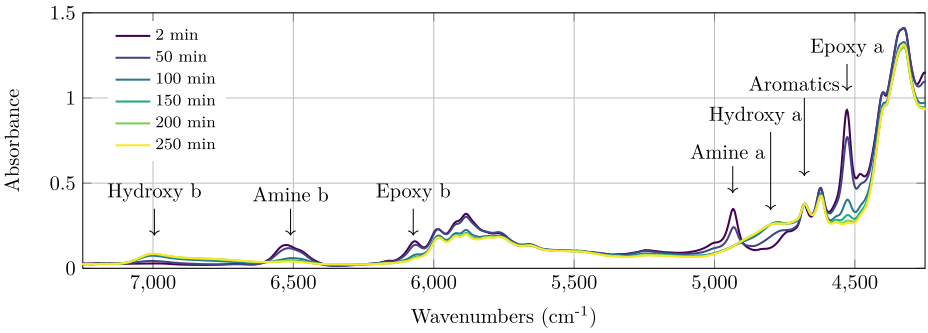

Fig. 3. Individual, exemplarily spectra of the studied epoxy system during the curing process.

be processed to determine the normalised time-dependent change of reactive groups. For the present system, we focus on the time-dependent change of epoxy rings, the primary, secondary and tertiary amines, as well as the hydroxyl groups. The aromatic signal was chosen as an invariant reference signal, because no influence of curing chemistry should affect this signal.

The relations between the functional groups and the absorption bands are shown in Table 3. The epoxy absorption band concentration is directly related to the concentration of reactive epoxy groups. In the following, only Epoxy a is considered as the respective epoxy absorption band, neglecting the overtone signals from CH stretching (Epoxy b). The same holds for the respective hydroxy absorption bands, for which only Hydroxy a is considered as the functional hydroxy group. The absorption band of Amine a directly corresponds to the functional primary amine group. As the absorption band of Amine b consists of both primary and secondary amine signals, the difference of Amine b and Amine a is calculated as the quantity of secondary amines.

Table 3
Relation between functional groups and absorption bands.

Functional group	Assignment of absorptions bands
Unlinked epoxy	Epoxy a
Primary amine	Amine a
Secondary amine	Amine b − Amine a
Hydroxy	Hydroxy a

2.3. Experimental near-infrared spectroscopy results – Absolute absorbance

The development of the relevant absorbance band signals as a function of time is presented in Fig. 4(b)–(e) together with the corresponding temperature history (a). Additionally, the absorbance band of the aromatics is added as a reference (f). The quantity of the aromatics does not change throughout the curing process, since the aromatics do not react during the curing process. This allows the change of the absorbance band signal to be used as an indicator for the temperature dependency. Due to different integration limits and peak values, the absolute signal intensities are not quantitatively comparable. However, a qualitative analysis is useful as it gives insights into the influence of the mixing ratio on the curing reaction and to identify the importance of the etherification reaction between epoxy and hydroxy in general.

The comparison of all curves with the reference signals at the beginning and the end of the curing procedure shows that especially the amines and the hydroxyl groups are influenced by the temperature. For the amines, this effect is small in comparison to the absolute signal. The hydroxyl groups are stronger influenced by the temperature, as a temperature change has a direct effect on hydrogen bonding, which in turn influences the absorption band signals. The evaluation of absolute signal intensities of the standard mixture shows that after consumption of around 50% of epoxy groups, 90% of primary amines are already reacted and the signal intensity of secondary amines is at its peak value. At this stage, the formation of secondary amines starts to decrease, which means that from this point, the reaction of secondary to tertiary amines is the dominant one and faster, compared to the reaction of primary to secondary amines. Towards the end of the curing time, the converged values of the standard mixture indicate that the system is fully cured. The absolute signal intensities of epoxy and primary amine converge against zero. The absolute signal intensity of secondary amines does not reach its starting value of zero, indicating that there is a small amount of secondary amines left in the cured system.

With an excess of hardener molecules, all epoxy groups are fully reacted as indicated by the signal intensity of epoxy groups that is converging towards zero. The complete consumption of epoxy is detectable after ≈ 120 min, whereas remaining signals of primary and secondary amines are observable. Due to the shortage of epoxy, not all hardener molecules can react, thus a small amount of primary and a substantial amount of secondary amines are left in the system. The constant signals of amines and hydroxyl groups from ≈ 120 min on

Table 2
NIR measurement assignment of absorption bands and the corresponding evaluation parameters.

Absorption band	Assignment	Integration limits (cm^{-1})
Epoxy a	Combination of CH stretching and CH_2 deformation	4560–4497
Epoxy b	Overtone from CH stretching	6110–6036
Amine a	Combination of primary NH_2 stretching and bending vibration	4971–4887
Amine b	Overtone of primary NH_2 plus secondary NH stretching	6610–6410
Hydroxy a	Combination of OH	4851–4750
Hydroxy b	Overtone of OH stretching	7090–6901
Aromatics	Combination of aromatic C=C and aromatic CH stretching	4702–4658

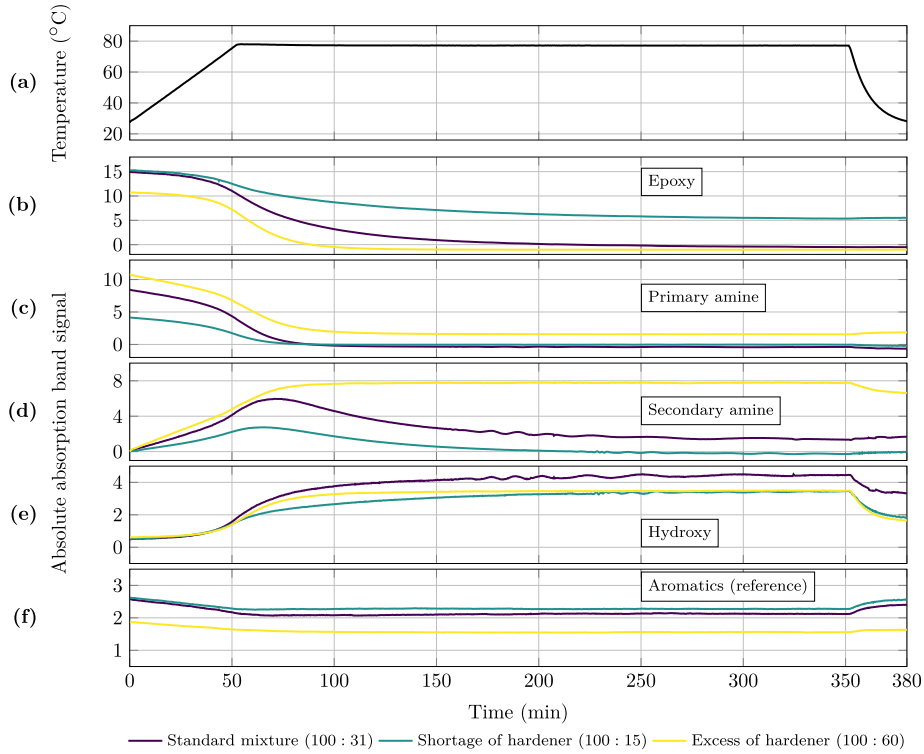

Fig. 4. Development of curing temperature (a) and relevant absolute absorption band signals (b)–(f) as a function of curing time for different stoichiometric mixtures.

clearly show that the complete consumption of epoxy stops the reaction in the mixture and no relevant contribution from reactivity between the hydroxyl and amine groups is observable (i.e., condensation reactions by ether formation).

The third measured mixing ratio with a shortage of hardener results in a cured system with a substantial amount of non-reacted epoxy groups left. The final signal intensities of primary and secondary amines, both converging against zero, indicate that all hardener molecules are fully reacted to tertiary amines. Compared to the standard mixture between 100 and 350 min, the decay of secondary amines signal and the formation of the hydroxyls signals shows a very similar pattern. This means the curves are only shifted in the vertical positions, due to different integration values, but they do not cross or converge to each other. This can be seen as an indicator, that even at a lack of amines, no hydroxyl groups react additionally by etherification with epoxy groups. The most likely reason is that the hydroxyl groups do not react at all with the epoxy, as it was also stated by Strehmel [42] for amine-cured systems without an accelerator. However, it should be noticed that the reaction of epoxy with hydroxyl groups does not result in additional hydroxyl groups, because ether is formed, hence, the concentration of hydroxyls keeps constant.

In general, it seems that even at the end of the reaction still slight changes are observable, although the main changes of all signals occur during the first half of the curing time. The increasing viscosity as well as the gel formation significantly prevents the transport of reactive groups to reach others, therefore the reaction is significantly slowed down at a certain level and finally stopped.

2.4. Experimental NIR results – Normalised change of reactive groups

For an analysis of the curing process and the following validation of the molecular modelling, it is useful to derive the normalised change of reactive groups from the absorption band measurements. This is achieved by first normalising the time-dependent change of the absorption bands (Fig. 4) and second, by calculating the normalised change of reactive groups from the absorption bands. The normalisation can be done for the absorption bands of Epoxy a, Amine a and Amine b, as these bands are related to functional groups that are only decreasing due to the chemical reaction (see Table 2). Therefore, the initial state refers to the reference value of the uncured system that is related to 100% of each absorption band. Based on the integration parameters, an integrated peak area of zero refers to 0% of the absorption band. The normalisation of the hydroxyl absorption band is rather difficult, as there is already an unknown quantity of hydroxyl groups at the initial state and the absorption band is increasing during the chemical reaction. Thus, it is not possible to determine a reference value either for the initial or the final state of hydroxyl groups. However, as the previous analysis of the time-dependent change of absorbance bands has shown,

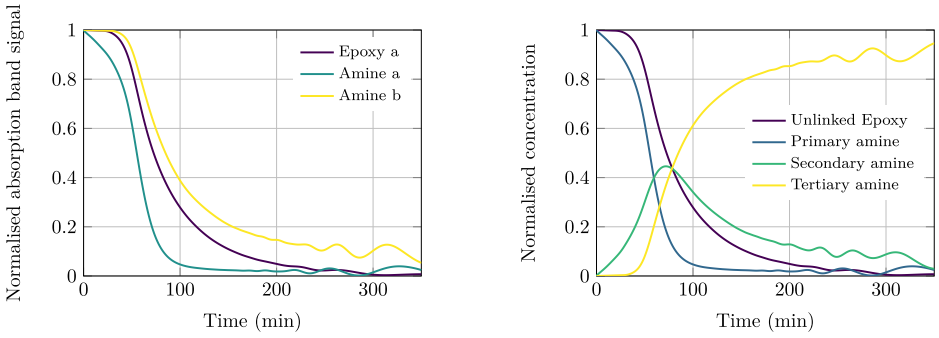

Fig. 5. Normalised NIR measurement data of the standard mixing ratio (100:31): (a) absorption bands (b) reactive groups.

the hydroxyl groups are not significantly involved in the curing process and thus neglected for the following analysis. The normalised change of the absorption band is shown in Fig. 5(a). A smoothing is applied to reduce oscillations and minor corrections of the NIR signal are applied to correct measurement inaccuracy. The concentration of the Epoxy a and both amine absorption bands is decreasing over time, as it is expected due to the curing reaction. The oscillations in the absorption band signals are likely caused by the chemical shrinkage of the epoxy system. The chemical shrinkage induces thermal stress in the glass cuvette, which leads to minimal motion of the cuvettes within the NIR device and finally to broken cuvettes at the end of the curing process. This phenomenon results in an oscillating base line offset that influences the integrated peak area.

After the normalisation, the concentration of the functional groups can be calculated from the normalised absorption band concentration. The relations between the functional groups and the absorption bands have already been shown in Table 3 and hold for the normalised absorption bands. In addition, for the normalised values it is possible to calculate the concentration of tertiary amines as the differences of Amine b to the initial value of 100%. The normalised changes of the relevant reactive groups for the standard mixing ratio are shown in Fig. 5(a). The concentration of unlinked epoxy groups is steadily decreasing, as the curing only happens irreversibly with the reaction of epoxy and amine groups to crosslinked monomer hardener molecules. Therefore also the concentration of the primary amines is decreasing continuously, with over 90% reacting to secondary amines within the first 100 min of the curing process. This can also be seen by the increase of secondary amines until a peak is reached at $\approx$ 75 min, after which the quantity of secondary amines decreases. The progress of the secondary amines indicates, that the reaction from primary to secondary amines is dominant within the first 75 min. The reaction from secondary to tertiary amines becomes dominant only after the majority of primary amines reacted to secondary amines. Finally, the curing reaction results in a large amount of $\approx$90% tertiary amines in the final state. After 350 min, the system is fully cured, indicated by the converged concentration of unlinked epoxy groups.

Fig. 6(a) shows the normalised change of reactive groups for the mixing ratio with a hardener shortage (100:15). The general evolution of reactive groups is qualitatively the same as for the standard mixing ratio. Due to the shortage of hardener, nearly all of the amine groups are fully reacted to tertiary amines, whereas only $\approx$60% of the epoxy groups are reacted. Although the normalised concentration of secondary amines is lower than the concentration of primary amines, both amines can be interpreted as fully reacted, due to the shortage of hardener. The normalised change of reactive groups for the mixture with an excess of hardener (100:60) is shown in Fig. 6(b). Due to the excess of hardener, the epoxy groups are fully reacted after $\approx$ 150 min, with a substantial amount of non-reacted amine groups left.

It is also worth mentioning that for all mixing ratios a strong decrease of primary amine groups without a corresponding decrease of unlinked epoxy groups can be seen within the first 30 min. This physically unlikely measurement effect needs to be interpreted with respect to the heating of the specimen and is also partly related to measurement inaccuracy. NIR absorption is temperature-dependent, with an increasing temperature leading to a decrease of signal intensity, as it can be seen in Fig. 4. For further information on the temperature dependency the reader is referred to Duemichen et al. [31] and Erdmann et al. [32]. Nevertheless, it is appropriate to use the measurement data obtained during heating, in order to observe the full curing process.

3. Molecular modelling method for crosslinking

3.1. Generation of the unlinked model

The unlinked model, as a representation of the uncured epoxy system, is randomly generated based on the molecule models of the monomer and curing agent. The chemical composition of the epoxy system (AIRSTONE 880E & AIRSTONE 886H from Olin Epoxy) is presented in Table 1, the corresponding chemical structures are shown in Fig. 1. Both the epoxy resin and the hardener are a mixture of three molecules, from which in both cases one molecule with a weight fraction less than 5% was neglected for the model generation. The modelled epoxy resin consists of two monomer molecules, Bisphenol A diglycidyl ether and 1,4-Butanediol diglycidyl ether. The molecule modelling is specified by an average weight fraction ratio of 85:15 and an average value of $n = 1.265$ for the repeating units of Bisphenol A diglycidyl ether. The modelled hardener is a mixture of α, ω-poly(oxypropylene) diamine and 3-(aminomethyl)-3,5,5-trimethyl-cyclohexanamine, for which an average weight fraction ratio of 62.5:37.5 was chosen. The number of repeating units for the first hardener molecule, α, ω-poly (oxypropylene) diamine, was chosen to $n = 9.5$. The specified weight fraction ratios and the number of repeating units are based on the data given by the corresponding data sheets [38,39].

Firstly, chemical models for each of the individual molecules are generated and equilibrated. These molecule models are duplicated according to box size, density and mixing ratio for a randomly and equally distributed placement in the simulation box. An optimised molecule arrangement is generated using the open source package PACKMOL

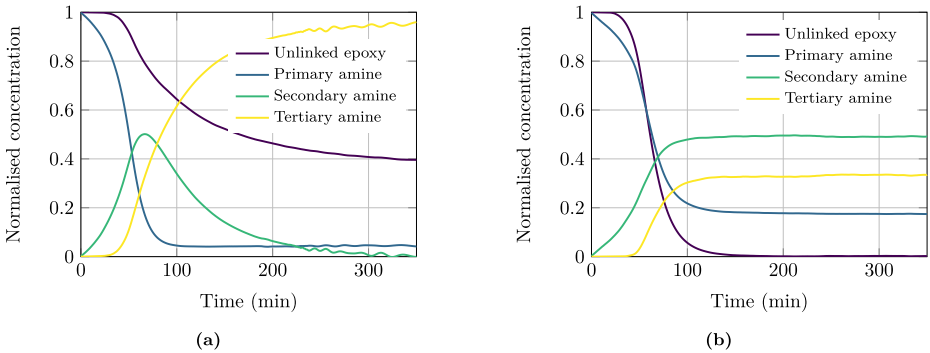

Fig. 6. Normalised change of reactive groups of modified mixing ratios: (a) shortage of hardener (100:15) (b) excess of hardener (100:60).

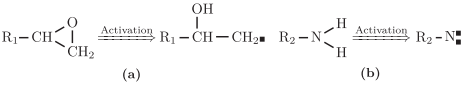

Fig. 7. Activation of (a) epoxy group and (b) amine group. A black square (■) indicates a possible covalent bond to a reaction partner.

[43]. As a preparation for the crosslinking simulation, all reactive groups are activated, as shown in Fig. 7, with the black square indicating a possible covalent bond to a reaction partner. The epoxy group is broken up and the oxygen is hydrated to a hydroxyl group, resulting in an reactive methylene group. Both hydrogen atoms of the amine groups are removed, resulting in a reactive primary amine. Furthermore, molecular mechanic energy minimisation is applied to equilibrate the system. The pre-processing implements the Open Babel Package [44,45].

3.2. Crosslinking simulation

The crosslinking simulation is the main part in the model generation and starts with the previously generated unlinked simulation model. The principle polymerisation reactions are presented in Fig. 2. The obtained NIR measurement data has shown that the etherification reaction has no influence on the curing kinetics for the epoxy system investigated. Therefore, this reaction is neglected in the following crosslinking simulation, which focusses on the reaction of amine groups with epoxy groups.

The simulations are done using the Molecular Dynamic Finite Element Method (MDFEM) [34,35], which incorporates the MD method into a FEM (Finite Element Method) framework. In principle, the MDFEM is an implementation of the MD method into a finite element (FE) framework. It implies that the atomistic interactions (i.e., bonded and non-bonded interactions) are defined by corresponding user defined elements. This leads to a FE calculation, which is comparable to a MD simulation. For further general information on MD implementations into the FEM, the reader is referred to Nasdala et al. [33] and Wackerfuß [46]. All simulations were performed using the DREIDING force field, in its form published by Mayo et al. [47]. Harmonic potentials are used for the bonded interactions and the Morse potential is applied for non-bonded interactions. This force field was chosen as it is applicable to a large number of atoms and proved to be an appropriate choice for MD simulations of polymers [4,36]. A Nosé-Hoover thermostat in combination with a Parrinello-Rahman barostat [48] is used for controlling the box temperature and pressure. The crosslinking simulation uses an isothermal-isobaric ensemble (NPT) with zero external pressure to allow for a sufficient relaxation and to trace the curing-induced volume change. Three-dimensional periodic boundary conditions were applied, allowing bond formation across box boundaries. The time increment size was chosen to a value of 1 fs. The crosslinking algorithm follows the common approach to use the distance between two reactive groups as the main criterion for a bond formation. The crosslinking simulation procedure is as follows:

Step 1: Initial relaxation within 500 ps under NPT ensemble, combined with a linear increase of temperature to the curing temperature;
Step 2: Distances between all possible reactions groups are calculated; all reaction distances larger than a chosen cut-off r_c for the reaction distance are discarded and the bond with the smallest reaction distance is formed;
Step 3: Equilibration of the system for a time period of 2.5 ps;
Step 4: Repeat step 2 and 3 until the end of overall simulation time is reached.

The time period of 500 ps for the initial relaxation is sufficient to equilibrate the system and increase the temperature to the curing temperature, which was chosen to the experimental value of 353.15 K (80 °C) for the used epoxy system. In order to generate a realistic representation of the cured epoxy system, it must be assured that a sufficiently high degree of crosslinking is reached. This can either be achieved through a large cut-off r_c, for which the values to be investigated range between 4 Å and 10 Å, or through a sufficiently long simulation time. The latter is directly related to unfavourable high computational cost. With a larger cut-off, more potential bonds are found in every crosslinking step and a high degree of crosslinking can be achieved in a reasonable simulation time. However, this might also lead to an increased overall simulation time, as a significant longer time period might be needed for a sufficient equilibration of the cured system, due to the large initial bond lengths. The trade-off between cut-off r_c and overall simulation time is the topic of a parameter study and a discussion in the following section. The value of 2.5 ps was chosen as this time period is large enough to let the system react to the structural change due to the newly created bond. A sufficient time period between

the bond formation is necessary for an appropriate equilibration, since the initial lengths of newly formed bonds can be unreasonably large and need to be equilibrated. Possible differences in the reactivity of primary and secondary amines are not explicitly prescribed, as only one cut-off value is used, independent of the reaction type. The variation in reactivity is considered implicitly due to the change of distance between the reactive groups caused by steric effects and physical interactions.

As the cut-off distances investigated (4 Å < r_c < 10 Å) are significantly larger than the equilibrium distance, large initial bond forces arise during the crosslinking. Using the harmonic potential for the bond energy, the attracting forces increase linearly with the bond length, resulting in enormous forces for initially formed bonds. This can lead to unstable simulations, unreasonable oscillation in the global potential energy of the system and finally in time divergence. On the other hand, using the Morse potential can lead to a very low bond energy for large bond lengths, what may result in an unrealistic equilibrium state of the system. To handle this issue the harmonic potential function was used with a linear activation within 100 time steps after bond formation. With an average time step of 1 fs, this results in a linear scaling of the potential from 0% to 100% within 0.1 ps. This issue was also noted by Doherty et al. [3], who used the harmonic potential within the bond generation procedure and by Heine et al. [7], who used a constant potential energy above a certain cut-off value. Also Mayo et al. [47] advised to use the harmonic potential for relaxation of artificially generated structures. The linear activation of the potential proved to be a sufficient choice in the present study and due to the moderate increase in bond energy, no convergence issues were observed. The algorithm can be generally applied to amine-cured, as well as anhydrite-cured epoxy systems. For epoxy systems different from the one investigated, the etherification might need to be considered, as it can have a significant influence. For this case, it is proposed to differentiate by using different cut-off radii for the reaction of epoxy and amine ($r_{c,Amine}$), as well as epoxy and hydroxy ($r_{c,Hydroxy}$). The probability of these two oppositional curing reactions can be adjusted within the crosslinking simulation by the ratio of these reaction cut-offs.

4. Results and discussion

This section presents and discusses the results obtained by using the proposed molecular modelling method. As the cut-off distance is the major parameter, that has an influence on the final crosslinking degree, an appropriate choice for this parameter is discussed first. Based on a chosen value, the molecular modelling method is validated by direct comparison of the time-dependent change of reactive groups with experimental results obtained by NIR. Furthermore, it is shown that the molecular modelling method is also applicable and predictive for modified material configurations. Therefore, crosslinking simulations are conducted for the investigated epoxy system with changed mixing ratios and are also compared to experimental NIR measurements. All simulations were carried out using a quadratic box with a side length of 60 Å and under periodic boundary conditions. All results show the average of 5 simulations and the degree of crosslinking is defined as the percentage of crosslinked epoxy groups (epoxy conversion).

4.1. Effect of cut-off distance

Crosslinking simulations were conducted for cut-off distances r_c of 2 Å, 4 Å, 6 Å, 8 Å and 10 Å to study the effect on the curing mechanism. Fig. 8 shows the degree of crosslinking as a function of time for the investigated cut-off radii, with error bars visualising the standard deviation of five simulations. A significant difference in the evolution of the epoxy conversion between the smallest cut-off radius of 2 Å and the larger radii (4 Å–10 Å) is identifiable. With cut-off distances larger then 2 Å a reaction partner is found in every crosslinking step within the first 0.5 ns. This results in a linear increase of the degree of crosslinking up to values between 62% for r_c = 4 Å and 86.5% for r_c = 10 Å. After the linear decrease, the reaction rate is significantly reduced, but not stopped. Still crosslinking occurs because of diffusion effects that lead to slow molecule movement and thus, new possible reaction partners can be found within r_c. The result for the smallest cut-off radius shows a significant slower increase in the degree of crosslinking, because of the distinct reduced probability of finding a reaction partner within r_c = 2 Å. After 3 ns the final degree of crosslinking has values of 48.5% for r_c = 2 Å and values between 84.2% and 94.8% for the larger cut-off values. For the two largest cut-off values of 8 Å and 10 Å, the degree of crosslinking can be interpreted as converged, as no change is observed within the last 0.5 ns. Fig. 8 shows that the maximum value of r_c = 10 Å lead to the most efficient crosslinking procedure, as the converged degree of crosslinking is reached within an reasonable time. Nevertheless, the results indicate that a high degree of crosslinking (> 90%) can be achieved by cut-off radii larger or equal then 4 Å with a respective increase of computational time. Furthermore it shows, that larger values(>10 Å) would not lead to an further increase in efficiency, as there is a negligible difference between the results obtained by values of r_c = 8 Å and r_c = 10 Å.

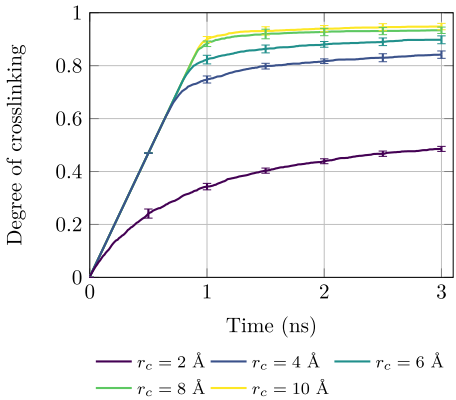

Fig. 8. Degree of epoxy conversion as a function of time for different cut-off radii, with error bars visualising the standard deviation.

For insights into the effect on the curing mechanism, the evolution of reactive amine groups for the r_c values investigated is shown in Fig. 9. The relative change of reactive amine groups as a function of the degree of crosslinking is presented by different symbols for each of the investigated cut-off radii. The results show a perfect agreement without an identifiable deviation in the curing mechanism for all cut-off values, with the only difference being the maximum degree of crosslinking that is reached within the defined time (3 ns). The maximum degree of crosslinking is shown with a dashed vertical lines for the respective values of r_c. Fig. 9 shows that the choice of r_c has no influence on the curing mechanism, but only on the efficiency i.e., the computational time needed to reach a desired degree of crosslinking. From the simulation results, shown in Fig. 8 and 9, it can be concluded that the curing process predicted by the present molecular modelling is not sensitive to the chosen cut-off value. However, a larger cut-off value provides us with higher efficiency without any difference in the curing mechanism and without any loss in accuracy.

However, for subsequently analysis of the physical material properties, it is crucial to ensure the polymer system to be in an equilibrated state. Fig. 10(a) shows the distribution of bond lengths of all crosslinks formed at the end of the crosslinking simulation. The equilibrium distance of newly formed bonds between hardener nitrogen atoms and epoxy carbon atoms has a value of r_{N-C} = 1.462 Å, indicated by a

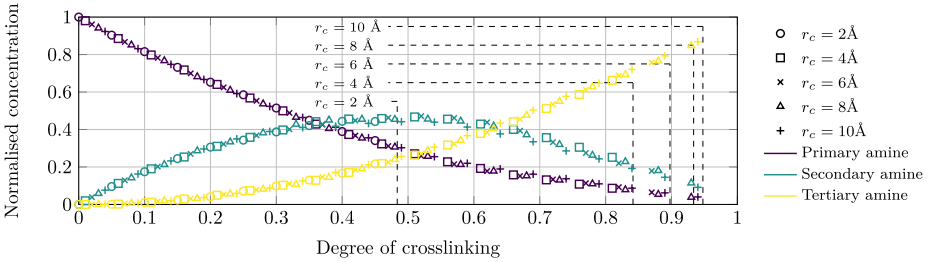

Fig. 9. Simulation results of the curing process in terms of the relative change of reactive amine groups as a function of the degree of crosslinking for all investigated values for r_c for the default mixing ratio of 100:31. Vertical dashed lines indicate the maximum degree of crosslinking for the respective values of r_c within the defined time of 3 ns.

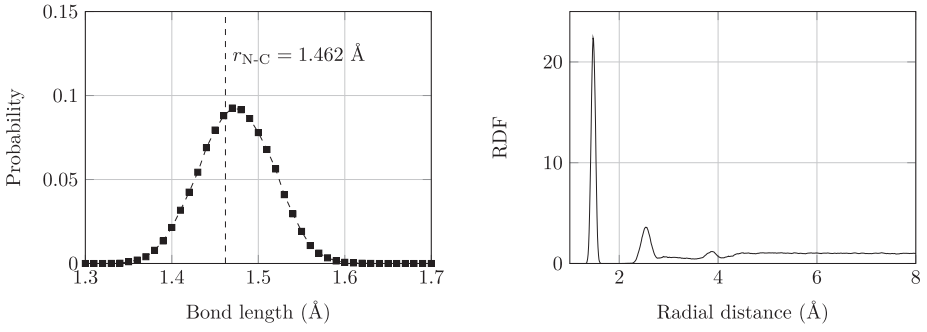

Fig. 10. Characteristics of the crosslinked system: (a) Distribution of bond length of newly formed crosslink bonds only (b) Radial distribution function of all nitrogen atoms to all other carbon atoms in the system.

vertical dashed line. The distribution of the bond length is in very good agreement and shows a reasonable distribution with its peak value very close to the equilibrium bond length. Fig. 10(b) shows the radial distribution function (RDF) of all nitrogen atoms to all other carbon atoms in the system. The RDF also depicts the main peak at the distance of the equilibrium bond length. Both results prove that the system is in a well equilibrated state and that all newly formed bonds, with initial bond lengths up to $r_c = 10$ Å, have reasonable bond lengths.

The investigation of the influence of the cut-off distance clearly shows that with the largest investigated cut-off value of $r_c = 10$ Å, a well equilibrated and fully crosslinked system can be achieved with a significant reduction of the simulation time, compared to lower values of the cut-off distance. These results show that a cut-off distance of $r_c = 10$ Å leads to the most efficient molecular modelling of a well equilibrated and fully crosslinked epoxy system. Therefore, this value is used for the following analysis and comparison of crosslinking simulation with NIR data.

4.2. Experimental validation using NIR measurements

As the time scales of the NIR-measured curing (≈ 5 h) and the molecular modelling method ($\approx 10^{-9}$ s) differ by magnitudes, a direct comparison of the time-dependent change of reactive groups is difficult. However, an analysis of the change of reactive groups relative to the degree of curing, specified by the decrease of unlinked epoxy groups, allows a time-independent comparison of the numerical method and the experimentally gained NIR data. Fig. 11 shows the curing results obtained by the NIR experiment (solid line) and the molecular modelling (dashed line). The final degree of crosslinking is comparable with values of ≈94% for the molecular modelling and a degree of crosslinking up to 100% for the NIR measurement, as it can be seen in Fig. 5(b). The general behaviour of the numerical results is in qualitatively good agreement with the experimental data. The strong reaction of primary to secondary amines without a reduction of unlinked epoxy groups observed in the NIR results is physically unlikely as it was explained in the NIR section. Considering this effect of the NIR measurement, caused by measurement inaccuracy and temperature dependency, the curves for the primary amines are shifted vertically and show a very good agreement. Furthermore, the peak value of the secondary amines is very well represented in the numerical results.

Beside the curing process of the epoxy system with the default mixing ratio, curing with shortage and excess of hardener were also investigated. The respective results are shown in Fig. 12. Fig. 12(a) shows the results for the mixing ratio with a shortage of hardener (100:15). The general qualitative curing behaviour is in fair agreement, although the strong reaction of primary to secondary amines at the beginning of the curing process without any reaction of epoxy groups leads to differences. These deviations decrease within the crosslinking process and the finally crosslinked system is in good agreement. An interpretation and explanation for this physically unlikely experimental data is given in the last paragraph of Section 2.4. The molecular modelling method yields a final degree of curing of 56%, which is close

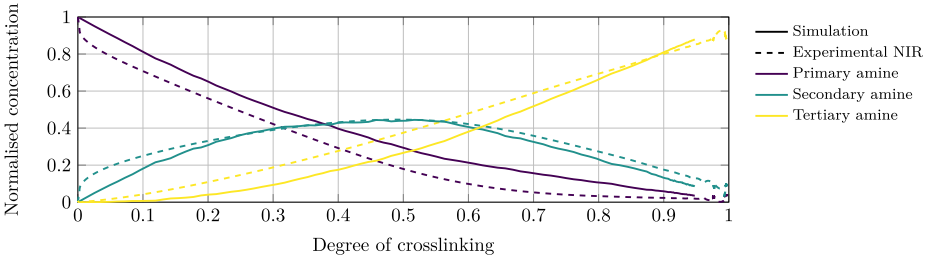

Fig. 11. Simulation and experimental results of the curing process in terms of the relative change of reactive amine groups as a function of the degree of crosslinking for the default mixing ratio of 100:31.

to the experimental degree of curing of 60% indicated by the NIR measurements. In both cases, all hardener has fully reacted to 100% tertiary amines, resulting in 0% of primary and secondary amines after the curing process. However, the molecular modelling is not able to cover the curing mechanism precisely compared to the results obtained with the default mixing ratio. Especially the asymptotic behaviour of tertiary amines, which lead to a plateau, is only poorly predicted. Fig. 12(b) shows the results for the mixing ratio with an excess of hardener (100:60). In both crosslinking procedures, the experimental and the molecular modelling method, a full reaction of all epoxy groups is achieved, since an excess of hardener is available. The results, which are shown in terms of normalised concentration of amine groups, are in good agreement with the NIR measurements.

4.3. Discussion

The present parameter study reveals the influence of the cut-off distance on the crosslinking mechanism and the final degree of curing with respect to the simulation time. It was shown that different cut-off distances do not change the qualitative evolution of reactive groups, but the overall time needed to reach a certain degree of crosslinking. The final choice of $r_c = 10$ Å results in an increase of efficiency without any loss of accuracy, as shown by the distribution of bond lengths. However, a further increase of the cut-off distance may lead to a long relaxation time in order to reach the equilibrium state.

Estridge [10] used MD for her research on competitive primary and secondary amine reactivity focussing on the structural evolution and derived material properties of an amine-cured epoxy system. The study points out that it is important to include an accurate kinetic crosslinking

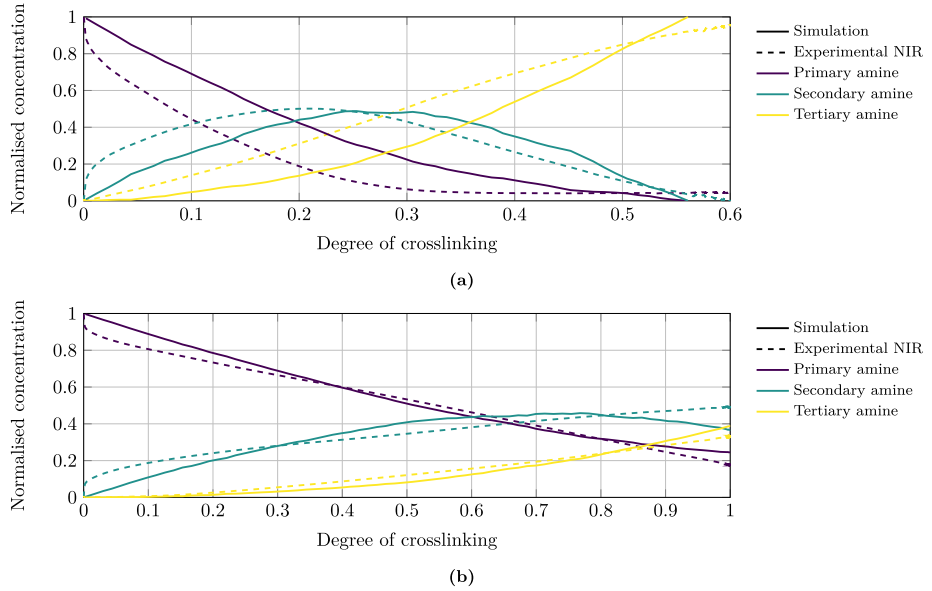

Fig. 12. Simulation and experimental results of the curing process in terms of the relative change of reactive amine groups as a function of the degree of crosslinking for the modified mixing ratios: (a) shortage of hardener (100:15) (b) excess of hardener (100:60).

mechanism, as it can have a significant effect on the material properties predicted. Nevertheless, no comparison or validation of the crosslinking kinetics were presented by Estridge [10], which makes it difficult to assess or define a specific reaction probability. The present comparison of the curing details of the molecular modelling method with experimental results of the in situ curing confirm the assumption that no specific reaction probability for the reaction from primary to secondary and from secondary to tertiary is needed to cover the realistic curing mechanism. The results underline that due to the steric effects and physical interactions, a reaction mechanism in close agreement with experimental results can be achieved. The focus of the present study is the experimental validation of the proposed molecular modelling of epoxy resin crosslinking. Research on the size of epoxy clusters or the behaviour of bond percolation was out of scope for the present study and interested readers are referred to [8,10–12].

The proposed molecular modelling method leads to results that are in good agreement with the experimental results for the default mixing ratio (100:31) and an excess of hardener (100:60) and to results that are still in fair agreement for the mixing ratio with a shortage of hardener (100:15). The main cause for the deviation between simulation and experimental results is the strong reaction of primary to secondary amines measured by NIR at the beginning of the curing process. However, this strong reaction does not correspond to the minor reaction of epoxy in the same time period. As already discussed in the NIR section, this effect must be interpreted as measurement inaccuracy as well as an unfiltered temperature influence on the signal intensity. The epoxy system considered with a shortage of hardener (100:15) consists of an increased quantity of high-molecular epoxy molecules. Compared to the other monomers, the main epoxy resin component Bisphenol A diglycidyl ether is a stiff and inflexible molecule. Thus the increased quantity of this molecule leads to a higher viscosity and less molecular movement in the system. This phenomenon influences the curing mechanism, as the low-molecular curing agents are disproportionately prevented to reach the reactive epoxy groups, which is related to a decrease in reaction evolution. The molecular modelling method cannot precisely cover this effect, since the artificial bond formation is not influenced by a changed viscosity. This explains the fair agreement of the results with a shortage of hardener (100:15) compared to the good agreement obtained for both other considered mixing ratios (100:31 and 100:60). Differences in the results may also arise from slightly different mixing ratios of epoxy and hardener components, for which the average value was chosen based on the specified range in the corresponding data sheets.

With the proposed method, a molecular modelling is presented that is validated against experimental results and transferable to other material systems or curing conditions. It allows us to investigate the influence of temperature or pressure on the curing process and thus helps to understand and predict curing mechanism of epoxy resins.

5. Conclusions

The curing procedure of thermosetting epoxy resins has an influence on the final network structure and thus on the material properties. Therefore, an accurate representation of the crosslinking process is crucial for understanding the underlying mechanism and deriving material properties with MD simulations.

We contributed to the challenge of generating realistic representations of the atomistic network structure of epoxy resins by presenting the first experimentally validated molecular modelling method for the crosslinking of epoxy resins. The method presented, which implements a step-wise bond formation based on the distance between reactive groups, is studied by applying it to a commercially available amine-cured epoxy system. Numerical studies on the curing process lead to a reasonable choice of $r_c = 10$ Å for the cut-off distance of the crosslinking algorithm in terms of efficiency and accuracy. The results of the parametric study show that this value decreases the simulation time significantly needed for a realistic crosslinking while still maintaining a well equilibrated system.

It was shown that NIR is a valuable analysis method for the characterisation of the curing process of epoxy systems, especially due to the possibility of identifying the time-dependent evolution of reactive groups. Experiments with three different mixing ratios were carried out for a validation of the molecular modelling method. Crosslinking simulations with the corresponding mixing ratios were conducted and a comparison to experimental NIR results showed that the fundamental curing mechanism is well represented. The present molecular modelling method provides a precise prediction of the chemical reactions and the corresponding evolution of reactive groups. Additionally, the final degree of curing is in good agreement with NIR results for the mixing ratios considered. This is achieved by considering only the inherent physical interactions and steric effects without specifying an explicit reaction probability for the different types of amine.

The proposed method enables material properties derived by MD simulations to be a reliable prediction, because the atomistic network structure is experimentally validated as a realistic representation of the cured polymer material. Moreover, the validated method allows us to gain deeper insights into the curing mechanism of epoxy resins. By deriving the influence of the curing process on the atomistic network structure, MD simulations effectively contribute to the virtual material development of thermosetting polymers by improving existing and designing new epoxy systems.

Funding

This work originates from the research project ‘Hybrid laminates and nanoparticle reinforced materials for improved rotor blade structures’ (‘LENAH – Lebensdauererhöhung und Leichtbauoptimierung durch nanomodifizierte und hybride Werkstoffsysteme im Rotorblatt’), funded by the Federal Ministry of Education and Research of Germany. The authors wish to express their gratitude for the financial support.

Competing interests

The authors declare that they have no competing interests.

Data availability

The raw/processed data required to reproduce these findings cannot be shared at this time as the data also forms part of an ongoing study.

CRediT authorship contribution statement

Robin Unger: Conceptualization, Data curation, Formal analysis, Investigation, Methodology, Software, Validation, Visualization, Writing - original draft, Writing - review & editing. **Ulrike Braun:** Data curation, Formal analysis, Investigation, Methodology, Validation, Writing - original draft, Writing - review & editing. **Johannes Fankhänel:** Conceptualization, Software, Validation, Writing - review & editing. **Benedikt Daum:** Conceptualization, Supervision, Validation, Writing - review & editing. **Behrouz Arash:** Supervision, Validation, Writing - review & editing. **Raimund Rolfes:** Funding acquisition, Project administration, Supervision, Writing - review & editing.

Acknowledgements

The authors would like to express special thanks to Hannah Quantrell who conducted the NIR results during her internship at the

Federal Institute for Materials Research and Testing. The authors acknowledge the support bythe LUIS scientific computing cluster, which is funded by Leibniz Universität Hannover, the Lower Saxony Ministry of Science and Culture (MWK) and the DFG.

References

[1] J.H. Hodgkin, G.P. Simon, R.J. Varley, Thermoplastic toughening of epoxy resins: a critical review, Polym. Adv. Technol. 9 (Jan. 1998) 3–10, https://doi.org/10.1002/(SICI)1099-1581(199801)9:1<3::AID-PAT727>3.0.CO;2-I.

[2] Matthew S. Radue, Benjamin D. Jensen, S. Gowtham, Danielle R. Klimek-McDonald, Julia A. King, and Gregory M. Odegard, "Comparing the mechanical response of di-, tri-, and tetra-functional resin epoxies with reactive molecular dynamics", in: Journal of Polymer Science Part B: Polymer Physics, Vol. 56 (Feb. 1, 2018), pp. 255–264, doi: https://doi.org/10.1002/polb.24539.

[3] D.C. Doherty, B.N. Holmes, P. Leung, R.B. Ross, "Polymerization molecular dynamics simulations. Cross-linked atomistic models for poly (methacrylate) networks", in: Computational and Theoretical Polymer Science, Vol. 8 (1998), pp. 169–178.

[4] Wu. Chaofu, Xu. Weijian, Atomistic molecular modelling of crosslinked epoxy resin, Polymer 47 (July 2006) 6004–6009, https://doi.org/10.1016/j.polymer.2006.06.025.

[5] Wu. Chaofu, Xu. Weijian, Atomistic molecular simulations of structure and dynamics of crosslinked epoxy resin, Polymer 48 (Sept. 2007) 5802–5812, https://doi.org/10.1016/j.polymer.2007.07.019.

[6] Irene Yarovsky, Evan Evans, Computer simulation of structure and properties of crosslinked polymers: application to epoxy resins, Polymer 43 (2002) 963–969.

[7] David R. Heine, Gary S. Grest, Christian D. Lorenz, Mesfin Tsige, Mark J. Stevens, Atomistic simulations of end-linked poly(dimethylsiloxane) networks: structure and relaxation, Ma cromolecules 37 (May 2004) 3857–3864, https://doi.org/10.1021/ma035760j 17 January 30, 2019.

[8] Vikas Varshney, Soumya S. Patnaik, Ajit K. Roy, Barry L. Farmer, "A Molecular Dynamics Study of Epoxy-Based Networks: Cross-Linking Procedure and Prediction of Molecular and Material Properties", in: Macromolecules Vol. 41 (Sept. 23, 2008), pp. 6837-6842, doi: 10.1021/ma801153e.

[9] Ananyo Bandyopadhyay, Pavan K. Valavala, Thomas C. Clancy, Kristopher E. Wise, Gregory M. Odegard, Molecular modeling of crosslinked epoxy polymers: the effect of crosslink density on thermomechanical properties, Polymer 52 (May 2011) 2445–2452, https://doi.org/10.1016/j.polymer.2011.03.052.

[10] Carla E. Estridge, The effects of competitive primary and secondary amine reactivity on the structural evolution and properties of an epoxy thermoset resin during cure: a molecular dynamics study, Polymer 141 (Apr. 2018) 12–20, https://doi.org/10.1016/j.polymer.2018.02.062.

[11] Shaorui Yang, Qu. Jianmin, Computing thermomechanical properties of crosslinked epoxy by molecular dynamic simulations, Polymer 53 (Sept. 2012) 4806–4817, https://doi.org/10.1016/j.polymer. 2012.08.045.

[12] Chunyu Li, Alejandro Strachan, "Molecular scale simulations on thermoset polymers: a review", in: Journal of Polymer Science Part B: Polymer Physics, Vol. 53 (Jan. 15, 2015), pp. 103–122, doi: https://doi.org/10.1002/polb.23489.

[13] Tomonaga Okabe, Yutaka Oya, Koichi Tanabe, Gota Kikugawa, Kenichi Yoshioka, Molecular dynamics simulation of crosslinked epoxy resins: curing and mechanical properties, Eur. Polymer J. 80 (July 2016) 78–88, https://doi.org/10.1016/j.eurpolymj.2016.04.019.

[14] Tomonaga Okabe, Tomohiro Takehara, Keisuke Inose, Noriyuki Hirano, Masaaki Nishikawa, Takuya Uehara, Curing reaction of epoxy resin composed of mixed base resin and curing agent: Experiments and molecular simulation, Polymer 54 (Aug. 2013) 4660–4668, https://doi.org/10.1016/j.polymer.2013. 06.026.

[15] Changwoon Jang, Thomas E. Lacy, Steven R. Gwaltney, Hossein Toghiani, Charles U. Pittman, "Relative Reactivity Volume Criterion for Cross-Linking: Application to Vinyl Ester Resin Molecular Dynamics Simulations", in: Macromolecules, Vol. 45 (June 12, 2012), pp. 4876–4885, doi: https://doi.org/10.1021/ma202754d.

[16] Chunyu Li, Alejandro Strachan, Molecular simulations of crosslinking process of thermosetting polymers, Polymer 51 (Nov. 2010) 6058–6070, https://doi.org/10.1016/j.polymer.2010.10.033.

[17] Chunyu Li, Alejandro Strachan, Molecular dynamics predictions of thermal and mechanical properties of thermoset polymer EPON862/DETDA, Polymer 52 (June 2011) 2920–2928, https://doi.org/10.1016/j.polymer.2011.04.041.

[18] Baris Demir, Tiffany R. Walsh, A robust and reproducible procedure for cross-linking thermoset polymers using molecular simulation, Soft Matter 12 (2016) 2453–2464, https://doi.org/10.1039/C5SM02788H.

[19] Joshua D. Monk, Justin B. Haskins, Charles W. Bauschlicher, John W. Lawson, Molecular dynamics simulations of phenolic resin: Construction of atomistic models, Polymer 62 (Apr. 2015) 39–49, https://doi.org/10.1016/j.polymer.2015.02.003.

[20] Joshua D. Monk, Eric W. Bucholz, Tane Boghozian, Shantanu Deshpande, Jay Schieber, Charles W. Bauschlicher, John W. Lawson, "Computational and Experimental Study of Phenolic Resins: Thermal-Mechanical Properties and the Role of Hydrogen Bonding", in: Macromolecules, Vol. 48 (Oct. 27, 2015), pp. 7670–7680, doi: https://doi.org/10.1021/acs.macromol.5b01183.

[21] Yasuyuki Shudo, Atsushi Izumi, Katsumi Hagita, Toshio Nakao, Mitsuhiro Shibayama, Large-scale molecular dynamics simulation of crosslinked phenolic resins using pseudo-reaction model, Polymer 103 (Oct. 2016) 261–276, https://doi.org/10.1016/j.polymer.2016.09.069.

[22] Atsushi Izumi, Toshio Nakao, Mitsuhiro Shibayama, "Atomistic molecular dynamics study of crosslinked phenolic resins", in: Soft Matter, Vol. 8 (2012), pp. 5283, doi: https://doi.org/10.1039/c2sm25067e.

[23] Nathan Sharp, Chunyu Li, Alejandro Strachan, Douglas Adams, R. Byron Pipes, "Effects of water on epoxy cure kinetics and glass transition temperature utilizing molecular dynamics simulations", in: Journal of Polymer Science Part B: Polymer Physics, Vol. 55 (Aug. 1, 2017), pp. 1150–1159, doi: https://doi.org/10.1002/polb.24357.18 January 30, 2019.

[24] Lik-ho Tam, Denvid Lau, Chao Wu, "Understanding interaction and dynamics of water molecules in the epoxy via molecular dynamics simulation", in: Molecular Simulation (Nov. 2018), pp. 1–9, doi: https://doi.org/10.1080/08927022.2018.1540869.

[25] Jihua Gou, Bob Minaie, Ben Wang, Zhiyong Liang, Chuck Zhang, Computational and experimental 616 study of interfacial bonding of single-walled nanotube reinforced composites, Comput. Mater. Sci. 31 (Nov. 2004) 225–236, https://doi.org/10.1016/j.commatsci.2004.03.002.

[26] Borja Coto, Ibai Antia, Javier Barriga, Miren Blanco, Jose-Ramon Sarasua, Influence of the geometrical properties of the carbon nanotubes on the interfacial behavior of epoxy/CNT composites: a molecular modelling approach, Comput. Mater. Sci. 79 (Nov. 2013) 99–104, https://doi.org/10.1016/j.commatsci.2013.05.057.

[27] Van Son Vo, Vu-Hieu Nguyen, Samia Mahouche-Chergui, Benjamin Carbonnier, Devis Di Tommaso, Salah Naili, From atomistic structure to thermodynamics and mechanical properties of epoxy/clay nanocomposites: investigation by molecular dynamics simulations, Comput. Mater. Sci. 139 (Nov. 2017) 191–201, https://doi.org/10.1016/j.commatsci.2017.07.024.

[28] Xueyu Song, Yi Sun, Wu. Xiaorong, Fanlin Zeng, Molecular dynamics simulation of a novel kind of polymer composite incorporated with polyhedral oligomeric silsesquioxane (POSS), Comput. Mater. Sci. 50 (Dec. 2011) 3282–3289, https://doi.org/10.1016/j.commatsci.2011.06.009.

[29] S. Neyertz, P. Brachet, D. Brown, F. Männle, The structure of amino-functionalized polyhedral oligomeric silsesquioxanes (POSS) studied by molecular dynamics simulations, Comput. Mater. Sci. 62 (Sept. 2012) 258–265, https://doi.org/10.1016/j.commatsci.2012.05.057.

[30] Surya D. Pandita, Liwei Wang, Ramani S. Mahendran, Venkata R. Machavaram, Muhammad S. Irfan, Dee Harris, Gerard F. Fernando, Simultaneous DSC-FTIR spectroscopy: comparison of cross-linking kinetics of an epoxy/amine resin system, Thermochim. Acta 543 (Sept. 2012) 9–17, https://doi.org/10.1016/j.tca.2012.04.024.

[31] E. Duemichen, M. Javdanitehran, M. Erdmann, V. Trappe, H. Sturm, U. Braun, G. Ziegmann, Analyzing the network formation and curing kinetics of epoxy resins by in situ near-infrared measurements with variable heating rates, Thermochim. Acta 616 (Sept. 2015) 49–60, https://doi.org/10.1016/j.tca.2015.08.008.

[32] Maren Erdmann, Volker Trappe, Heinz Sturm, Ulrike Braun, Erik Duemichen, Cure conversion of structural epoxies by cure state analysis and in situ cure kinetics using nondestructive NIR spectroscopy, Thermochim. Acta 650 (Apr. 2017) 8–17, https://doi.org/10.1016/j.tca.2017.01.010.

[33] Lutz Nasdala, Andreas Kempe, Raimund Rolfes, Are finite elements appropriate for use in molecular dynamic simulations? Compos. Sci. Technol. 72 (May 2012) 989–1000, https://doi.org/10.1016/j.compscitech.2012.03.008.

[34] Lutz Nasdala, Andreas Kempe, Raimund Rolfes, "The molecular dynamic finite element method (MDFEM)", in: Computers Materials and Continua, Vol. 19 (2010), p. 57.

[35] Lutz Nasdala, Andreas Kempe, Raimund Rolfes, "Molecular Dynamic Finite Element Method (MDFEM)", in: Computational Finite Element Methods in Nanotechnology, CRC Press, 2013, pp. 331–372.

[36] J. Fankhänel, D. Silbernagl, M. Ghasem Zadeh Khorasani, B. Daum, A. Kempe, H. Sturm, R. Rolfes, Mechanical properties of boehmite evaluated by atomic force microscopy experiments and molecular dynamic finite element simulations, J. Nanomater. 2016 (2016) 1–13, https://doi.org/10.1155/2016/5017213.

[37] M. Jux, J. Fankhänel, B. Daum, T. Mahrholz, M. Sinapius, R. Rolfes, Mechanical properties of epoxy/boehmite nanocomposites in dependency of mass fraction and surface modification – an experimental and numerical approach, Polymer 141 (Apr. 2018) 34–45, https://doi.org/10.1016/j.polymer.2018.02.059.

[38] Olin Epoxy AIRSTONE 886H Hardener, Material Safety Data Sheet, UPPC GmbH, Schemmenberger Str. 39, 88487 Mietingen-Baltringen, Germany, Apr. 4, 2011.

[39] Olin Epoxy AIRSTONE 880E Epoxy Resin, Material Safety Data Sheet, UPPC GmbH, Schemmenberger Str. 39, 88487 Mietingen-Baltringen, Germany, Apr. 4, 2011. 19 January 30, 2019.

[40] N. Poisson, G. Lachenal, H. Sautereau, Near-and mid-infrared spectroscopy studies of an epoxy reactive system, Vib. Spectrosc. 12 (1996) 237–247.

[41] Gilbert Lachenal, Alain Pierre, Nicolas Poisson, FT-NIR spectroscopy: trends and

application to the kinetic study of epoxy/triamine system (comparison with DSC and SEC results), Micron 27 (Oct. 1996) 329–334, https://doi.org/10.1016/S0968-4328(96)00022-4.
[42] Veronika Strehmel, Bildung und Struktur vernetzter temperaturstabiler polymerer Materialien, Martin Luther University of Halle-Wittenberg, Habilitation, Halle-Wittenberg, 2000.
[43] L. Martínez, R. Andrade, E.G. Birgin, J.M. Martínez, PACKMOL: a package for building initial configurations for molecular dynamics simulations, J. Comput. Chem. 30 (Oct. 2009) 2157–2164, https://doi.org/10.1002/jcc.21224.
[44] Noel M. O'Boyle, Michael Banck, Craig A. James, Chris Morley, Tim Vandermeersch, Geoffrey R. Hutchison, "Open Babel: an open chemical toolbox", in: Journal of Cheminformatics, Vol. 3 (2011), p. 33, doi: https://doi.org/10.1186/1758-2946-3-33.
[45] The Open Babel Package, version 2.3.1 http://openbabel.org.
[46] Jens Wackerfuß, "Molecular mechanics in the context of the finite element method", in: International Journal for Numerical Methods in Engineering, Vol. 77 (Feb. 12, 2009), pp. 969–997, doi: https://doi.org/10.1002/nme.2442.
[47] Stephen L. Mayo, Barry D. Olafson, William A. Goddard, DREIDING: a generic force field for molecular simulations, J. Phys. Chem. 94 (1990) 8897–8909.
[48] Simone Melchionna, Giovanni Ciccotti, Brad Lee Holian, "Hoover NPT dynamics for systems varying in shape and size", in: Molecular Physics, Vol. 78 (Feb. 20, 1993), pp. 533–544, doi: https://doi.org/10.1080/00268979300100371.

Chapter 4

Prediction of non-linear viscoelasticity of epoxy resins

4.1 Research context

Cured epoxy resins exhibit a temperature-dependent non-linear viscoelastic material response under loading. Accurate representation and prediction of this complex behaviour using molecular simulations are highly desirable for two main reasons. Firstly, simulations can be used to investigate nano-scale effects and derive an understanding of the physical mechanism occurring at the atomistic length scale. Secondly, molecular simulations can consistently be implemented into multi-scale frameworks and thus replace time- and cost-intensive experimental testing needed for the material characterisation. However, the significant difference in timescales is a huge challenge in predicting the material response and a direct determination of time-dependent material properties is not possible (see Section 5.1 and Figure 1.4 on page 8).
In the following publication, the challenge of bridging the timescales and predicting the viscoelasticity of epoxy resins over a broad range of strain rates and temperatures is met. Since the viscoelastic properties of polymers are related to the inter- and intramolecular mechanisms acting at atomistic length and timescale, molecular dynamics simulations at the nano-scale can be used to identify the parameters of viscoelastic theories. A comprehensive analysis of existing theories and their capabilities to predict the viscoelastic material behaviour over a broad range of temperatures and strain rates was missing in the current literature. The following publication is concerned with this challenge and presents a comparison and assessment of three models for the viscoelasticity of polymers, namely the Eyring model [24, 25], the Argon model [5–7] and the Cooperative model [30, 70]. Experimental validation on the predictive capabilities after parameter identification using purely molecular simulation data is provided.

4.2 Methods

The study on the predictive capabilities of the viscoelastic theories is based on molecular simulations that were performed by using the Large-scale Atomic/Molecular Massively Parallel Simulator (LAMMPS) [63]. The simu-

lation models were generated using the developed curing simulation presented in Chapter 3. The derived numerical data is used for identifying the parameters of the theories with an in-house implementation of a grid search optimisation algorithm. With the calibrated theories an extrapolation to experimental timescales is performed and validated with experimental tensile test results. Therefore, tensile tests at the default test configuration (DIN EN ISO 527) at differing temperatures and strain rates were conducted by the Institute of Composite Structures and Adaptive Systems of the German Aerospace Center (DLR).

4.3 Results and outlook

The presented experimental validation confirms that a successful prediction of viscoelastic properties is possible based on purely molecular simulation data. The calibrated Argon model can be used to extrapolate over a huge range of timescales in good agreement with experimental results. An acceptable agreement was found for the calibrated Eyring model, whereas the Cooperative model does not lead to reasonable results after calibration. The results emphasise that the underlying nano scale physics of viscoelasticity are covered by the molecular simulations. The publication is a contribution to the challenge of bridging the different timescales between MD (nanoseconds) and experiments (seconds to hours) concerning the viscoelasticity of cross-linked epoxy resins. Furthermore, it underlines the capabilities of the Argon model in the context of constitutive multi-scale approaches for an accurate representation of viscoelasticity of cross-linked epoxy resins.

4.4 Paper B: Non-linear viscoelasticity of epoxy resins: Molecular simulation-based prediction and experimental validation

The following paper is published in Polymer, Volume 180, October 2019.

Author contribution statement:

The main work was done by the author of this thesis. Wibke Exner contributed the experimental tensile tests and reviewed the corresponding paragraphs. Behrouz Arash contributed with conceptualisation, advisory and supporting work. Raimund Rolfes contributed with advisory and supporting work.

Graphical Abstract

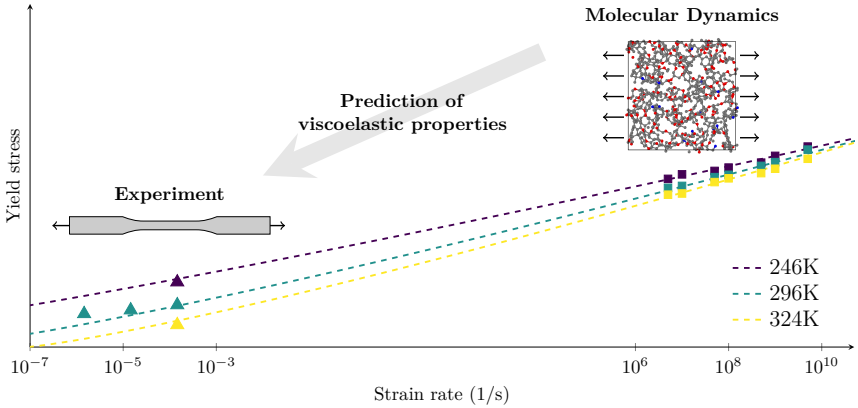

Polymer 180 (2019) 121722

Contents lists available at ScienceDirect

Polymer

journal homepage: www.elsevier.com/locate/polymer

Non-linear viscoelasticity of epoxy resins: Molecular simulation-based prediction and experimental validation

Robin Unger[a,*], Wibke Exner[b], Behrouz Arash[a], Raimund Rolfes[a]

[a] Institute of Structural Analysis, Leibniz Universität Hannover, Appelstraße 9A, 30167, Hannover, Germany
[b] Institute of Composite Structures and Adaptive Systems, DLR (German Aerospace Center), Lilienthalplatz 7, Braunschweig, 38108, Germany

HIGHLIGHTS

- Theories for the viscoelasticity of polymers are calibrated using molecular simulation results.
- The effect of temperature and strain rates on the yield stress is analysed.
- A prediction of yield stress at experimental time scales is presented and evaluated.
- The Argon model describes the underlying nanoscale physics of viscoelasticity in good agreement with experimental results.

ARTICLE INFO

Keywords:
Epoxy resin
Non-linear viscoelasticity
Molecular dynamics
Experimental validation

ABSTRACT

The precise knowledge of the temperature-dependent non-linear viscoelastic material behaviour of polymers is of great importance for engineering applications. The present work is a contribution to meet the challenge of bridging the inherently different time scales of molecular dynamics (MD) and experiments by providing a consistent comparison and assessment of viscoelastic theories. For this reason, the physically motivated theories for viscoelasticity of Eyring and Argon as well as the Cooperative model are evaluated with regard to their predictive capability for the characteris7ation of the viscous behaviour over a broad range of temperatures and strain rates. MD simulations of tensile tests are performed and the effect of strain rate and temperature on the yield stress is examined. The distinctive feature of this study is to demonstrate that viscoelastic theories can be successfully calibrated using only MD results. For a comparison to experimental data, we conduct tensile tests at three different strain rates and at three temperatures in the glassy regime. Experimental validation confirms the predictive capability of the Argon model, which can provide an accurate formulation of epoxy viscoelasticity for physically motivated constitutive models. The present study not only underlines the ability of MD simulations for identifying and characterising physical phenomena on the molecular level, but also shows that molecular simulations can substitute experimental tests for the characterisation of the viscoelastic material behaviour of polymers.

1. Introduction

Highly cross-linked epoxy resins are of great interest for engineering applications that demand a light-weight but high-performance polymer matrix, such as aircraft structures and wind turbine rotor blades. The macroscopic material properties are the result of the underlying microstructure, which can be tailored by modifying the chemical composition or mixing ratio. An accurate material characterisation is of great importance for the dimensioning of structures in industrial applications made of polymers [1]. This includes the experimental derivation of the time- and temperature-dependent material behaviour, which is relevant for applications in a broad range of temperatures (aerospace structures) or under complex load conditions at varying strain rates (rotor blades). A full characterisation of viscoelastic materials is, however, time- and cost-consuming as extensive experimental tests are required. Furthermore, it is difficult to obtain information about the underlying mechanism of macroscopic phenomena that is related to nanoscale physics.

Molecular dynamics (MD) simulations for material research can supplement experimental studies leading to a more comprehensive analysis of material behaviour [2]. Many studies have been conducted on the challenge of deriving thermo-mechanical properties of bulk polymers [3,4] and nanoparticle reinforced polymer composites [5,6]. Results obtained by MD simulations can also be used within a

* Corresponding author.
E-mail address: r.unger@isd.uni-hannover.de (R. Unger).

https://doi.org/10.1016/j.polymer.2019.121722
Received 9 July 2019; Received in revised form 12 August 2019; Accepted 17 August 2019
Available online 22 August 2019
0032-3861/

multiscale framework in order to calibrate constitute models used on larger length scales [7]. Furthermore, simulations can be utilised to get insights into nanoscale effects and generate an understanding of the underlying mechanisms of action, which occur at length scales that are examinable by MD [8,9]. It is generally agreed that a direct determination of time-dependent material properties from MD simulations is not possible, as the feasible time in MD simulations ranges in the order of nanoseconds. This important challenge of overcoming the significant differences of time scales can be achieved by utilising theories for the viscoelasticity of polymers. MD simulation results can be used to calibrate these theories by identifying parameters and thus enable the prediction of the viscoelastic material response at experimental strain rates.

One fundamental theory for the viscosity of polymers was presented by Eyring [10], with the concept of viscoelasticity being a thermally activated rate process. The Eyring formulation of viscosity was originally derived from the transition state theory, which describes the reaction rates of elementary chemical reactions [11]. The macroscopic yielding is understood as the viscous plastic flow of polymer chains between adjacent equilibrium states, moving in the direction of minimum potential energy. Ree et al. [12–14] formulated a further enhanced Ree-Eyring formulation that includes two rate processes for high-stress/low-temperature and low-stress/high-temperature behaviour, respectively. Bauwens et al. [15] and Bauwens-Crowet et al. [16,17] presented an experimental study on the tensile behaviour of glassy polymers, in which the Eyring model was able to describe the yield stress behaviour well for temperatures larger than a characteristic material-dependent temperature. The Ree-Eyring theory showed an excellent fit without any observable temperature limitation, confirming the assumption that more than one rate process is involved. Subsequent studies showed that the Eyring theory can predict the yield behaviour of polymers in acceptable agreement to experimental data within certain temperature ranges [18,19].

Fotheringham et al. [20,21] presented the cooperative model by modifying the Ree-Eyring theory by two aspects. Firstly, an internal stress is added, which describes inherent structural defects either from the load or temperature history. Secondly, the model assumes a cooperative movement of several polymer segments involving a certain number of elementary transitions. In contrast to the Ree-Eyring model, which explicitly considers two elementary transitions, the cooperative model uses a parameter to depict the number of elementary transitions. Richeton et al. [22,23] extended the cooperative model for temperatures above the glass transition temperature, leading to a unique model with very good agreement over a broad range of strain rates and temperatures after calibration with experimental data.

Similar theories were presented by Argon [24,25] and Robertson [26], both focussing on a macroscopic representation of the molecule movement at the atomistic length scale. Argon stated that the intermolecular resistance against the formation of molecule kinks interferes the chain rearrangement. A corresponding energy barrier (activation energy) was derived and used in the context of the Eyring theory. Cook et al. [27] presented a reasonable fit of the Argon model for the yield stress under uniaxial loading of different epoxy polymers for low temperatures. However, the calibrated model showed a deviation for high temperatures, which is in line with results published by Brooks et al. [28] and Richeton et al. [23]. The Argon model was enhanced by Boyce et al. [29] to take the effect of hydrostatic pressure into account and was incorporated into the widely known Arruda-Boyce model [30,31]. Poulain et al. [32] used the Argon theory to model the viscoelastic deformation behaviour of a highly cross-linked epoxy system in good agreement to experimental results. As opposed to the Argon theory, the Robertson theory considers the intramolecular resistance against deformation as the main resistance against deformation. The work done by externally applied stress or strain is considered to be equal to the energy needed to change the rotational conformations from the low energy *trans* state to the high energy *cis* state. Duckett et al. [33] enhanced the Robertson model to include the effect of hydrostatic pressure, leading to a good agreement of tension and compression yield data to experiments.

Existing literature gives strong evidence that, in general, MD can be used for a prediction of viscoelastic material properties of thermosetting polymers. Arash et al. [7] used the Eyring model as part of a multiscale viscoelastic damage model for nanoparticle/epoxy nanocomposites. The Eyring model was calibrated using MD simulations and led to a viscoelastic material behaviour consistent with experimental results at room temperature. Park et al. [34] calibrated the Ree-Eyring model using yield stresses at different temperatures obtained by MD simulation. An experimental validation showed that the predicted quasi static yield was in acceptable agreement for temperatures in the glassy regime. The Argon model was also successfully implemented into a multiscale model for the thermo-plastic material behaviour of an epoxy system in the glassy regime [35]. MD simulation data was used to extrapolate the yield stress to quasi static strain rates for different temperatures and the prediction was validated by experimental results. However, a comprehensive study on the capabilities of the available theories is desirable to underline the potential and to show limitations of MD simulations in this context. A direct comparison of physically based theories over a wide range of temperatures and strain rates is still missing in the literature.

The innovative nature of the present study is to meet this challenge by presenting a consistent analysis with a comparison and assessment of existing theories and their capabilities to predict the viscoelastic material behaviour over a broad range of temperatures and strain rates. The present approach underlines that existing theories calibrated only by MD simulation data obtained at high strain rates can successfully bridge the difference between MD and experimental time scales. The viscoelastic properties of polymers are related to the inter- and intramolecular mechanisms acting at atomistic length and time scale (i.e. molecular chain sliding and rearrangement) as it will be presented in the following section. Therefore, molecular dynamic simulations at the nanoscale in conjunction with viscoelastic theories are sufficient to predict the viscoelastic material behaviour, since the underlying mechanism are covered by the simulation. To prove this, an experimental validation is included using tensile test results obtained at a range of strain rates and temperatures to underline the capabilities of molecular simulation. The current study can help to enhance physically motivated constitute models, by providing new insights into the nanoscale mechanism. This meets the demand of molecular simulation-guided constitutive modelling requiring a reliable prediction of the viscoelasticity [7,36]. An industrially available epoxy resin is used and realistic simulation models are assured by use of an experimentally validated molecular modelling. The scope of the present work is limited to theories, which are physically motivated and consist of parameters that can be related to physical properties. For an overview of pure phenomenological theories, the reader is referred to Voyiadjis et al. [37]. Derivation of elastic material properties is not part of the present investigation, as this aspect has already been extensively discussed in literature [2,6,38].

2. The viscoelastic nature of polymers

The viscoelastic deformation of a polymer is the result of inter- and intramolecular movement or deformation of molecule segments. Starting from such an atomistic perspective of viscoelasticity, physically motivated and phenomenological theories were developed to describe the viscous flow as a function of external properties such as stress and temperature. The scope of the present study is limited to physically based theories, as these can be used to extrapolate the viscoelastic behaviour of polymers under loading after careful calibration. In the following, an overview of related theories is provided, comprising the Eyring theory, the Cooperative model and the Argon theory. All these formulations share their motivation that the viscoelastic material

behaviour results from molecule arrangement. In Section 4, the theories presented are applied to simulation results by using the yield stress for parameter identification.

2.1. Eyring theory

Eyring [11] presented a theory of viscosity, derived from the transition state theory (TST), which describes the reaction rates of elementary chemical reactions. The TST assumes that an activated complex exits at a higher energy level along the reaction coordinate, as illustrated in 1. To overcome this energy barrier, also called the transition state between reactants and products, additional activation energy is required, although the reaction is exothermic. The TST can be used to calculate the reaction rates at which two reactants react to an energetic favourable equilibrium state.

Based on the original concept of the TST, the viscoelasticity is assumed to be a thermally activated rate process [10,39,40]. The rate process represents the viscous flow and the macroscopic deformation is the result of molecule movement in the direction of energetically favourable equilibrium states. Externally applied stress or strain allows a molecule rearrangement to a more energy-efficient state by providing the necessary activation energy to overcome the energy barrier. Consequentially, the Eyring model was formulated that can describe the basic phenomena of viscoelasticity with inherent non-linearity. Derived from the transition state theory, the strain rate $\dot{\varepsilon}$ is defined by:

$$\frac{\mathrm{d}\varepsilon}{\mathrm{d}t} = \dot{\varepsilon} = \dot{\varepsilon_0}^{E} \exp\left(-\frac{\Delta H^E}{kT}\right)\sinh\left(\frac{\sigma V^E}{kT}\right) \tag{1}$$

The temperature is denoted as T, k is the Boltzmann constant and σ is the external stress (see Fig. 1). The parameters ΔH and V express the activation energy and volume respectively, and $\dot{\varepsilon_0}$ is a pre-exponential factor describing the frequency of molecule arrangements to an energetically favourable state. The superscript ^{E} is used for all parameters of the Eyring model. Fig. 2 visualises the concept of the Eyring viscosity with σV being the energy difference in the direction of flow due to the externally applied stress.

Expressing the hyperbolic sine in terms of the difference of exponentials leads to:

$$\dot{\varepsilon} = \dot{\varepsilon}_0^E \exp\left(-\frac{\Delta H^E}{kT}\right)\frac{1}{2}\left[\exp\left(\frac{\sigma V^E}{kT}\right) - \exp\left(-\frac{\sigma V^E}{kT}\right)\right] \tag{2}$$

The last term is assumed to be negligible, as it vanishes for increasing stress values, which leads to an explicit formulation in terms of strain and stress:

$$\dot{\varepsilon} = \frac{\dot{\varepsilon_0}^E}{2} \exp\left(-\frac{\Delta H^E - \sigma V^E}{kT}\right) \tag{3}$$

$$\sigma = \frac{kT}{V^E}\left(\ln\frac{2\dot{\varepsilon}}{\dot{\varepsilon_0}^E} + \frac{\Delta H^E}{kT}\right) \tag{4}$$

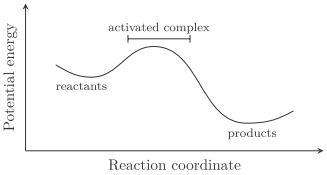

Fig. 1. Energy profile along the reaction coordinate based on the transition state theory.

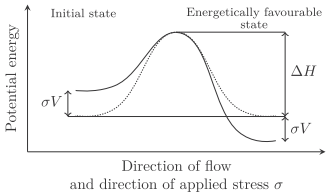

Fig. 2. Energy profile in the direction of flow with (solid line) and without (dashed line) externally applied stress, based on the Eyring theory of viscosity.

2.2. Cooperative model

Experimental results reveal the general phenomena that the viscoelastic behaviour is not strictly proportional to the strain rate or temperature. The variation of the yield stress is larger at high strain rates or low temperatures than at low strain rates or high temperatures. The Eyring model is not capable of describing this non-linearity in terms of strain rate and temperature, as it represents the viscoelastic response as a result of only one rate process. This leads to an enhanced formulation, based on the Ree-Eyring theory, by Ree et al. [12–14]. The Ree-Eyring model consists of two activation processes (α and β) and the prediction of yield stress is given by:

$$\frac{\sigma_y}{T} = \dot{\varepsilon}_{0,\alpha}^{RE}\left[\ln\dot{\varepsilon} + \frac{\Delta H_\alpha^{RE}}{kT}\right] + \dot{\varepsilon}_{0,\beta}^{RE}\sinh^{-1}\left[\dot{\varepsilon}\exp\left(\frac{\Delta H_\beta^{RE}}{kT}\right)\right] \tag{5}$$

The α process represents the behaviour at low strain rates and high temperatures, whereas the β process refers to high strain rates and low temperatures. The supercript $^{\mathrm{RE}}$ indicated parameters of the Ree-Eyring model.

With two independent rate processes, the Ree-Eyring theory showed a good agreement to experimental data, especially at low temperatures for which an identifiable non-linear increase in yield stress with respect to decreasing temperature is observable. The overproportional increase of yield stress is covered by the Ree-Eyring model due to the β process. However, a more generalised formulation with an unknown number n of elementary transitions was presented with the cooperative model by Fotheringham et al. [20,21]. It extended the Eyring model based on two main assumptions. Firstly, it was assumed that several molecule segments move cooperatively, so that n elementary transitions must be taken into account. Secondly, an internal stress σ_i was assumed to exist dependent on temperature. The strain rate of the cooperative model is given by:

$$\dot{\varepsilon} = \dot{\varepsilon_0}^{C}\exp\left(-\frac{\Delta H^C}{kT}\right)\sinh^n\left(\frac{V^C(\sigma - \sigma_i(T))}{kT}\right) \tag{6}$$

The hyperbolic sine function is raised to an n-th power indicating that an unknown number n of elementary transitions occurs cooperatively. The internal stress σ_i is the sum of a constant $\sigma_i(0)$ and a temperature-dependent part of the internal stress:

$$\sigma_i(T) = \sigma_i(0) - mT \tag{7}$$

Here, m is a material parameter and $\sigma_i(0)$ is a constant stress at zero Kelvin. The superscript ^{C} is used for the parameters of the Cooperative model.

Richeton et al. [22,23] formulated the cooperative model consistent with the time-temperature superposition principle proposed by Bauwens et al., leading to a formulation for the yield stress:

$$\sigma_y = \sigma_i(0) - mT + \frac{2kT}{V^C}\sinh^{-1}\left(\frac{\dot{\varepsilon}}{\dot{\varepsilon_0}^C\exp\left(-\frac{\Delta H^C}{kT}\right)}\right)^{\frac{1}{n}} \tag{8}$$

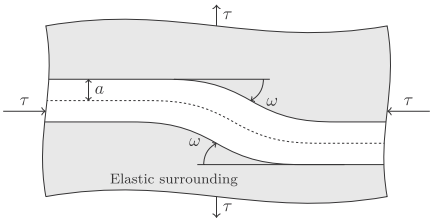

Fig. 3. Basic process of molecular chain deformation based on the Argon model of viscoelasticity.

Furthermore, an extension to temperatures above the glass transition temperature was proposed and it was shown that the parameters of the cooperative model can be related to the parameters of the α and β processes of the Ree-Eyring model [22].

2.3. Argon theory

A theory for the viscoelastic deformation of polymers, physically motivated by the intermolecular resistance against the formation of a pair of molecule kinks, was presented by Argon [24,25]. The underlying process of deformation at a molecular scale is shown in Fig. 3.

Under shear loading, a polymer molecule with a radius of a is assumed to deform with pairwise kinks with an angle of ω. The resistance against this deformation arises from the elastic interactions with its neighbouring polymer molecules. The intermolecular energy change (i.e. the activation energy) for a pair of kinks is calculated using the theory of disclinations developed by Li et al. [41]. The activation energy ΔH^A increases with increasing shear stress τ and is given as:

$$\Delta H^A = \frac{3\pi G\omega^2 a^3}{16(1-\nu)}\left[1 - 6.75(1-\nu)^{\frac{5}{6}}\left(\frac{\tau}{G}\right)^{\frac{5}{6}}\right] \tag{9}$$

The activation energy depends on the elastic properties, G is the shear modulus and ν is the Poisson ratio, and geometrical properties with the molecule kink angle ω and the molecule radius a. With this explicit definition of the activation energy, Argon follows the theory of Eyring that the viscous flow is a thermally activated process to account for the shear rate dependency:

$$\dot{\gamma} = \dot{\gamma_0^A}\exp\left(-\frac{\Delta H^A}{kT}\right) \tag{10}$$

The superscript ^{A} denotes the parameters of the Argon theory. Although the theory was originally formulated for shear stress, strong evidence can be found that it is also applicable to uniaxial loading [23,27,28,32,35,42]. Combining equations (9) and (10) leads to an explicit expression for the (uniaxial) strain rate and stress:

$$\dot{\varepsilon} = \dot{\varepsilon_0^A}\exp\left(-\frac{3\pi G\omega^2 a^3}{16(1-\nu)kT}\left[1 - 6.75(1-\nu)^{\frac{5}{6}}\left(\frac{\sigma}{G}\right)^{\frac{5}{6}}\right]\right) \tag{11}$$

$$\sigma = \frac{0.102G}{1-\nu}\left[1 - \frac{16(1-\nu)}{3\pi G\omega^2 a^3}kT\ln\left(\frac{\dot{\varepsilon_0^A}}{\dot{\varepsilon}}\right)\right]^{\frac{6}{5}} \tag{12}$$

A reduction to three unknown is possible leading to a formulation with an athermal yield stress σ_0^A and an equivalent activation energy ΔH^A.

$$\sigma = \sigma_0^A\left[1 - \frac{kT}{\Delta H^A}\ln\left(\frac{\dot{\varepsilon_0^A}}{\dot{\varepsilon}}\right)\right]^{\frac{6}{5}} \tag{13}$$

The close similarity to the Eyring model can be seen by eliminating the outer brackets and substituting the athermal yield stress by $\frac{\Delta H^A}{V^A}$, with V^A being the equivalent activation energy in terms of the Eyring model.

Table 1
Overview of the chemical composition of the epoxy system (names, mixing ratios and CAS identification numbers). Corresponding chemical structures are shown in Fig. 4.

	Name	Parts (wt%)	CAS-No.
Resin (AIRSTONE 880E)	Bisphenol A diglycidyl ether	75 – 100	25068-38-6
	1,4-Butanediol diglycidyl ether	10 – 25	2425-79-8
	Alkyl (C12–C14) glycidyl ether	1 – 5	68609-97-2
Hardener (AIRSTONE 886H)	α,ω-poly(oxypropylene)diamine	50 – 75	9046-10-0
	3-(aminomethyl)-3,5,5-trimethyl-cyclohexanamine	25 – 50	2855-13-2
	2,4,6-tris[(dimethylamino) methyl]phenol	1 – 5	90-72-2

3. Material and methods

3.1. Material system

The epoxy system chosen for the presented study is a commercially available amine-cured epoxy system from Olin Epoxy, namely the epoxy resin of type AIRSTONE 880E and the hardener of type AIRSTONE 886H. The AIRSTONE epoxy system is a low-viscosity infusion system tailored for the infusion process of large and thick composite parts, such as wind turbine blades. Table 1 gives an overview of the chemical composition with the corresponding chemical structures shown in Fig. 4. The mixing ratio by weight is specified by 100 parts epoxy to 31 parts hardener. The cured epoxy system has a density of 1.1 g/cc and a glass transition temperature of 82 °C. All information is taken from the material data sheets [43,44].

3.2. Molecular dynamics

3.2.1. Molecular modelling

An accurate molecular modelling procedure is essential in order to obtain a realistic representation of the cured epoxy system, which is crucial for a reliable derivation of the material properties [45–48]. The molecular modelling applied is implemented in the Molecular Dynamics Finite Element Method (MDFEM) framework [49–51] and was experimentally validated for the used epoxy system [52]. For the model generation, the third chemical component of both the epoxy and the hardener is neglected, as the weight fraction is less than five percent. Each of the considered resin and hardener molecules consists of two reactive sites, which are the epoxy end groups for the resin molecules and the amine groups (NH_2) for the hardener molecules. The main chemical reaction, leading to the final network topology is the reaction of the amine group (NH_2) with an epoxy group. Each amine group can react with two epoxy groups, whereas the epoxy groups can only react with one reactive amine group. No reaction of hydroxy groups with epoxy groups (etherification) is considered, as it was experimentally shown that this reaction is not part of the curing mechanism. The cross-linking procedure follows the common approach to use the distance between two reactive groups as the criterion for bond formation. The initial simulation box is generated by randomly distributing the unlinked molecules and applying an energy minimisation. The pre-processing implements the open source packages PACKMOL [53] and Open Babel [54]. This simulation box, representing the uncured and liquid epoxy system, is used for the simulation of the cross-linking procedure by use of the MDFEM framework with the following steps:

(1) Initial equilibration within 500 ps under NPT ensemble, combined with a linear increase of temperature to the curing temperature (80 °C);

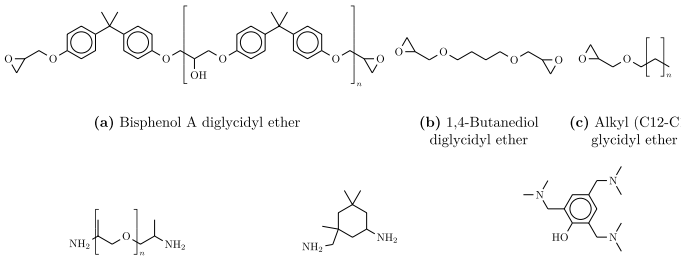

(a) Bisphenol A diglycidyl ether

(b) 1,4-Butanediol diglycidyl ether

(c) Alkyl (C12-C14) glycidyl ether

(d) α,ω-poly(oxypropylene)diamine

(e) 3-(aminomethyl)-3,5,5-trimethyl-cyclohexanamine

(f) 2,4,6-tris[(dimethylamino)methyl]phenol

Fig. 4. Chemical structures of all molecules of the studied epoxy system: (a)–(c) chemical components of the epoxy resin, (d)–(f) chemical components of the hardener.

(2) Distances between all possible reactive groups are calculated; all reaction distances larger than the chosen cut-off of 10 Å for the reaction distance are discarded and the bond with the smallest reaction distance is formed;
(3) Equilibration of the system for a time period of 2.5 ps ;
(4) Repeat step 2 and 3 until the end of overall simulation time is reached.

The respective parameters (duration of equilibration and cut-off) were chosen with respect to efficiency while maintaining a well equilibrated system [52]. The DREIDING force field in its form published by Mayo et al. [55] is used. In all steps, the harmonic potentials are used for the bonded interactions and the Morse potential is applied for non-bonded interactions. As the cut-off distance is significantly larger than the equilibrium distance, the large initial bond forces can lead to unreasonable oscillation in the global potential energy of the system and to diverging simulations. To avoid this issue, the harmonic bond potential of newly created cross-links was linearly activated within 0.1 ps after bond formation. An isothermal–isobaric ensemble (NPT) with atmospheric external pressure is used with a time step size of 1 fs. The box temperature and pressure is controlled by a Nosé-Hoover thermostat and a Parrinello-Rahman barostat [56]. The overall simulation time of the cross-linking procedure is 4 ns and three-dimensional periodic boundary conditions are applied allowing bond formation across box boundaries.

3.2.2. Tensile simulation

To characterise the mechanical response of the system, the Large-scale Atomic/Molecular Massively Parallel Simulator (LAMMPS) [57] is used to perform tensile tests. An isothermal-isobaric ensemble (NPT) with Nose-Hoover thermostat and barostat is used with a strain rate-dependent time step size. The DREIDING force field is used with the Morse potential for the bonded interactions and the harmonic potentials for the angle and dihedral interactions. The Morse potential was chosen to take the non-linear increase of the bond force into account for large bond lengths. The non-bonded interactions are calculated using the Lennard-Jones (12,6) potential with neighbour updating and a cut-off value of 15Å. Each of the four cross-linked simulation models was used for a tensile test in all three directions, resulting in twelve independent simulation results that will be used for the analysis. The tensile deformation is applied by increasing the box length in the tensile direction at a constant strain rate and remapping the atom coordinates in every time step accordingly. The pressures in the lateral directions, perpendicular to the tensile direction, are controlled at zero to allow for the natural Poisson contraction. Periodic boundary conditions are applied along all directions. To ensure comparability over different strain rates, it is important to use a constant output frequency in terms of strain instead of absolute time or time steps. Otherwise, only a very small number of output data is available for the fastest strain rate, which affects the derived material properties. For the present study, a constant output frequency of $\Delta\varepsilon = 10^{-4}$ was chosen, which means that one output is written at every strain increase of $\Delta\varepsilon$. To fulfil this requirement, it is necessary to reduce the time step size to values as low as 0.02 fs for the highest strain rate of 5×10^9 1/s, whereas the maximum time step size is limited to 1 fs. Table 2 gives an overview of the applied time step sizes for the investigated strain rates.

3.3. Experiments

3.3.1. Manufacturing

The epoxy resin considered in this work is presented in detail in Section 3.1 and was mixed according to the manufacturer's guideline with a mixing ratio between epoxy and hardener of 100: 31 in weight. After a short de-gassing process at room temperature, the mixture was poured into a mould. The resin plates with a thickness of 2.7 mm (Fig. 5 (a)) were cured at 80° C for 5 h. Test specimens were cut to standardized dog-bone shape according to DIN EN ISO 527 with a CNC milling machine (Fig. 5 (b)). Fig. 6 shows the specimen geometry with an overall length of 230 mm and a thickness of 2.7 mm. The exact width and thickness of each specimen was measured at three cross-sections in the narrow dog-bone regime (indicated by dashed lines in Fig. 6) and the average cross-sectional area was used for the stress calculation.

3.3.2. Mechanical tests

Tensile tests were conducted according to DIN EN ISO 527 using a Zwick 1481 electromechanical universal axial testing machine and the strain was measured by an extensometer of type MTS 776. Tensile tests

Table 2
Time step sizes for the investigated strain rates, based on a constant output frequency in terms of strain with a value of $\Delta\varepsilon = 10^{-4}$.

Strain rate (1/s)	Time step size (fs)
$\dot{\varepsilon}$	Δt
5×10^9	0.02
1×10^9	0.1
5×10^8	0.2
1×10^8	1.0
5×10^7	1.0
1×10^7	1.0
5×10^6	1.0

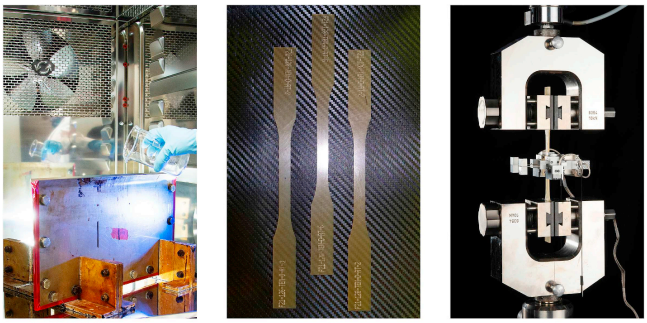

(a) (b) (c)

Fig. 5. Experimental procedure: (a) Manufacturing using molding process, (b) Dog-bone test specimen prepared for testing, (c) Tensile test with extensometer until failure.

until failure (Fig. 6 (c)) were conducted at standard laboratory conditions (23° C and 50% humidity) at three different test speeds of 0.01 mm/min, 0.1 mm/min and 1 mm/min. Experiments at significantly larger test speeds were not conducted as it is difficult to obtain reliable results for an analysis of the strain rate effect. The reason is that it is challenging to assure a constant strain rate for tensile tests with a duration until failure ranging in the order of seconds. To study the effect of temperature, two additional configurations were tested at a higher temperature of 53°C and a lower temperature of − 27°C, both with the standardized test speed of 1 mm/min and 50% relative humidity. For these two configurations, the test machine was heated up or cooled down (with nitrogen cooling) to the target temperature and kept constant for at least 30 min to assure a constant temperature.

4. Results and discussion

4.1. Molecular dynamics results

4.1.1. Molecular modelling

For the present study, four quadratic boxes with a size of 60 Å× 60 Å× 60 Å are generated. The unlinked simulation boxed are generated based on the molecular modelling procedure presented in section 3.2.1. The resultant simulation box consists of 133 molecules of the first epoxy component (Bisphenol A diglycidyl ether) and 81 molecules of the second epoxy component (1,4-Butanediol diglycidyl ether). The number of curing agents molecules is calculated to 40 molecules of the first curing agent component (α,ω-poly(oxypropylene) diamine) and 70 of the second component (3-(aminomethyl)-3,5,5-trimethyl-cyclohexanamine). In total, this results in 10547 atoms in each simulation box.

The curing simulation lead to an average value for the degree of cross-linking of 94.77% in terms of an epoxy conversion with a standard deviation of 1.21%. To characterise the curing process and the final network topology, the evolution of reactive amine groups as a function of the epoxy conversion is shown in Fig. 7. The majority (87.64%) of curing agents has reacted twice to its final state of tertiary amines. Only 8.76% of secondary amines and 3.6% of (non-reacted) primary amines are left after the cross-linking procedure. The challenge of a realistic model generation was part of a previous study by Unger et al. [52] to which the reader is referred for a detailed presentation of the applied molecular modelling and an experimental validation.

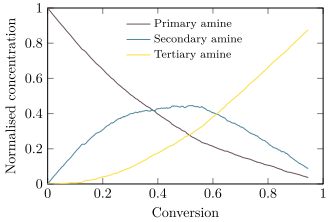

Fig. 7. Evolution of reactive groups during the cross-linking simulation in terms of the relative change of reactive amine groups as a function of the epoxy conversion.

The used molecular modelling procedure assures a well equilibrated system due to the sequential bond formation of only one bond per cross-linking time-step followed by a relaxation. But as the potentials of bonded and non-bonded interactions are updated for the tensile simulations an additional relaxation is necessary. To assure a well equilibrated system with the updated potentials, the system was relaxed individually at each temperature (246 K, 296 K, 326 K) for 20 ns. Fig. 8 shows the average density for all simulation boxes as a function of the relaxation time for all three temperatures considered. After initial small changes in the density the system is converged to the equilibrium state. The density at room temperature converges to a value of 1.13 g/cc,

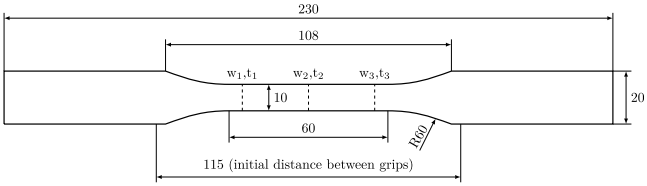

Fig. 6. Planar dimensions of the dog-bone specimens with a thickness of 2.7 mm used for tensile tests, all dimensions are in millimeters. Dashed lines indicate the positions of measured width and thickness for calculating the average cross-section.

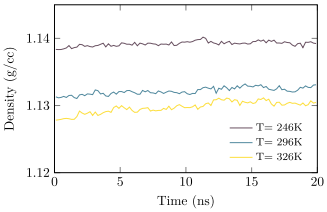

Fig. 8. Density as a function of additional relaxation time after updating the bonded and non-bonded potentials for the tensile simulation.

which is in very good agreement to the manufacturers specification of 1.1 g/cc. The general behaviour of increasing density with decreasing temperature due to thermal expansion is also covered by the simulation. A qualitative analysis of the thermochemical properties (coefficient of thermal expansion, glass transition temperature) is out of scope for the present study.

4.1.2. Tensile simulation

MD simulations with a tensile loading at strain rates ranging from $\dot{\varepsilon} = 5 \times 10^6$ 1/s to $\dot{\varepsilon} = 5 \times 10^9$ 1/s at temperatures of 246 K(≈−27 °C), 296 K(≈23 °C) and 326 K(≈53 °C) were performed for the parameter identification. The temperatures are chosen according to the temperatures applied at the experimental tensile tests and cover a range of 80 K within the glassy regime ($T_g = 82$ ° C≈ 355 K). Fig. 9 shows the resultant mechanical response in terms of averaged stress-strain curves for exemplary strain rates and all investigated temperatures. The stress-strain response shows a typical behaviour, with a linear increase of stress in the low strain elastic regime. It can be seen that the initial stiffness is independent of the strain rate. This is followed by a softening which leads to a viscous flow, indicated with nearly constant stress at increasing strain. The expected and commonly known material behaviour is identifiable in the non-linear regime with the maximum stress at which viscous flow occurs rising with increasing strain rate. A comparison of results obtained at different temperatures shows that the maximum stress for a constant strain rate decreases with increasing temperature.

Fig. 10 shows one representative stress-strain curve of the cured epoxy system obtained by a single molecular dynamics simulation at a strain rate of $\dot{\varepsilon} = 1 \times 10^7$1/s. A piecewise cubic spline interpolation is used to fit the data points. The spline was obtained by optimising the position of the centre knot in terms of minimising the least square error between the fit and the simulation data. For the following parameter identification of the viscoelastic models the yield point is defined as the first maximum of the spline. The definition to chose the point at which the derivative of stress with respect to the strain is zero is a common criterion [7,27,32,35,58]. At this point, the elastic strain rate is

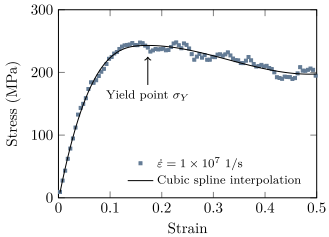

Fig. 10. Representative tensile stress-strain response of a cured epoxy system at a strain rate of $\dot{\varepsilon} = 1 \times 10^{-7}$ with highlighted yield stress.

assumed to vanish and the strain is dominantly induced by the viscous flow without a significant elastic contribution. The yield point is highlighted in Fig. 10 at a yield stress of 243.05 MPa.

Fig. 11 shows the mean values and the standard deviation of the yield stresses for all investigated combinations of strain rates and temperatures. The standard deviation ranges between ≈ 14 MPa and ≈ 26 MPa being in the common order of MD simulation scattering. However, the effect of strain rates and temperature on the yield stress is clearly identifiable and shows the expected behaviour. The yield stress increases with increasing strain rate and decreasing temperature.

4.2. Parameter identification of viscoelastic theories

The parameter identification was conducted by an in-house grid search algorithm, that was executed iteratively with decreasing boundaries to find an optimised set of parameters for the presented theories. As most of the parameters that need to be identified have a physical interpretation, it is possible to define reasonable boundaries a priori in order to reduce computational cost. The objective function given by the root mean square deviation between predicted yield stress values and yield stress obtained by MD simulation results was minimised without any constraints (single objective optimisation). The parameter identification was conducted with all mean values for each combination of strain rate and temperature obtained from MD simulation results after eliminating distinct outliers (Fig. 11).

The final identified parameters for the three investigated theories are presented in Table 3 and are found to be in a reasonable range with respect to their physical meaning and existing values in literature. For example, the activation volume of the Eyring model V^E was calibrated to a value of 0.79 nm^3 by Arash et al. [7] for the same epoxy system, but without considering the effect of temperature. Bardella [59] calibrated the Eyring model for an epoxy system with values for the activation volume and energy of 1.53 nm^3 and 0.634 × 10^{-19} J, respectively.

The parameter set of the Cooperative model consists of values in a

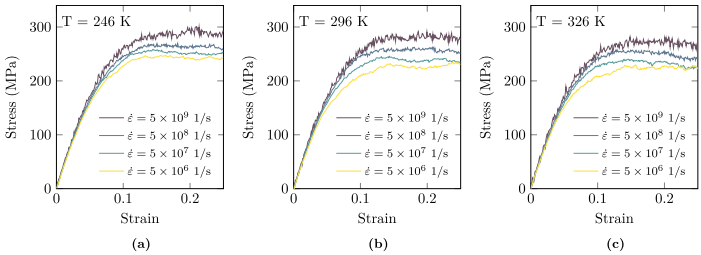

Fig. 9. Stress-strain response obtained by MD simulations at various strain rates and three different temperatures (all below the glass transition temperature): (a) 246 K, (b) 296 K, (c) 326 K.

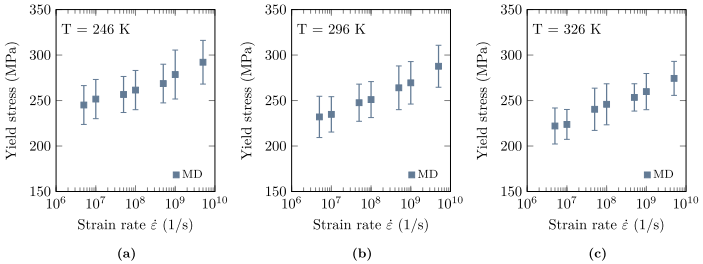

Fig. 11. Yield stress obtained from MD simulations at varying strain rates and temperatures of (a) 246 K, (b) 296 K, (c) 326 K. Error bars visualise the standard deviation.

Table 3
Viscoelastic model parameters identified by MD simulations.

	Parameter		Value
Eyring	V^E	(nm^3)	0.552
	ΔH^E	(J)	1.786×10^{-19}
	$\dot{\varepsilon}_0^E$	(1/s)	3.281×10^{12}
Cooperative	$\sigma_i(0)$	(MPa)	294
	m	(MPa/K)	0.44
	V^C	(nm^3)	0.0501
	$\dot{\varepsilon}_0^C$	(1/s)	1.122×10^{13}
	ΔH^C	(J)	1.584×10^{-20}
	n	(−)	12.2
Argon	σ_0^A	(MPa)	324.34
	ΔH^A	(J)	1.977×10^{-19}
	$\dot{\varepsilon}_0^A$	(1/s)	1.0447×10^{12}

reasonable range compared to experimentally identified values for three different thermosetting polymers [22], except for the value of the constant stress at zero Kelvin. The presented values found for $\sigma_i(0)$ range between 190 MPa and 210 MPa after experimental calibration, whereas the MD-identified parameter has a value of 294 MPa. The Argon model was calibrated by Richeton et al. [23] for two materials, Poly(methyl methacrylate) (PMMA) and polycarbonate PC, with values for the athermal yield stress of 1311 MPa (PMMA) and 205 MPa (PC). The activation energy was identified with values of 2.939×10^{-19} J for PMMA and 3.4041×10^{-19} J for PC, being in agreement to the presented values for the investigated epoxy system. Fig. 12 shows the yield stress as a function of the strain rate for all calibrated models, as well as the underlying MD simulation results. The root mean square deviation between MD results and prediction are calculated to be 12.78 MPa for the Eyring model, 12.99 MPa for the Argon model and 10.76 MPa for the cooperative model. Due to its close similarity in the formulation, the Eyring and Argon model show a very similar behaviour in the range of molecular strain rates and a nearly identical value for the root mean square deviation. On the other hand, the Cooperative model can approximate the MD results with higher accuracy due to its complex formulation with six parameters resulting in a smaller root mean square deviation.

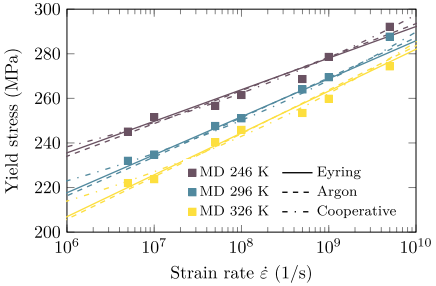

Fig. 12. Simulation results obtained by MD and calibrated viscoelastic models for all investigated temperatures.

4.3. Experimental results

Experimental tensile tests were performed according to the test procedure presented in Section 3.3. For the following analysis, the temperatures will be given in Kelvin and the strain rate will be used instead of the test speed. At room temperature, three test speeds were examined resulting in strain rates between $\dot{\varepsilon} = 1.44 \times 10^{-6}$ (1/s) and $\dot{\varepsilon} = 1.44 \times 10^{-4}$ (1/s) based on the specimen geometry (Fig. 6). The experimental stress-strain curves are shown in Fig. 13 with the yield stress highlighted, using the same criterion (horizontal tangent) as for the MD results.

The effect of strain rate and temperature on the elastic material properties is out of the scope for the present study. However, it is worth mentioning that only the temperature has an effect on the initial stiffness in the elastic regime but no influence of the strain rate is identifiable. The yield stress shows the qualitatively same behaviour as presented by the MD results, the yield stress is increasing with decreasing temperature and increasing strain rate. For the highest temperature, no effects of thermal degradation (i.e. significant loss of initial stiffness or unidentifiable yield stress) nor rubbery behaviour was observable, as the highest temperature of 326 K is about 30 K lower than the glass transition temperature.

4.4. Experimental validation

The following investigation considers the prediction of the viscoelastic behaviour in terms of the yield stress as the start of viscous flow, at different temperatures. All studied temperatures are significantly lower than the glass transition temperature ($T_g = 82\,^\circ C \approx 355$ K), thus the present study is limited to the viscoelasticity in the glassy regime. A validation is presented by a comparison to experimental results. Fig. 14 presents the calibrated models (lines) and the underlying MD results (squares) together with the experimental results (triangles) for all investigated temperatures.

These figures reveal the strain rate dependency by showing the increase of yield stress for an increasing strain rate of the calibrated models. First of all, a significant deviation of the prediction by the cooperative model is identifiable, although this model showed the

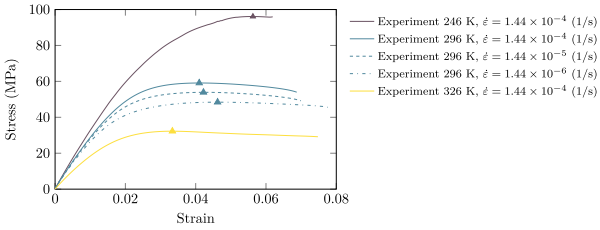

Fig. 13. Stress-strain curves obtained by experimental testing under uniaxial tensile loading. The triangle mark shows the respective yield stress.

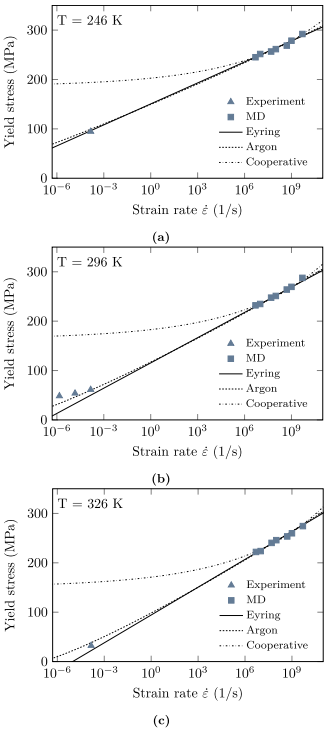

Fig. 14. Comparison of predicted yield stress and experimental results at temperatures of (a) 246 K, (b) 296 K, (c) 326 K.

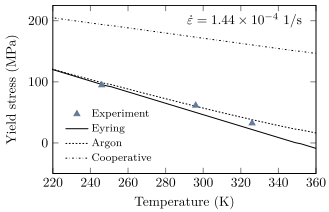

Fig. 15. Comparison of predicted yield stress and experimental results for a constant strain rate.

smallest deviation to MD results after parameter identification. The cooperative model significantly underestimates the decrease of yield stress for a decreasing strain rate for all temperatures. This leads to overestimated values for the yield stress at experimental strain rates by at least a factor of two. The Eyring model, with a linear dependency to the logarithmic strain rate, shows a good prediction for the lowest temperature of 246 K and an acceptable fit for the two higher temperatures at the largest strain rate. The prediction of the Eyring model for the two smaller strain rates is rather poor compared to the Argon model. The Argon model is able to cover the non-linear behaviour well due to its exponential factor of 6/5. In general, the Argon model is in good agreement with the experimental data with a slight but identifiable underestimation for the smallest strain rate. However, the temperature dependency is very well represented by the Argon model, as depicted in Fig. 15 by showing the yield stress as a function of temperature for the default strain rate of $\dot{\varepsilon} = 1.44 \times 10^{-4}$ 1/s. This figure again shows a substantial overestimation of the cooperative model.

The results shown for the Eyring and the Argon model are qualitatively in agreement with insights presented by Cook et al. [27], who reported that the Argon model predicts the yield stress over a broad range of temperatures in better agreement to the experimental data, compared to the Eyring equation. However, it should be noted that both the Eyring and Argon model cannot be used for a consistent prediction at temperatures above the glass transition temperature. The prediction by the cooperative model shows a substantial deviation to the experimental results. This can be explained by the difficulty in finding a suitable value for the strain rate-independent constant stress at zero Kelvin $\sigma_i(0)$, when using only MD results for the calibration. Our results are in contrast to promising results published by several authors, in which all of them used experimental results for the calibration [22,28,60].

Our present study identifies the Argon model to be well suited for predicting the viscoelasticity of epoxy polymers in the glassy regime after careful calibration using only MD results. The physical phenomena on the molecular level are well represented by the Argon model and it can be used for a sufficiently accurate prediction of the yield stress in good agreement to experimental results. Furthermore, the three parameters of the Argon model are related to physical quantities and thus allow for a characterisation of underlying physics acting at viscous deformation. This makes the Argon model valuable in the context of physically based constitute models, as it generally allows an extrapolation of the viscoelastic properties. The Argon model can easily substitute the Eyring model in existing constitutive models due to its close similarity and same number of parameters with related physical meaning.

It should be noted that the MD results do not need to be obtained at temperatures equivalent to the desired prediction temperatures, as it is present in this study. Nevertheless, an accurate prediction of

viscoelasticity, including extrapolation, is only given, if a sufficiently large temperature range is used for calibration. A limitation of the current study is the constant activation volume, or the related athermal stress in the Argon model with respect to the temperature. It is generally agreed that the activation volume increases with increasing temperature, as the physically underlying process of molecular movement involves a larger volume at higher temperatures [27,28,60]. Although this effect seems to be negligible, at least for the Argon model, it would be attractive to study the effect in further studies for all models. The prediction of the glass transition temperature of polymers using MD simulations is desirable, but also comes with the challenge of bridging the different time scales (i.e. significant differences of the heating or cooling rate) [61]. Because of this complexity molecular dynamic based prediction is a research topic for its own and thus it is out of scope for the present study. Detailed insights into successful molecular dynamics based approaches dealing with the extrapolation from atomistic to experimental time scales were presented by Li et al. [38], Vollmayr et al. [62], Buchholz et al. [63], and Han et al. [64].

5. Conclusion

The present work confirms that a successful prediction of viscoelastic properties is possible by solely using results obtained by molecular tensile test simulations. A comparison to experimental results is presented that includes three different strain rates and three different temperatures in the glassy regime. Three theories for the viscoelasticity of polymers are examined, namely the widely known Eyring theory, the further developed Argon theory and the more complex cooperative model. The prediction by the Eyring model was found to be in adequate agreement, whereas the Argon model was able to predict the yield stress in good agreement to experimental results. The results show that the cooperative model is not suitable for a description of viscoelasticity if only MD results are used for the calibration.

We contributed to the challenge of bridging the different time scales between MD (nanoseconds) and experiments (seconds to hours) with respect to the viscoelasticity of cross-linked epoxy resins. The present study is important for the implementation of viscoelasticity in physically motivated constitute models, as we have shown that the Argon model is able to describe the physical phenomena on the molecular level in good agreement to experimental results. Our study encourages the use of the Argon model for two reasons. (1) It ensures a comprehensive and accurate representation of viscoelasticity of cross-linked epoxy resins on a continuum length scale. (2) It can successfully be calibrated by only using MD results and thus significantly reduce the amount of experimental testing. In future studies, the effect of cross-linking density, network topology and polymerisation degrees on the finite strain viscoelastic behaviour can furthermore improve constitutive models and lead to a more reliable material behaviour in numerical continuum simulations. Additionally, it is desirable to investigate the effect of nanoparticles on the viscoelasticity, as potential insights and developments will help to clarify the underlying mechanism of actions in nanocomposites. The application of a coarse-grained model is desirable to study a system with larger length and time scales compared to today's feasible molecular dynamic simulations [65–67].

Funding

This work originates from the research project 'Hybrid laminates and nanoparticle reinforced materials for improved rotor blade structures' ('LENAH – Lebensdauererhöhung und Leichtbauoptimierung durch nanomodifizierte und hybride Werkstoffsysteme im Rotorblatt'), funded by the Federal Ministry of Education and Research of Germany. The authors wish to express their gratitude for the financial support.

Competing interests

The authors declare that they have no competing interests.

Data availability

The raw/processed data required to reproduce these findings cannot be shared at this time, as the data also forms part of an ongoing study.

Acknowledgements

The authors acknowledge the support by the LUIS scientific computing cluster, which is funded by Leibniz Universität Hannover, the Lower Saxony Ministry of Science and Culture (MWK) and the DFG.

References

[1] A. Wineman, "Nonlinear viscoelastic solids—a review", Math. Mech. Solids 14 (May 2009) 300–366, https://doi.org/10.1177/1081286509103660.
[2] Chunyu Li, Alejandro Strachan, Molecular scale simulations on thermoset polymers: a review, J. Polym. Sci. B Polym. Phys. 53 (Jan. 15, 2015) 103–122, https://doi.org/10.1002/polb.23489.
[3] Matthew S. Radue, Benjamin D. Jensen, S. Gowtham, Danielle R. Klimek-McDonald, Julia A. King, Gregory M. Odegard, Comparing the mechanical response of di-, tri-, and tetra-functional resin epoxies with reactive molecular dynamics, J. Polym. Sci. B Polym. Phys. 56 (Feb. 1, 2018) 255–264, https://doi.org/10.1002/polb.24539.
[4] Nathan Sharp, Chunyu Li, Alejandro Strachan, Douglas Adams, R. Byron Pipes, Effects of water on epoxy cure kinetics and glass transition temperature utilizing molecular dynamics simulations, J. Polym. Sci. B Polym. Phys. 55 (Aug. 1, 2017) 1150–1159, https://doi.org/10.1002/polb.24357.
[5] Mehrzad Mortezaei, Mohammad Hossein Navid Famili, Mehrdad Kokabi, The role of interfacial interactions on the glass-transition and viscoelastic properties of silica/polystyrene nanocomposite, Compos. Sci. Technol. 71 (May 2011) 1039–1045, https://doi.org/10.1016/j.compscitech.2011.02.012.
[6] B. Arash, Q. Wang, V.K. Varadan, Mechanical properties of carbon nanotube/polymer composites, Sci. Rep. 4 (May 2015), https://doi.org/10.1038/srep06479.
[7] Behrouz Arash, Wibke Exner, Raimund Rolfes, A viscoelastic damage model for nanoparticle/epoxy nanocomposites at finite strain: a multiscale approach, J. Mech. Phys. Solids 128 (July 2019) 162–180, https://doi.org/10.1016/j.jmps.2019.04.004.
[8] J. Fankhänel, D. Silbernagl, M. Ghasem Zadeh Khorasani, B. Daum, A. Kempe, H. Sturm, R. Rolfes, Mechanical properties of boehmite evaluated by atomic force microscopy experiments and molecular dynamic finite element simulations, J. Nanomater. 2016 (2016) 1–13, https://doi.org/10.1155/2016/5017213.
[9] M. Jux, J. Fankhänel, B. Daum, T. Mahrholz, M. Sinapius, R. Rolfes, Mechanical properties of epoxy/boehmite nanocomposites in dependency of mass fraction and surface modification - an experimental and numerical approach, Polymer 141 (Apr. 2018) 34–45, https://doi.org/10.1016/j.polymer.2018.02.059.
[10] Eyring Henry, Viscosity, plasticity, and diffusion as examples of absolute reaction rates, J. Chem. Phys. 4 (Apr. 1936) 283–291, https://doi.org/10.1063/1.1749836.
[11] Eyring Henry, The activated complex in chemical reactions, J. Chem. Phys. 3 (Feb. 1935) 107–115, https://doi.org/10.1063/1.1749604.
[12] Taikyue Ree, Eyring Henry, Theory of non-Newtonian flow. II. Solution system of high polymers, J. Appl. Phys. 26 (July 1955) 800–809, https://doi.org/10.1063/1.1722099.
[13] Taikyue Ree, Eyring Henry, Theory of non-Newtonian flow. I. Solid plastic system, J. Appl. Phys. 26 (July 1955) 793–800, https://doi.org/10.1063/1.1722098.
[14] Taikyue Ree, Eyring Henry, The relaxation theory OF transport phenomena, Rheology, Elsevier, 1958, pp. 83–144, , https://doi.org/10.1016/B978-0-12-395695-8.50008-2.
[15] J.C. Bauwens, C. Bauwens-Crowet, G. Homes, Tensile yield-stress behavior of poly (vinyl chloride) and polycarbonate in the glass transition region, J. Polym. Sci. A-2 Polym. Phys. 7 (1969) 1745–1754.
[16] C. Bauwens-Crowet, J.C. Bauwens, G. Homes, Tensile yield-stress behavior of glassy polymers, J. Polym. Sci. A-2 Polym. Phys. 7 (1969) 735–742.
[17] C. Bauwens-Crowet, J.-C. Bauwens, Georges Homes, The temperature dependence of yield of polycarbonate in uniaxial compression and tensile tests, J. Mater. Sci. 7 (1972) 176–183.
[18] Jung Yul Lim, Henry J. Donahue, Sang Yong Kim, Strain rate, temperature, and microstructure-dependent yield stress of poly(ethylene terephthalate), Macromol. Chem. Phys. 204 (Mar. 2003) 653–660, https://doi.org/10.1002/macp.200390033.
[19] Anthony E. Mayr, Wayne D. Cook, Graham H. Edward, "Yielding behaviour in model epoxy ther-mosets—I. Effect of strain rate and composition", Polymer 39 (1998) 3719–3724.
[20] D.G. Fotheringham, B.W. Cherry, C. Bauwens-Crowet, "Comment on "the compression yield be haviour of polymethyl methacrylate over a wide range of temperatures and strain-rates"", J. Mater. Sci. 11 (1976) 1368–1371.
[21] D.G. Fotheringham, B.W. Cherry, The role of recovery forces in the deformation of linear polyethylene, J. Mater. Sci. 13 (May 1978) 951–964, https://doi.org/10.1007/BF00544690.

[22] J. Richeton, S. Ahzi, L. Daridon, Y. Rémond, A formulation of the cooperative model for the yield stress of amorphous polymers for a wide range of strain rates and temperatures, Polymer 46 (July 2005) 6035–6043, https://doi.org/10.1016/j.polymer.2005.05.079.
[23] J. Richeton, S. Ahzi, L. Daridon, Thermodynamic investigation of yield-stress models for amorphous polymers, Philos. Mag. 87 (Aug. 21, 2007) 3629–3643, https://doi.org/10.1080/14786430701381162.
[24] A.S. Argon, A theory for the low-temperature plastic deformation of glassy polymers, Philos. Mag. 28 (Oct. 1973) 839–865, https://doi.org/10.1080/14786437308220987.
[25] A.S. Argon, M.I. Bessonov, Plastic deformation in polyimides, with new implications on the theory of plastic deformation of glassy polymers, Philos. Mag. 35 (Apr. 1977) 917–933, https://doi.org/10.1080/14786437708232634.
[26] Richard E. Robertson, Theory for the plasticity of glassy polymers, J. Chem. Phys. 44 (May 15, 1966) 3950–3956, https://doi.org/10.1063/1.1726558.
[27] Wayne D. Cook, Anthony E. Mayr, Graham H. Edward, "Yielding behaviour in model epoxy ther mosets—II. Temperature dependence", Polymer 39 (1998) 3725–3733.
[28] N.W.J. Brooks, R.A. Duckett, I.M. Ward, Temperature and strain-rate dependence of yield stress of polyethylene, J. Polym. Sci. B Polym. Phys. 36 (1998) 2177–2189.
[29] Mary C. Boyce, David M. Parks, Ali S. Argon, Large inelastic deformation of glassy polymers. Part I: rate dependent constitutive model, Mech. Mater. 7 (1988) 15–33.
[30] Ellen M. Arruda, Mary C. Boyce, A three-dimensional constitutive model for the large stretch be havior of rubber elastic materials", J. Mech. Phys. Solids 41 (1993) 389–412.
[31] Ellen M. Arruda, Mary C. Boyce, Evolution of plastic anisotropy in amorphous polymers during finite straining, Int. J. Plast. 9 (Jan. 1993) 697–720, https://doi.org/10.1016/0749-6419(93)90034-N.
[32] X. Poulain, A.A. Benzerga, R.K. Goldberg, Finite-strain elasto-viscoplastic behavior of an epoxy resin: experiments and modeling in the glassy regime, Int. J. Plast. 62 (Nov. 2014) 138–161, https://doi.org/10.1016/j.ijplas.2014.07.002.
[33] R.A. Duckett, S. Rabinowitz, I.M. Ward, The strain-rate, temperature and pressure dependence of yield of isotropic poly(methylmethacrylate) and poly(ethylene terephthalate), J. Mater. Sci. 5 (Oct. 1970) 909–915, https://doi.org/10.1007/BF00574864.
[34] Hyungbum Park, Joonmyung Choi, Byungjo Kim, Seunghwa Yang, Hyunseong Shin, Maenghyo Cho, Toward the constitutive modeling of epoxy matrix: temperature-accelerated quasi-static molecular simulations consistent with the experimental test, Compos. B Eng. 142 (June 2018) 131–141, https://doi.org/10.1016/j.compositesb.2018.01.018.
[35] N. Vu-Bac, M.A. Bessa, Timon rabczuk, and wing kam liu, "A multiscale model for the quasi-static thermo-plastic behavior of highly cross-linked glassy polymers", Macromolecules 48 (Sept. 22, 2015) 6713–6723, https://doi.org/10.1021/acs.macromol.5b01236.
[36] Ying Li, Shan Tang, Martin Kröger, Wing Kam Liu, Molecular simulation guided constitutive modeling on finite strain viscoelasticity of elastomers, J. Mech. Phys. Solids 88 (Mar. 2016) 204–226, https://doi.org/10.1016/j.jmps.2015.12.007.
[37] George Z. Voyiadjis, Amir Shojaei, Guoqiang Li, A generalized coupled viscoplastic–viscodamage–viscohealing theory for glassy polymers, Int. J. Plast. 28 (Jan. 2012) 21–45, https://doi.org/10.1016/j.ijplas.2011.05.012.
[38] Chunyu Li, Alejandro Strachan, Molecular dynamics predictions of thermal and mechanical properties of thermoset polymer EPON862/DETDA, Polymer 52 (June 2011) 2920–2928, https://doi.org/10.1016/j.polymer.2011.04.041.
[39] Kauzmann Walter, Eyring Henry, The viscous flow of large molecules, J. Am. Chem. Soc. 62 (1940) 3113–3125.
[40] Samuel Glasstone, Keith Laidler, Eyring Henry, The Theory of Rate Processes, McGraw-Hill, New York, 1941.
[41] J.C.M. Li, J.J. Gilman, Disclination loops in polymers, J. Appl. Phys. 41 (Oct. 1970) 4248–4256, https://doi.org/10.1063/1.1658452.
[42] V. Sundararaghavan, A. Kumar, Molecular dynamics simulations of compressive yielding in cross-linked epoxies in the context of Argon theory, Int. J. Plast. 47 (Aug. 2013) 111–125, https://doi.org/10.1016/j.ijplas.2013.01.004.
[43] Olin Epoxy AIRSTONE 886H Hardener, Material Safety Data Sheet, UPPC GmbH, Schemmenberger Str. vol. 39, Mietingen-Baltringen, Germany, Apr. 4, 2011, p. 88487.
[44] Olin Epoxy AIRSTONE 880E Epoxy Resin, Material Safety Data Sheet, UPPC GmbH, Schemmenberger Str. vol. 39, Mietingen-Baltringen, Germany, Apr. 4, 2011, p. 88487.
[45] Chaofu Wu, Weijian Xu, Atomistic molecular simulations of structure and dynamics of crosslinked epoxy resin, Polymer 48 (Sept. 2007) 5802–5812, https://doi.org/10.1016/j.polymer.2007.07.019.
[46] E. Carla, Estridge, "The effects of competitive primary and secondary amine reactivity on the structural evolution and properties of an epoxy thermoset resin during cure: a molecular dynamics study", Polymer 141 (Apr. 2018) 12–20, https://doi.org/10.1016/j.polymer.2018.02.062.
[47] Chunyu Li, Alejandro Strachan, Molecular simulations of crosslinking process of thermosetting polymers, Polymer 51 (Nov. 2010) 6058–6070, https://doi.org/10.1016/j.polymer.2010.10.033.
[48] Vikas Varshney, Soumya S. Patnaik, Ajit K. Roy, Barry L. Farmer, A molecular dynamics study of epoxy-based networks: cross-linking procedure and prediction of molecular and material properties, Macromolecules 41 (Sept. 23, 2008) 6837–6842, https://doi.org/10.1021/ma801153e.
[49] Nasdala Lutz, Andreas kempe, and raimund rolfes, "molecular dynamic finite element method (MDFEM)", Comput. Finite Elem. Methods Nanotechnol, CRC Press, 2013, pp. 331–372.
[50] Nasdala Lutz, Andreas Kempe, and Raimund Rolfes, "Are finite elements appropriate for use in molecular dynamic simulations?", Compos. Sci. Technol. 72 (May 2012) 989–1000, https://doi.org/10.1016/j.compscitech.2012.03.008.
[51] Nasdala Lutz, Andreas Kempe, and Raimund Rolfes, "The molecular dynamic finite element method (MDFEM)", Comput. Mater. Continua (CMC) 19 (2010) 57.
[52] Robin Unger, Ulrike Braun, Johannes Fankhänel, Benedikt Daum, Behrouz Arash, Raimund Rolfes, Molecular modelling of epoxy resin crosslinking experimentally validated by near-infrared spectroscopy, Comput. Mater. Sci. 161 (Apr. 2019) 223–235, https://doi.org/10.1016/j.commatsci.2019.01.054.
[53] L. Martínez, R. Andrade, E.G. Birgin, J.M. Martínez, "PACKMOL: a package for building initial configurations for molecular dynamics simulations", J. Comput. Chem. 30 (Oct. 2009) 2157–2164, https://doi.org/10.1002/jcc.21224.
[54] The open Babel package, version 2.3.1 http://openbabel.org.
[55] Stephen L. Mayo, Barry D. Olafson, William A. Goddard, DREIDING: a generic force field for molecular simulations, J. Phys. Chem. 94 (1990) 8897–8909.
[56] Simone Melchionna, Giovanni Ciccotti, Brad Lee Holian, Hoover NPT dynamics for systems varying in shape and size, Mol. Phys. 78 (Feb. 20, 1993) 533–544, https://doi.org/10.1080/00268979300100371.
[57] Steve Plimpton, Fast Parallel algorithms for short-range molecular dynamics, Journal of Computational Physics, vol. 117, Mar. 1995, pp. 1–19, , https://doi.org/10.1006/jcph.1995.1039.
[58] I.M. Ward, J. Sweeney, Mechanical Properties of Solid Polymers, third ed., Wiley, Chichester, West Sussex, United Kingdom, 2013, p. 461.
[59] Lorenzo Bardella, A phenomenological constitutive law for the nonlinear viscoelastic behaviour of epoxy resins in the glassy state, Eur. J. Mech. A Solid. 20 (2001) 907–924.
[60] J. Richeton, S. Ahzi, K.S. Vecchio, F.C. Jiang, A. Makradi, Modeling and validation of the large deformation inelastic response of amorphous polymers over a wide range of temperatures and strain rates, Int. J. Solids Struct. 44 (Dec. 2007) 7938–7954, https://doi.org/10.1016/j.ijsolstr.2007.05.018.
[61] Malcolm L. Williams, Robert F. Landel, John D. Ferry, The temperature dependence of relaxation mechanisms in amorphous polymers and other glass-forming liquids, J. Am. Chem. Soc. 77 (July 1955) 3701–3707, https://doi.org/10.1021/ja01619a008.
[62] Katharina Vollmayr, Kob Walter, Kurt Binder, How do the properties of a glass depend on the cooling rate? A computer simulation study of a Lennard-Jones system, J. Chem. Phys. 105 (Sept. 15, 1996) 4714–4728, https://doi.org/10.1063/1.472326.
[63] Joachim Buchholz, Wolfgang Paul, Fathollah Varnik, Kurt Binder, Cooling rate dependence of the glass transition temperature of polymer melts: molecular dynamics study, J. Chem. Phys. 117 (Oct. 15, 2002) 7364–7372, https://doi.org/10.1063/1.1508366.
[64] Jie Han, Richard H. Gee, Richard H. Boyd, Glass transition temperatures of polymers from molecular dynamics simulations, Macromolecules 27 (1994) 7781–7784.
[65] Behrouz Arash, Harold S. Park, Timon Rabczuk, Coarse-grained model of the J-integral of carbon nanotube reinforced polymer composites, Carbon 96 (Jan. 2016) 1084–1092, https://doi.org/10.1016/j.carbon.2015.10.058.
[66] Aramoon Amin, Timothy D. Breitzman, Christopher Woodward, Jaafar A. El-Awady, Coarse-grained molecular dynamics study of the curing and properties of highly cross-linked epoxy polymers, J. Phys. Chem. B 120 (Sept. 8, 2016) 9495–9505, https://doi.org/10.1021/acs.jpcb.6b03809.
[67] Atiyeh Alsadat Mousavi, Behrouz Arash, Xiaoying Zhuang, Timon Rabczuk, A coarse-grained model for the elastic properties of cross linked short carbon nanotube/polymer composites, Compos. B Eng. 95 (June 2016) 404–411, https://doi.org/10.1016/j.compositesb.2016.03.044.

Chapter 5

Temperature-dependent viscoelastic damage behaviour of nanocomposites

5.1 Research context

Adding nano-scale additives to a polymer matrix can lead to significantly increased specific material properties, which are highly desirable in engineering applications, especially for lightweight structures. These nanocomposites exhibit a non-linear material behaviour affected by various factors such as the polymer network topology, nanoparticle-matrix interaction and strain rate. Additionally, as polymers generally show a strong temperature-dependent behaviour, the effect of temperature is an important challenge for the accurate representation and prediction of the material behaviour (see Section and Figure 1.3 on page 7). With regard to material modelling for engineering applications, this complex material behaviour is challenging in two ways. Firstly, a constitutive model must be capable at all to accurately capture and represent the non-linear material response. Secondly, for constitutive models that pass the first aspect, generally extensive experimental testing is required for the parameter identification process.

To meet both aspects, it is desirable to use physically-based constitutive models in combination with molecular simulations for the parameter identification. It has been shown that these kind of multi-scale frameworks are valuable tools that require less experimental data due to the derivation of material parameters from molecular simulations. Several approaches can be found in the literature [3, 4, 10, 26, 46, 87], from which especially the viscoelastic damage model for nanoparticle/epoxy nanocomposites presented by Arash et al. [3] is noteworthy. It was shown that some parameters can be obtained from molecular simulations and lead to material and structural behaviour in good agreement with experimental results. However, the effect of temperature was not included in this model.

In the following publication, the constitutive damage model for nanoparticle/epoxy nanocomposites is extended to take the effect of temperature into account. The predictive capability of the extended model is assessed, and the ability of molecular simulations to identify the model parameter is evaluated. The gained knowledge and developed methods of both previous publication are the fundamentals on which this study builds up on.

5.2 Methods

The curing simulations, presented in Chapter 3 are used to generate the simulation models and to identify one parameter of the proposed constitutive model. Molecular tensile and shear simulations were performed by using the Large-scale Atomic/ Molecular Massively Parallel Simulator (LAMMPS) [63]. The Argon model that was found to be an accurate representation for the viscoelasticity (see Chapter 4) was implemented in the model and replaced the former used Eyring model. With this study, the capabilities of MD simulations to replace experimental tests are investigated. For the parameter identification and the validation, experimental tensile tests at different test configurations and with different materials were conducted by the Institute of Composite Structures and Adaptive Systems of the German Aerospace Center (DLR). Tensile tests at the default test configuration (DIN EN ISO 527) were performed for the pure epoxy material and nanocomposites with nanoparticle weight fractions of 5 %, 10 % and 15 %. Additionally, the pure epoxy material was tested at three different temperatures and three different strain rates. The parameter identification uses an in-house implementation of a genetic algorithm.

5.3 Results and outlook

With the present publication, a unique extension to finite temperatures for a physically-based constitutive model is proposed that accurately captures the characteristic temperature-dependent viscoelastic damage behaviour of nanoparticle/epoxy nanocomposites. The capabilities of the multi-scale constitutive model and the corresponding parameter identification are studied with two cases. Firstly, only experimental results, obtained from tensile tests at different strain rates and temperatures are used to calibrate the model. The aim of this first case is, to investigate the general predictive capabilities of the material model and provide an assessment against independent experimental results, not used in the identification process. It is shown that the material model is capable of reproducing the complex, non-linear material behaviour in good agreement with experimental results for variations of the temperature, strain rate and nanoparticle weight fraction.
Secondly, molecular simulations are used to identify parameters and by doing so, the required number of experimental tests is reduced considerably. With the second case, it is underlined that experiments can partly be replaced by numerical simulations without a significant loss in accuracy. An experimental validation demonstrates that the material response is in fair agreement with experimental data for variations of the strain rate, temperature and nanoparticle weight fractions. Finally, a quantitative assessment of the accuracy of both studied cases for the parameter identification is provided by using the stored strain energy as a criterion.
The present publication provides a better understanding of the thermo-

viscoelastic behaviour of nanoparticle/epoxy nanocomposites and discusses the associated challenges of modelling these materials accurately. For further enhancement, experimental data obtained from cyclic loading conditions is desirable to investigate the prediction of the hysteresis behaviour. Incorporating coarse-grained methods would allow reducing the computational cost and would make larger length and timescales accessible in numerical simulations. Due to its general formulation, the proposed constitutive model can easily be extended for the analysis of specific physical and chemical phenomena that affect the material response such as water absorption [73, 74, 86], thermal degradation [64] or physical ageing mechanisms [57].

5.4 Paper C: Effect of temperature on the viscoelastic damage behaviour of nanoparticle/epoxy nanocomposites: Constitutive modelling and experimental validation

The following paper is published in Polymer, Volume 197, February 2020. In contrast to both previous publications the absolute temperature is denoted as Θ.

Author contribution statement:

The main work was done by the author of this thesis. Wibke Exner contributed the experimental tensile tests and reviewed the corresponding paragraphs. Behrouz Arash contributed with conceptualisation, advisory and supporting work. Raimund Rolfes contributed with advisory and supporting work.

Graphical Abstract

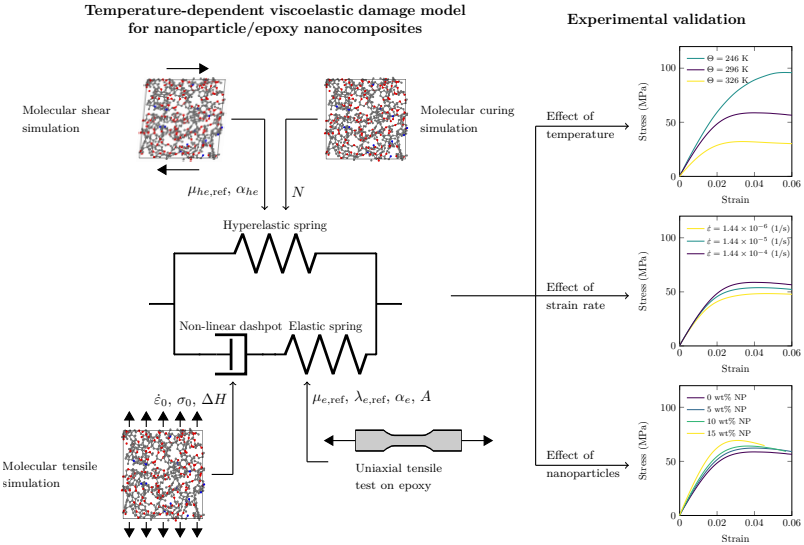

Polymer 191 (2020) 122265

Contents lists available at ScienceDirect

Polymer

journal homepage: www.elsevier.com/locate/polymer

Effect of temperature on the viscoelastic damage behaviour of nanoparticle/epoxy nanocomposites: Constitutive modelling and experimental validation

Robin Unger [a,*], Behrouz Arash [a], Wibke Exner [b], Raimund Rolfes [a]

[a] Institute of Structural Analysis, Leibniz Universität Hannover, Appelstraße 9A, 30167 Hannover, Germany
[b] Institute of Composite Structures and Adaptive Systems, DLR (German Aerospace Center), Lilienthalplatz 7, Braunschweig, 38108, Germany

ARTICLE INFO

Keywords:
Nanocomposites
Constitutive modelling
Viscoelasticity
Damage behaviour

ABSTRACT

The accurate prediction of the complex material response of nanoparticle/epoxy nanocomposites for thermomechanical load cases is of great interest for engineering applications. In the present work, three main contributions with respect to multi-scale modelling of the viscoelastic damage behaviour of nanocomposites are presented. Firstly, a constitutive model for the viscoelastic damage behaviour at finite temperatures below the glass-transition temperature is proposed. The constitutive model captures the main characteristics of the material response including the non-linear hyperelasticity, softening behaviour and the effect of temperature. Secondly, the material model is calibrated using purely experimental results to evaluate the best capability of the model in reproducing the stress–strain response at different strain rates and temperatures. The calibrated model predicts the material behaviour across a range of nanoparticle weight fractions with good agreement with experimental results. Finally, a combined approach of experimental testing and molecular simulations is proposed to identify the parameters of the constitutive model. This study shows that the proposed simulation-based framework can be used to significantly reduce the number of experimental tests required for identification of material parameters without a significant loss of accuracy in the material response prediction. The predictive capability of the atomistically calibrated constitutive model is validated, with additional experimental results not used within the parameter identification, in terms of an accurate representation of the viscoelastic damage behaviour of nanoparticle/epoxy nanocomposites at finite temperatures. The present study underlines the capabilities of numerical molecular simulations intended for the characterisation of material properties with respect to physically based constitutive modelling and multi-scale approaches.

1. Introduction

To increase the efficiency of today's lightweight structures, it is essential to develop innovative material concepts which exhibit significantly improved specific material properties. It has been shown that nanocomposites made of a polymer matrix and nanoscale additives can meet these requirements [1,2]. Among different nano-modified polymer nanocomposites, promising results with respect to improved mechanical properties have been shown for Boehmite nanoparticles (BNP) in an epoxy resin matrix [3–6].

Innovative material concepts, such as nanocomposites, come with the need to accurately predict the complex material response for structural analysis in order to exploit their full potential. Continuing research activity is leading to a variety of phenomenological [7–12] or physically motivated [13–15] constitutive models that can predict the material response for certain load cases. Physically motivated constitutive models are favourable as they, in general, allow an extrapolation outside the range of calibration and their parameters can be related to underlying mechanisms or physical quantities.

For cross-linked epoxy systems, these models must be able to reproduce the complex material behaviour that shows a non-linear stress–strain response affected by various factors such as the polymer network topology, strain rate and temperature. The behaviour of nanocomposites that additionally contain nanoscale matrix additives may be more complex, since nanoparticle size and agglomeration, as well as the interaction between matrix and particle, have an effect on the mechanical response [5,16]. Noteworthy approaches with a good agreement with experimental results have been published in the past [8,14,15,17]. A constitutive model for rubber materials at finite deformations was proposed by Arruda and Boyce [14]. The hyperelasticity

* Corresponding author.
E-mail address: r.unger@isd.uni-hannover.de (R. Unger).

https://doi.org/10.1016/j.polymer.2020.122265
Received 18 November 2019; Received in revised form 4 February 2020; Accepted 5 February 2020
Available online 11 February 2020
0032-3861/

of the underlying macromolecular network structure was represented by the eight-chain model, which captured the cooperative nature of the polymer network deformation accurately. Bardella [8] proposed a constitutive model for the non-linear viscoelasticity of epoxy resins in the glassy regime. Although the constitutive model is phenomenological, the physically motivated Eyring model was used to account for the rate-dependent viscoelastic deformation and led to a prediction of the stress–strain behaviour in good agreement with cyclic experimental results. Kontou [15] presented a constitutive model with the focus on the material response in the glassy regime very close to the glass-transition temperature. The main characteristics of yield, strain softening/hardening and the rate/temperature dependence were captured and an evolution law for the activation volume of the Eyring model was proposed. A good agreement was presented between the tensile behaviour under monotonic loading and stress relaxation at various strain rates and temperatures. Melro et al. [18] presented an elasto-plastic constitutive model that was considerably extended by Rocha et al. [17], leading to a complex formulation that accounts for viscoelastic/viscoplastic/damage behaviour of an epoxy resin. After calibration using monotonic and cyclic tension tests, the model was able to predict the material response in terms of rate-dependent plasticity. However, the authors note that the results of cyclic tests were not accurately predicted, since the underlying mechanism coming from a combination of plasticity and non-linear viscoelasticity was not covered by the model. Relevant approaches to the material behaviour of semi-crystalline polymers were published by Qi and Boyce [19], Qi [20], Vandommelen et al. [21], Ahzi et al. [22] and Ayoub et al. [23]. These studies focus on the interaction between (soft) amorphous parts and (hard) crystalline parts of the polymer macrostructure that affect the resultant material behaviour.

In order to further incorporate numerical methods, the material properties needed for continuum-level formulations can be derived from a molecular dynamics (MD) simulation, leading to the development of physically based constitutive models and consistent multi-scale approaches [24]. Two main benefits arise from the use of molecular simulations. Firstly, analysis on the atomistic length scale can provide an understanding of micro- and macro-scale phenomena that are governed by nanoscale physics [25]. Molecular phenomena at length scales that are hardly examinable by experiment can be investigated under the requirement that the force field applied provides an accurate description of atomic interactions. Secondly, MD simulations can be used to reduce time- and cost-intensive experimental testing in the context of material science. Minor changes on the molecular level may accumulate to produce a significantly different material response on the structural level. Numerical methods on the atomistic length scale can provide an efficient first prediction of these effects, whereas extensive testing would otherwise be required. In general, the development period can be significantly reduced by implementing computational methods, and these can be supplemented by an experimental confirmation for a final design.

Yu et al. [26] used atomistic simulations of nanocomposites consisting of cross-linked epoxy and different sized alumina (Al_2O_3) nanoparticles. A sequential bridging method was used that incorporates an effective interface as a representation of the particle–matrix interaction. A multi-scale framework for the prediction of the viscoelastic material properties of linear polymers was proposed by Li et al. [27]. Nanoscale MD simulations were used to derive a coarse-grained model which was used to obtain homogenised micro-scale material properties. A constitutive model has been proposed for the micro-scale that is based on the tube model of primitive paths. The authors note that the viscoelastic properties of entangled polymers can be directly predicted from the molecular level. Vu-Bac et al. [28] presented a multi-scale model for the prediction of the thermo-plastic behaviour that incorporates MD simulations. The yield surface was defined by using molecular simulation results in combination with the Argon model to account for rate dependency. Furthermore, the temperature effect on the elasto-plastic behaviour was also upscaled from the nanoscale model. A viscoelastic damage model for a nanocomposite, made of Boehmite nanoparticles and an epoxy matrix, was presented by Arash et al. [29], in which MD simulation results were combined with experimental data for the parameter identification. The Guth–Gold model is implemented to capture the amplified effective stiffness resulting from well-dispersed nanoparticles. The constitutive model was able to predict the uniaxial material response and results of the four-point bending test in very close agreement with experimental results for nanoparticle weight fractions up to 20%. This model was further enhanced to take the effect of short-fibre reinforcement into account [30].

Sophisticated phenomenological constitutive models that can reproduce the complex temperature-dependent material response of viscoelastic nanocomposites often come with the drawback of a large number of parameters, which require extensive experimental testing to be identified. Mostly, the material properties are determined regardless of their underlying physical meaning, leading to an inaccurate prediction of the material response outside the range of calibration. Physically based constitutive models are more favourable, since the parameters are related to physical quantities and thus allow for a more general prediction of the material response. Unfortunately, the accurate experimental identification of parameters related to physical mechanisms on the atomistic length scale is generally challenging and time and cost intensive. Considering rate and temperature effects together with the influence of matrix cross-linking and nanoscale additives increases the complexity even further.

The present study contributes three main innovations to the field of multi-scale modelling of the viscoelastic material behaviour of nanoparticle/epoxy nanocomposites. Firstly, the constitutive model presented by Arash et al. [29] is extended to finite temperatures below the glass-transition temperature. The effect of temperature on the elastic and hyperelastic response is captured by a modified Kitagawa model and the Argon model is used for the temperature-dependent viscoelasticity. Secondly, the material model is calibrated using purely experimental data obtained from tensile tests at different temperatures and strain rates. This calibration reveals the best predictive capabilities of the constitutive model, which is validated with independent experimental results for a range of nanoparticle weight fractions up to 15%. Thirdly, a combination of experimental and numerical MD simulation results is used to calibrate the constitutive model. This study shows that the simulation-based framework proposed can be used to significantly reduce the number of experimental tests required to calibrate the constitutive model without significant loss in accuracy. The present results emphasise the capabilities of atomistic simulations when used in the context of multi-scale modelling for the parameter identification in physical constitutive models.

2. Constitutive model for nanoparticle/epoxy nanocomposite

In the present study, the continuum formulation of a viscoelastic damage model proposed by Arash et al. [29] for nanoparticle/epoxy nanocomposites is extended to finite temperatures below the glass-transition temperature. For completeness, the constitutive model is repeated in the following and the implemented extensions are presented. The respective one-dimensional rheological model of the physically motivated constitutive model is presented in Fig. 1. The material response for large deformations due to rearrangement of molecule chains is described by the hyperelastic spring. The linear spring accounts for the initial linear response and the non-linear dashpot characterises the strain-rate dependency due to changes in the atomistic configuration.

A multiplicative decomposition into inelastic $\mathbf{F}_i$ (i.e. non-linear dashpot) and elastic deformation $\mathbf{F}_e$ (i.e. elastic spring) is used for the total deformation gradient

$$\mathbf{F} = \mathbf{F}_e\mathbf{F}_i. \tag{1}$$

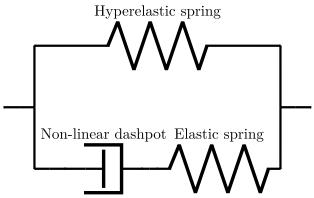

Fig. 1. Schematic representation of the constitutive model, consisting of a hyperelastic spring in parallel with a serial connection of a non-linear dashpot and an elastic spring.

The overall free energy can be decomposed into an equilibrium (hyperelasticity) and a non-equilibrium (viscoelasticity) part

$$\psi(\mathbf{C}, \mathbf{F}_i, d) = (1-d)\left[\psi_{eq}(\mathbf{C}) + \psi_{neq}\left(\mathbf{F}_i^{-T}\mathbf{C}\mathbf{F}_i^{-1}\right)\right], \tag{2}$$

with the right Cauchy–Green tensor being defined as $\mathbf{C} = \mathbf{F}^T\mathbf{F}$. Damage is modelled by a scalar damage variable $d \in [0, 1)$ with initial conditions $d = 0$. The eight-chain model [14] is used for the response of the equilibrium part (ψ_{eq}), i.e., the hyperelastic spring. The part of the free energy associated with the equilibrium deformation is given by

$$\psi_{eq} = nk\Theta\left(\sqrt{N}\Lambda_{chain}\beta + N\ln\frac{\beta}{\sinh\beta}\right), \tag{3}$$

$$\beta = l^{-1}\left(\frac{\Lambda_{chain}}{\sqrt{N}}\right). \tag{4}$$

Here n is the chain density, k is Boltzmann's constant and Θ is the absolute temperature. The number of rigid links between two cross-links is defined as N and the Langevin function is $l(x) = \coth(x) - 1/x$. The amplified chain stretch is given as

$$\Lambda_{chain} = \sqrt{X\left(\lambda_{chain}^2 - 1\right) + 1}, \tag{5}$$

as proposed by Bergström and Boyce [31], with λ_{chain} being the respective stretch of each chain in the eight-chain model defined as $\lambda_{chain} = \sqrt{\bar{I}_1/3}$. The first invariant $\bar{I}_1 = \mathrm{tr}\left[\bar{\mathbf{B}}\right]$ of the left Cauchy–Green tensor $\bar{\mathbf{B}} = \bar{\mathbf{F}}\bar{\mathbf{F}}^T$ is used with $\bar{\mathbf{F}} = J^{-1/3}\mathbf{F}$ and $J = \det[\mathbf{F}]$.

To take the effect of nanoparticles into account, the Guth–Gold model is implemented, which defines the effective stiffness of a matrix with well-dispersed nanoparticles as $\langle E\rangle = XE_m$ [32,33]. The amplification factor X is defined as $X = 1 + 3.5\nu + 18\nu^2$ for a given volume fraction of ν, as proposed by Qi [20]. This model is used, since the viscoelastic properties are dominated by the epoxy material response, in which the nanoparticles act as rigid body reinforcement. No large deformation or failure of nanoparticles is assumed due to their significantly higher stiffness. Therefore, the effect on the nanocomposite material behaviour can be considered using the amplification factor X, which only depends on the volume fraction.

The non-equilibrium part ψ_{neq} associated with the non-linear viscoelastic deformation is given by the viscoelastic combination of an elastic spring and a non-linear dashpot. The Hencky model is used for the elastic spring of the non-equilibrium part ψ_{neq} [34,35]

$$\psi_{neq} = X\mu_e\left|\mathbf{E}_e^0\right|^2 + \frac{1}{2}X\lambda_e\left(\mathrm{tr}\mathbf{E}_e\right)^2. \tag{6}$$

Here, the logarithmic elastic strain $\mathbf{E}_e = \ln\left(\mathbf{V}_e\right)$ is used and the deviatoric part is defined as $\mathbf{E}_e^0 = \ln\left(J_e^{1/3}\mathbf{V}_e\right)$, with $J_e = \det\left(\mathbf{F}_e\right)$. The left stretch tensor $\mathbf{V}_e$ of the elastic deformation gradient is obtained from the polar decomposition $\mathbf{F}_e = \mathbf{V}_e\mathbf{E}_e$, in which $\mathbf{R}_e$ is the rotation tensor. The Lamé moduli μ_e and λ_e are used to characterise the initial linear material response. It is noteworthy that among the various commonly used finite strain measures, the Hencky or logarithmic strain tensor has a wide applicability in modelling elastic behaviour at finite deformations [36,37].

Finally, the total Cauchy stress is given by the damage-reduced sum of total stress from hyperelastic rubbery ($\mathbf{T}_{eq}$) and viscoelastic ($\mathbf{T}_{neq}$) contributions

$$\mathbf{T} = (1-d)\left(\mathbf{T}_{eq} + \mathbf{T}_{neq}\right), \tag{7}$$

$$\mathbf{T}_{eq} = \frac{X\mu_{he}(\Theta)}{J\Lambda_{chain}}\frac{l^{-1}\left(\frac{\Lambda_{chain}}{\sqrt{N}}\right)}{\frac{1}{\sqrt{N}}}\mathrm{dev}\left[\bar{\mathbf{B}}\right], \tag{8}$$

$$\mathbf{T}_{neq} = \frac{X}{J_e}\left(2\mu_e(\Theta)\mathbf{E}_e^0 + \lambda_e(\Theta)\mathrm{tr}\left[\mathbf{E}_e\right]\mathbf{I}\right). \tag{9}$$

Here, it is worth noting that the material parameters μ_{he}, μ_e and λ_e are now specified as a function of the temperature Θ to account for the effect of finite temperatures on the elastic and hyperelastic response. As shown by Arash et al. [29], the time derivative of the inelastic deformation gradient can be expressed by

$$\dot{\mathbf{F}}_i = \frac{\dot{\varepsilon}_i}{\sigma_{neq}}\mathrm{dev}\left[\mathbf{T}_{neq}\right]\mathbf{F}_i. \tag{10}$$

with the assumption that the rate of spin is zero and only a rate of stretching exists. Here, $\dot{\varepsilon}_i$ denotes the viscoelastic flow rate, which depends on the equivalent stress σ_{neq} for which the Frobenius norm of the deviatoric part of the driving stress is used, $\sigma_{neq} = \left\|\mathrm{dev}\left[\mathbf{T}_{neq}\right]\right\|_F$. In contrast to the original formulation that incorporates the Eyring model, the Argon model is used for the viscoelastic flow rate

$$\dot{\varepsilon}_i = \dot{\varepsilon}_0\exp\left[\frac{\Delta H}{k\Theta}\left(\left(\frac{\sigma_{neq}}{\sigma_0}\right)^{5/6} - 1\right)\right]. \tag{11}$$

The Argon model is characterised by three parameters: a pre-exponential factor $\dot{\varepsilon}_0$, the activation energy ΔH and an athermal yield stress σ_0. In a recent study by Unger et al. [38] it was shown that the Argon model leads to a better agreement with experimental results across a broad range of strain rates and temperatures compared to the Eyring model. Finally, the damage evolution is characterised by the damage parameter A and has the form

$$\dot{d} = A(1-d)\Lambda_{chain}^{max}, \tag{12}$$

as proposed by Qi [20] and Miehe [7]. The amplified chain stretch evolves to

$$\Lambda_{chain}^{max} = \begin{cases} 0 & \Lambda_{chain} < \Lambda_{chain}^{max} \\ \Lambda_{chain} & \Lambda_{chain} \geq \Lambda_{chain}^{max} \end{cases} \tag{13}$$

as proposed by Qi and Boyce [19].

Beside the replacement of the Eyring model with the Argon model, the main extension to the original formulation is the effect of temperature on the material response (see Eqs. (8) and (9)). The general temperature dependency of the Young's modulus is shown in Fig. 2(a), as presented by Sperling [39]. In the glassy regime (1), the stiffness decreases slightly with increasing temperature, whereas close to the glass-transition region a significant drop is observable [40,41]. In the actual glass-transition region (2), the modulus decreases by several decades to a rubbery plateau region (3), where a nearly constant value is reached.

For the present approach, an accurate representation of the behaviour in the glassy regime is necessary. One common model which takes the temperature-dependent Young's modulus into account is the Kitagawa model. The general behaviour of the original Kitagawa formulation is shown in Fig. 2(b) by the green line. It was first proposed in [42] and successfully implemented in constitutive models by Poulain et al. [9] and Vu-Bac et al. [28]. However, due to its formulation, the original Kitagawa model cannot account for the sudden drop in the Young's modulus at temperatures that are still in the glassy regime but close to the glass-transition region. In order to cover these important phenomena, a modified version of the Kitagawa model [42]

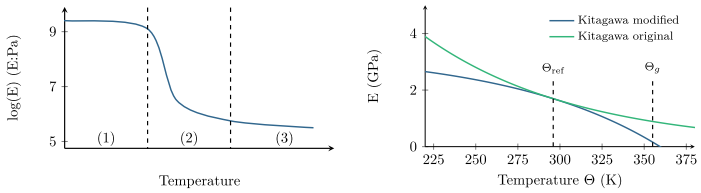

Fig. 2. Effect of temperature on the Young's modulus: (a) Schematic representation by Sperling [39], divided into three regions of viscoelastic behaviour for an amorphous polymer: (1) Glassy regime, (2) Glass transition from glassy into rubbery regime and (3) Rubbery plateau region, and (b) Comparison of original and modified Kitagawa model for temperatures in the glassy regime (region 1 in left Figure (a)).

is implemented with the following equations for the elastic response ($\mu_e(\Theta)$, $\lambda_e(\Theta)$) and hyperelastic response ($\mu_{he}(\Theta)$)

$$\mu_e(\Theta) = \mu_{e,\text{ref}}\left(2 - \exp\left[\alpha_e\left(\Theta - \Theta_{\text{ref}}\right)\right]\right), \tag{14}$$

$$\lambda_e(\Theta) = \lambda_{e,\text{ref}}\left(2 - \exp\left[\alpha_e\left(\Theta - \Theta_{\text{ref}}\right)\right]\right), \tag{15}$$

$$\mu_{he}(\Theta) = \mu_{he,\text{ref}}\left(2 - \exp\left[\alpha_{he}\left(\Theta - \Theta_{\text{ref}}\right)\right]\right). \tag{16}$$

These functions are phenomenologically motivated and depend on a reference value obtained at a reference temperature Θ_{ref}, together with a corresponding scaling parameter α. Fig. 2(b) shows the behaviour of the modified Kitagawa model that is able to capture the sudden drop in stiffness close to the glass transition temperature Θ_g. Individual scaling parameters α_e and α_{he} are used for elasticity and hyperelasticity. In both cases, the Poisson's ratio is assumed to be temperature independent. It is important to note that, with the present approach, the constitutive model is limited to temperatures below the glass-transition region, as the modified Kitagawa model converges to $-\infty$ for $\Theta \to \infty$ (see Fig. 2(b)).

3. Material and methods

3.1. Material

3.1.1. Epoxy system

For the present study, the epoxy resin AIRSTONE 880E and the hardener AIRSTONE 886H, both commercially available from Olin Epoxy, were chosen. The AIRSTONE epoxy system is particularly characterised by a low viscosity, which allows for the infusion of large and thick-walled structures, such as wind turbine rotor blades. The chemical composition is specified on the material data sheet [43,44] and summarised in Table 1. Fig. 3 shows the corresponding chemical structures of the resin and hardener, and the mixing ratio by weight is specified as 100 parts epoxy to 31 parts hardener. The density of the cured system is given by the manufacturer as 1.1 g/cc. The glass-transition temperature is specified to be 82 °C (≈ 355 K).

3.1.2. Boehmite nanoparticles

Boehmite nanoparticles (BNP), commercially available from Sasol Germany GmbH, were chosen as a nanoscale matrix additive. The spray-dried boehmite nanoparticles have a primary size of 14 nm and are modified by adding a taurine group at the nanoparticle surface (HP14T). These nanoparticles have already been comprehensively studied in the context of nanocomposites [3,45–48]. The crystalline structure of the oxide-hydroxide mineral (γ-AlO(OH)) was characterised by Bokhimi et al. [49] using X-ray powder diffraction. Fig. 4 shows the respective orthorhombic unit cell, which consists of a double-layered structure of oxygen octahedrons around central aluminium atoms. For a study on the mechanical behaviour of pure boehmite, the reader is referred to Fankhänel et al. [4].

3.2. Molecular dynamics

The molecular curing simulation uses an in-house MD framework (MDFEM), developed by Nasdala et al. [50], Nasdala et al. [51] and Nasdala et al. [52], whereas the molecular tensile and shear simulations were performed using the Large-scale Atomic/Molecular Massively Parallel Simulator (LAMMPS) [53]. The DREIDING force field by Mayo et al. [54] is used with different potentials for the molecular modelling and load simulations. All simulations are performed with periodic boundary conditions and a maximum time-step size of 1 fs. The following sub-sections present the specific procedure for the molecular modelling, as well as for the tensile and shear tests performed. The results and derivation of material properties for the present constitutive model are given in Section 4.

3.2.1. Molecular curing simulations

There is strong evidence that accurate molecular modelling is of great importance for the prediction of realistic material parameters of polymeric materials [55–58]. To achieve a reliable prediction of the material behaviour it is essential that the molecular network topology is a realistic representation of the cured epoxy system. The molecular modelling employed uses the experimentally validated procedure proposed by Unger et al. [59], in which the distance between two reactive groups is used as the criterion for bond formation. The final dense network topology is generated by the reaction of the epoxy groups of the resin with the amine groups (NH_2) of the hardener. The two chemical reactions are shown in Fig. 5. The primary amines which are initially present can react with one reactive epoxy site to form secondary amines (Fig. 5(a)) and then with an additional epoxy group to form the final tertiary amines (Fig. 5(b)). The epoxy groups can only react once, as it has been shown experimentally that no reaction between the hydroxyl groups of the epoxy molecules and the reactive epoxy sites (etherification) takes place [59].

The open-source packages PACKMOL [60] and Open Babel [61] are employed in the pre-processing. Before starting the cross-linking simulation, the simulation box, created by randomly distributing unlinked molecules, is subjected to a prior energy minimisation. The cross-linking simulation is started with the uncured epoxy system and the following steps are conducted:

(1) Initial equilibration and linear increase of the temperature to the curing temperature within 500 ps;
(2) Bond formation of one bond with the shortest possible length, below the chosen cut-off of 10 Å for the reaction distance, between two reactive sites;
(3) Subsequent equilibration for a time period of 2.5 ps;
(4) Iteration of step 2 and 3 until chosen simulation duration is reached.

The respective parameters (duration of the individual steps and cut-off value) were chosen to ensure a well-equilibrated system within a

Table 1
Overview of the chemical composition of the epoxy system (names, mixing ratios and CAS identification numbers). Corresponding chemical structures are shown in Fig. 3.

	Name	Proportion (wt%)	CAS No.
Resin	Bisphenol A diglycidyl ether	75–100	25068-38-6
(AIRSTONE 880E)	1,4-Butanediol diglycidyl ether	10–25	2425-79-8
	Alkyl (C12-C14) glycidyl ether	1–5	68609-97-2
Hardener	α, ω-poly(oxypropylene)diamine	50–75	9046-10-0
(AIRSTONE 886H)	3-(aminomethyl)-3,5,5-trimethyl-cyclohexanamine	25–50	2855-13-2
	2,4,6-tris[(dimethylamino)methyl]phenol	1–5	90-72-2

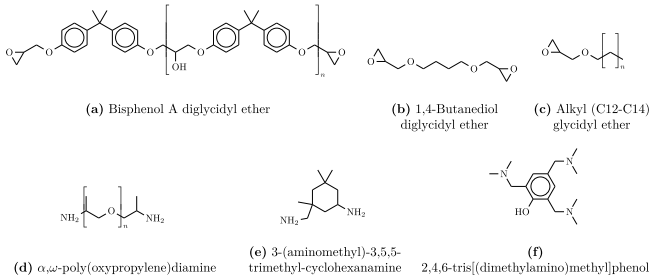

Fig. 3. Chemical structures of all molecules in the epoxy system studied: (a)–(c) chemical components of the epoxy resin and (d)–(f) chemical components of the hardener.

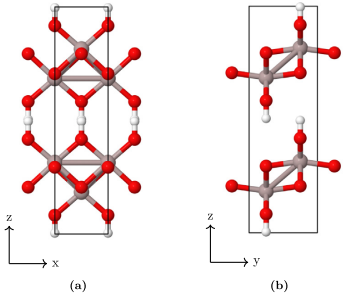

Fig. 4. Lateral view of the atomistic boehmite unit cell structure: (a) in the x–z plane and (b) in the y–z plane.

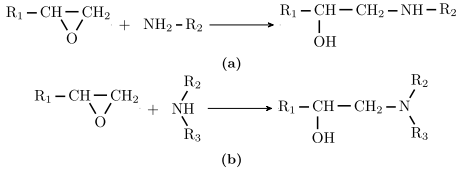

Fig. 5. Polymerisation reactions during curing: (a) epoxy site with a primary amine to form a secondary amine, (b) epoxy site with a secondary amine to form a tertiary amine.

reasonable computational time. Harmonic potentials are used for all bonded interactions and the Morse potential is used for the physical interactions. For all steps, an isothermal–isobaric ensemble (NPT) with atmospheric external pressure is used, with temperature and pressure controlled by a Nosé–Hoover thermostat and Parrinello–Rahman barostat [62]. The time step size was kept constant at 1 fs. Three-dimensional periodic boundary conditions are used within the dynamic cross-linking, allowing bond formation across box boundaries. For more detailed information on the molecular curing procedure, the assumptions made and the experimental validation, the reader is referred to Unger et al. [59] Using the cross-linked simulation model of the fully cured epoxy system, molecular loading simulations were performed, and these are presented in the following.

3.2.2. Molecular tensile simulations

Molecular tensile tests were performed to characterise the viscoelastic dashpot. The bonded interactions are represented by the Morse potential and the harmonic potentials are used for the angle and dihedral interactions. Physical interactions are modelled using the Lennard-Jones (12,6) potential. A cut-off value of 15 Å was chosen for the physical interactions combined with neighbour updating. The tensile tests were performed using an isothermal–isobaric ensemble (NPT) with a gradually increasing deformation in the tensile direction. The atom positions are remapped every time step and the external pressure in the lateral direction is kept at zero to allow a natural Poisson's ratio. Temperature and pressure are controlled by a Nosé–Hoover thermostat and Parrinello–Rahman barostat, respectively. For the derivation of material properties, a constant output frequency in terms of strain was chosen instead of an absolute time. The present study was conducted with a constant output frequency of $\Delta\epsilon = 10^{-4}$, so that for an increase of one percent in strain, one thousand outputs are written. Due to this requirement, the time step size needs to be reduced to a minimum of 0.02 for the fastest strain rate of 5×10^9 1/s. However, a constant output frequency in terms of strain rate assures a comparable accuracy across all strain rates investigated. The investigated strain rates and corresponding time step sizes are presented in Table 2. For further information on the procedure of atomistic tensile simulation, the reader is referred to [38].

3.2.3. Molecular shear simulations

In the present study, the time-independent configuration change of the cured epoxy is characterised by shear test simulations. For these

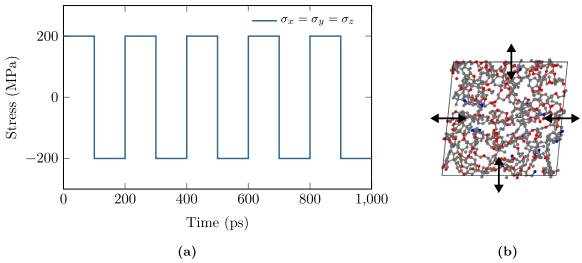

Fig. 6. Schematic illustration of molecular shear simulations: (a) hydrostatic pressure loading cycles applied to sheared simulation box and (b) visualisation of cyclic perturbations in hydrostatic tensile/compression acting on sheared simulation box.

Table 2
Time step sizes for the investigated strain rates, based on a constant output frequency in terms of strain with a value of $\Delta\varepsilon = 10^{-4}$.

Strain rate (1/s) $\dot{\varepsilon}$	Time step size (fs) Δt
5×10^9	0.02
1×10^9	0.1
5×10^8	0.2
1×10^8	1.0
5×10^7	1.0
1×10^7	1.0
5×10^6	1.0

tests, the simulation configuration (ensemble, force field potentials, etc.) was identical to that used for the tensile simulations. The cross-linked and relaxed simulation boxes are deformed at a shear rate of 10^7 1/s to a maximum shear strain of one percent in the x–y, x–z and y–z directions. In order to derive the shear modulus of the material under quasi-static loading, an artificial relaxation procedure is used, as presented by Yu et al. [63]. Small cyclic perturbations in the hydrostatic tensile/compressive stresses are applied to the system to enforce a relaxation to the quasi-static response by allowing local energy barriers to be overcome. The time period of the cyclic stresses was chosen to be 100 ps. The amplitude was chosen as $\sigma_x = \sigma_y = \sigma_z = \pm 200$ MPa, but is not sensitive to the relaxation process [63]. The hydrostatic pressure loading cycles applied to the sheared simulation box are shown in Fig. 6(a) and Fig. 6(b) illustrates the cyclic pertubations in hydrostatic tensile/compression acting on the sheared simulation box. This approach led to good results for the rate-independent shear modulus, as presented by Arash et al. [29] and Arash et al. [30].

3.3. Experiments

3.3.1. Manufacturing

Manufacturing the nanocomposite test specimen starts with mixing the boehmite nanoparticles, introduced in Section 3.1.2, with the resin component of the epoxy system, presented in 3.1.1. As the nanoparticles are supplied as a dry powder with clustered agglomerations, a dispersion process employing a three-roll mill (Exakt, 80E) is used, which is shown in Fig. 7(a). Possible agglomerations are broken up by the mechanical shear loads until the nanoparticles are well dispersed, no further particle size reduction is observed and only a negligible number of minor agglomerates is left. Using the dispersed nanoparticles, the final nanocomposite system is mixed according to the manufacturer's guidelines, with an epoxy-hardener mixing ratio of 100 : 31 by weight. The mixture is de-gassed at room temperature and poured into a mould with a depth of 2.7 mm for the curing. The nanocomposite plates are cured at 80° C for 5 hours. A CNC milling machine is used to cut the plates into a standardised dog-bone shape according to DIN EN ISO 527, shown in Fig. 7(b). The test specimen with a cross-sectional area of 10 mm × 2.7 mm is shown in Fig. 8. For the stress calculation, the average of the exact width and thickness measured at three cross-sections along the narrow section of the dog bone (indicated by dashed lines in Fig. 8) was used for each specimen.

3.3.2. Mechanical tests

A electromechanical universal axial testing machine (Zwick 1481) combined with an extensometer of type MTS 776 was used for tensile tests in a climatic chamber according to DIN EN ISO 527 (see Fig. 7(c)). In order to investigate the strain rate effect, tensile tests to failure were conducted at three different test speeds: 0.01 mm/min, 0.1 mm/min and 1 mm/min under standard laboratory conditions (23 °C and 50% humidity). Based on the specimen geometry (Fig. 8), this results in strain rates between 1.44×10^{-6} 1/s and 1.44×10^{-4} 1/s. The effect of temperature was investigated by additional tensile tests at the standardised test speed of 1 mm/min, at temperatures of 53 °C and −27 °C and both at 50% relative humidity. The testing environment was kept constant at the desired temperature for at least 30 minutes prior testing. The effect of nanoparticle content was studied using the standardised test configuration (test speed of 1 mm/min at standard laboratory conditions) for weight fractions of 5, 10 and 15 percent.

4. Results and discussion

This section presents and discusses two different cases of parameter identification for the present extension of the constitutive model to temperatures below the glass-transition temperature. As the experimental results are essential for both cases, they are presented at the beginning in Section 4.1.

In the first case, the constitutive model is calibrated using purely experimental results from tensile tests at different temperatures and strain rates. Thus, it is possible to calibrate all parameters of the constitutive model, including the temperature dependency of all elements and the strain rate dependency due to the non-linear dashpot. By using purely experimental results for the calibration, the general capabilities of the material model are investigated, i.e., it can be assessed how well the constitutive model reproduces the material response. A validation for this case is performed by the comparison of predicted and experimentally measured stress–strain response for three nanocomposite materials with nanoparticle fractions of 5, 10 and 15 percent by weight, which were not used in the parameter identification.

In the second case, experimental results are used only for the calibration of the temperature-dependent material response. The experiments at different strain rates are replaced by MD simulations that allow the parameters of the Argon model used for the non-linear dashpot to be identified. Also, the hyperelastic spring is calibrated using simulation data from atomistic shear tests. The aim is to investigate

Table 3
Overview of the utilisation of experimental test configurations for the first case (parameter identification using purely experimental data).

	Temperature Θ (K)	Strain rate $\dot{\varepsilon}$ (1/s)	BNP weight fraction (%)	
Parameter identification	296	1.44×10^{-4}	0	Reference (EN ISO 527)
	246	1.44×10^{-4}	0	Variation of temperature
	326	1.44×10^{-4}	0	Variation of temperature
	296	1.44×10^{-5}	0	Variation of strain rate
	296	1.44×10^{-6}	0	Variation of strain rate
Experimental validation	296	1.44×10^{-4}	5	Nanocomposite
	296	1.44×10^{-4}	10	Nanocomposite
	296	1.44×10^{-4}	15	Nanocomposite

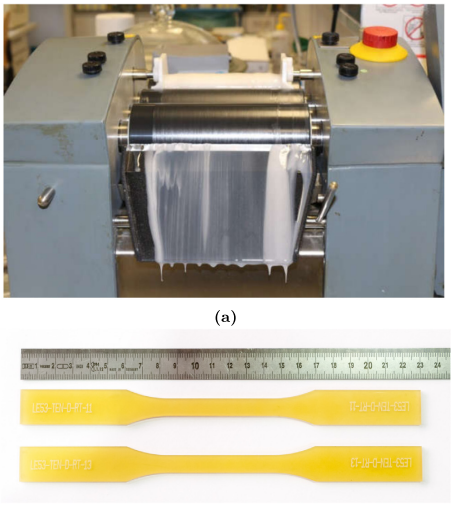

Fig. 7. Experimental procedure: (a) Dispersion process using a three-roll mill, (b) Nanocomposite dog-bone test specimen prepared for testing and (c) Tensile test to failure in climatic chamber with extensometer.

and assess the capabilities of numerical simulations for the parameter identification in constitutive models. Finally, a summary and discussion of results are given and an assessment of the predictive capabilities of the multi-scale model is provided.

4.1. Experimental results

Experimental tensile tests were conducted using variations of the standardised test configuration. Firstly, tests at two different temperatures, Θ = 246 K and Θ = 326 K, were performed at the standardised strain rate, without any nanoparticles added. Secondly, two variations of the strain rate were tested at room temperature, also without any nanoparticles added. The third variation focused on the effect of nanoparticles, as weight fractions of 5, 10 and 15 percent were investigated using the standardised test configuration. The results are presented in Fig. 9. The effect of temperature on the stress–strain response, shown in Fig. 9(a), follows the expected behaviour as the stress increases with decreasing temperature. This leads to a higher initial stiffness and yield stress. The temperatures cover a range of 80 K in the glassy regime with the glass-transition temperature at 82 °C (≈ 355 K). Fig. 9(b) shows the effect of the strain rate as the yield stress increases with increasing strain rate. The initial stiffness is not sensitive to the strain rates tested. The effect of the nanoparticle weight fraction is shown in Fig. 9(c). With increasing nanoparticle content, the initial stiffness and the yield stress increase. Beside this reinforcing effect on strength and stiffness, a failure at lower strain values is observable (i.e., more brittle material behaviour) with increasing nanoparticle fraction.

4.2. Case 1 - parameter identification using purely experimental data

The first case investigates the general capabilities of the constitutive model to reproduce the material behaviour. Table 3 gives an overview of the experimental data used for the parameter identification and experimental validation. The parameters were identified based on all available experimental data obtained with the pure epoxy material (no nanoparticle content). Three individual stress–strain results with Boehmite nanoparticle (BNP) weight fractions between 5 and 15 percent are used for the assessment of the predictive capabilities.

4.2.1. Parameter identification

All parameters of the constitutive model were identified by a single-objective genetic algorithm [64] of an in-house optimisation framework. Several optimisation runs were conducted until convergence, each with a starting population of 900, to assure the global maximum is found. The complete stress–strain curve of five individual experimental results is used in the optimisation. For each stress–strain curve, the error was defined by the square root of the sum of squares (euclidean norm) of the difference between the experimental data and material model prediction. The objective function was chosen to be the euclidean norm of all five individual errors. The identified parameter set with the smallest error is presented in Table 4, for which the reference temperature was chosen to be room temperature.

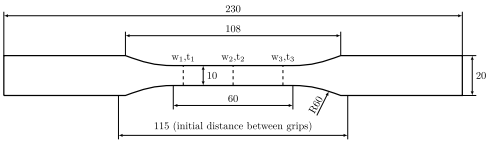

Fig. 8. Planar dimensions of the dog-bone specimens (see Fig. 7(b)) with a thickness of 2.7 mm used for tensile tests. All dimensions are in millimetres. Dashed lines indicate the positions of measured width and thickness for calculating the average cross-section.

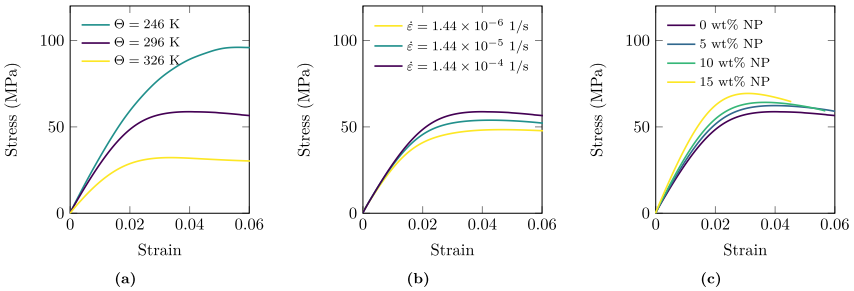

Fig. 9. Experimental tensile test results: (a) Effect of temperature at the default strain rate of $\dot{\varepsilon} = 1.44 \times 10^{-4}$, (b) Effect of strain rate at the default temperature of $\Theta = 296$ K and (c) Effect of nanoparticle weight fraction at the default test configuration of $\Theta = 296$ K and $\dot{\varepsilon} = 1.44 \times 10^{-4}$.

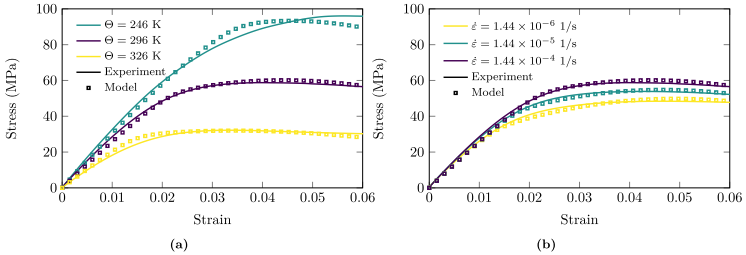

Fig. 10. Comparison of experimental stress–strain response and prediction for the configurations used within the parameter identification: (a) variation of temperature and (b) variation of strain rate.

The predictions of the yield stress for the variation of temperatures (a) and strain rates (b) are shown in Fig. 10. The calculated stress–strain response agrees very well with the experimental data. The largest deviation is identifiable for the default strain rate at the lowest temperature of 246 K, with the strain at yield point occurring earlier compared to the experimental results. However, the initial stiffness and post-peak softening behaviour is well predicted for all configurations. Furthermore, the effect of different strain rates is perfectly reproduced with a very good agreement with experimental data.

4.2.2. Experimental validation

Fig. 11 shows the prediction of the stress–strain response for the configurations with nanoparticle weight fractions of 5%, 10% and 15%. Comparison with these experimental data, which were not used in the parameter identification, allows an assessment of the predictive capabilities. For the configuration with the largest fraction of nanoparticles (15 wt%), a deviation of the yield stress is identifiable. The constitutive model underestimates the yield stress by approximately 5 MPa (≈ 7%). For the configurations with nanoparticle fractions of 5 and 10 weight percent, the yield stress agrees very well with experimental data. These results highlight the predictive capability of the constitutive model, which is able to reproduce the material behaviour across a range

Table 4
Identified parameters using five individual experimental stress–strain curves (Case 1 - Parameter identification using purely experimental results). The reference temperature was chosen to be $\Theta_{ref} = 296$ K.

	Parameter		Value
Hyperelastic spring	$\mu_{hr,ref}$	(MPa)	353.67
	α_{hr}		0.0159
	N		12.67
Linear spring	$\mu_{v,ref}$	(MPa)	623.42
	$\lambda_{v,ref}$	(MPa)	2493.70
	α_v		1.709×10^{-6}
Non-linear dashpot	$\dot{\varepsilon}_0$	(1/s)	8.9207×10^{11}
	σ_0	(MPa)	140.65
	ΔH	(J)	2.0324×10^{-19}
Damage	A		336.58

Table 5
Overview of which experimental results were used for the parameter identification and experimental validation for the second case (parameter identification using experimental and numerical data).

	Temperature Θ (K)	Strain rate $\dot{\varepsilon}$ (1/s)	BNP weight fraction (%)	
Parameter identification	296	1.44×10^{-4}	0	Reference (EN ISO 527)
	246	1.44×10^{-4}	0	Variation of temperature
	326	1.44×10^{-4}	0	Variation of temperature
Experimental validation	296	1.44×10^{-5}	0	Variation of strain rate
	296	1.44×10^{-6}	0	Variation of strain rate
	296	1.44×10^{-4}	5	Variation of nanoparticle fraction
	296	1.44×10^{-4}	10	Variation of nanoparticle fraction
	296	1.44×10^{-4}	15	Variation of nanoparticle fraction

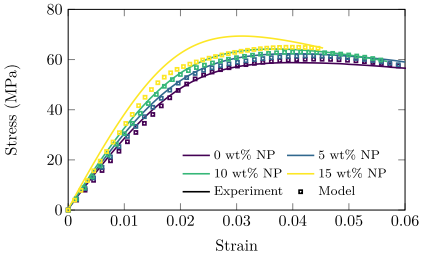

Fig. 11. Experimental validation in terms of prediction of stress–strain response for experiments which were not used in the parameter identification, with nanoparticle weight fractions between 5% and 15%.

of strain rates, temperatures and nanoparticle fractions. A detailed summary and comparison with the results of the following second case studied are given in Section 4.4.

4.3. Case 2 - parameter identification using experimental and numerical data

The second case investigates the capabilities of MD simulations for the replacement of experiments. Therefore, molecular simulation boxes are generated and investigated under tensile and shear loading to derive input parameters for the constitutive model. This section is structured as follows.

Firstly, the molecular modelling is presented, which is essential for a reliable derivation of the material properties and from which the parameter N (number of rigid links between two cross-links) is obtained. Subsequently, the results of molecular simulations with tensile and shear load cases are presented. Molecular tensile tests at combinations of various strain rates and temperatures are conducted to characterise the material's viscoelastic response by identifying the parameters for the Argon model ($\dot{\varepsilon}_0$, σ_0 and ΔH). Molecular shear tests are performed to determine the shear modulus ($\mu_{he,\mathrm{ref}}$) needed for the hyperelastic equilibrium response within the constitutive model. For this case, the assumption is made that both temperature scaling parameters are identical (i.e., $\alpha_e = \alpha_{he}$), which allows the derivation of the reference shear modulus $\mu_{he,\mathrm{ref}}$ at the reference temperature only, which is chosen to be room temperature (Θ_{ref} = 296 K). By following this approach, experimental results obtained from tensile tests at just three different temperatures are required for the identification of the remaining parameters ($\mu_{e,\mathrm{ref}}$, $\lambda_{e,\mathrm{ref}}$, α_e, A). Table 5 shows which experimental results were used for the parameter identification and experimental validation. An experimental validation is conducted using the results obtained with a variation of the strain rate and with different Boehmite nanoparticle weight fractions.

4.3.1. Molecular curing simulation

In the present study, four simulation boxes with a size of 60 Å × 60 Å × 60 Å were generated according to the molecular modelling procedure presented in Section 3.2.1. Due to the constant ratio of the first and second epoxy/hardener molecules, as well as the specified ratio of 100 parts epoxy to 31 parts hardener, all simulation boxes consist of the same number of individual molecules and 10547 atoms. The final degree of epoxy conversion converges to a value of 94.77% with a standard deviation of 1.21%. The evolution of reactive amine groups as a function of the epoxy conversion is shown in Fig. 12. The solid lines show the results of the numerical molecular modelling, whereas the dashed lines show the results of experimental near-infrared spectroscopy data from a previous study [59]. The simulation results are in good agreement with experimental data and lead to a final network topology characterised by 87.64% tertiary amines and 8.76% secondary amines. Only 3.6% of all amine groups are in the initial state of (non-reacted) primary amines. For a detailed presentation and discussion of these results, the reader is referred to Unger et al. [59]. From the cross-linked simulation box, the parameter N, the number of rigid links between two cross-links, is obtained with a value of 2.44.

Due to the sequential bond formation followed by a subsequent period of equilibrium for 2.5 ps, the procedure ensures a well-equilibrated simulation box. However, since the potentials of both bonded and non-bonded interactions are changed for the following load simulations,

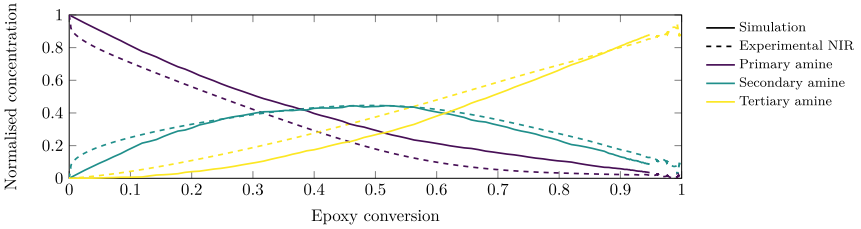

Fig. 12. Evolution of reactive groups during the cross-linking simulation in terms of the relative change of reactive amine groups as a function of the epoxy conversion.

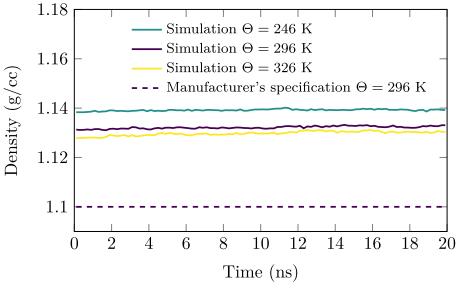

Fig. 13. Density as a function of additional relaxation time after updating the bonded and non-bonded potentials for the tensile simulation.

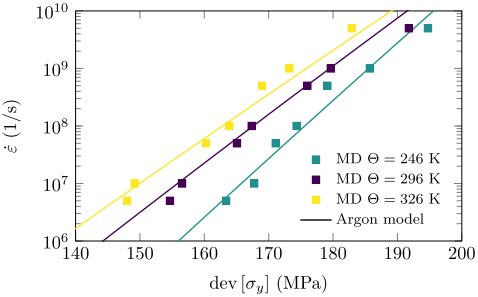

Fig. 15. Strain rate as a function of the deviatoric yield stress for all investigated temperatures: Simulation data obtained by MD (squares) and prediction using the Argon model after parameter identification (solid lines).

an additional equilibration is necessary. Therefore, each simulation box was relaxed at each temperature at which the load simulations were performed (246 K, 296 K, 326 K) individually. For this additional relaxation the isothermal–isobaric ensemble (NPT) with atmospheric external pressure is used, with temperature and pressure controlled by a Nosé–Hoover thermostat and Parrinello–Rahman barostat [62]. The time step size was kept constant at 1 fs and the relaxation time was chosen to be 20 ns to ensure a completely equilibrated system. As criteria for a proper relaxation the potential energy, temperature, pressure and density were analysed and all four values converged within the 20 ns relaxation time. The average density for all simulation boxes as a function of the relaxation time is shown in Fig. 13, with solid lines for each temperature. The manufacturer's specification for the density at room temperature is indicated by a dashed vertical line. For the case of room temperature, the density converges to a value of 1.13 g/cc, which is in very close agreement with the manufacturer's specification of 1.1 g/cc. It is worth noting that the general effect of temperature on the density (i.e., thermal expansion) is qualitatively covered, as the density decreases with increasing temperature. A quantitative study of the thermomechanical properties (coefficient of thermal expansion and glass-transition temperature) is out of the scope of this study.

4.3.2. Molecular tensile simulations

Molecular tensile tests were performed according to the procedure presented in Section 3.2.2 at temperatures of 246 K (≈ −27 °C), 296 K (≈ 23 °C) and 326 K (≈ 53 °C) with strain rates between 5×10^6 1/s and 5×10^9 1/s. The temperatures cover a range of 80 K in the glassy regime with the glass-transition temperature at 82 °C (≈ 355 K).

To identify the parameters of the Argon model for the viscoelastic dashpot, the values of the yield stress as a function of the strain rate and temperature are used. Firstly, an optimised piecewise cubic spline interpolation is used to fit each individual simulation result in order to avoid any effects caused by typical MD stress fluctuations. Secondly, the yield stress was defined as the point at which the derivative of the stress with respect to the strain is zero (i.e., the first maximum of the spline interpolation). This common criterion is used because it is assumed that the elastic strain rate vanishes at the yield point [9,28,29,40,65]. The horizontal tangent of the stress–strain response at the yield point indicates that the material is flowing without significant elastic contribution (i.e., only viscous flow appears for increasing strain above the yield point). Fig. 14 shows the average deviatoric yield stress with the standard deviation as a function of strain rate for each individual temperature. First of all, the strain rate effect is clearly visible with an increasing yield stress for increasing strain rate. By comparing the yield stress for a constant strain rate over all temperatures, the expected behaviour with changing temperature is identifiable. The yield stress decreases with increasing temperature. The largest standard deviation of all the averaged results shown has a value of ≈ 17 MPa, and is in the typical range of MD simulation scatter.

The results shown in Fig. 14 were used to identify the parameters of the Argon model ($\dot{\varepsilon}_0$, σ_0 and ΔH). An in-house single-objective grid search algorithm was used iteratively with decreasing boundaries and no constraints. Due to the underlying physical motivation of the Argon model, it is possible to define reasonable boundaries for the optimisation as the parameters have a physical meaning. To find the ideal

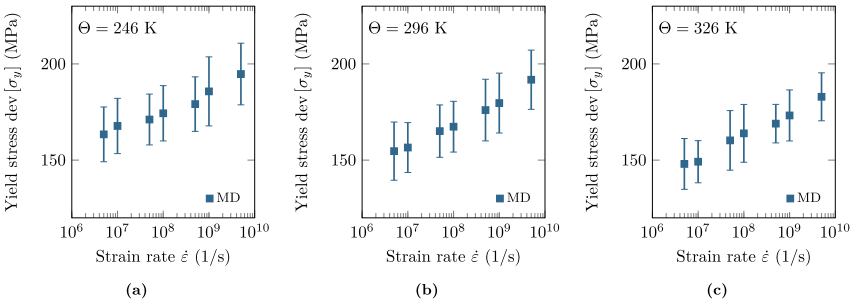

Fig. 14. Stress–strain response obtained by MD simulations at three different temperatures (all below the glass-transition temperature) and a range of strain rates: (a) 246 K, (b) 296 K and (c) 326 K.

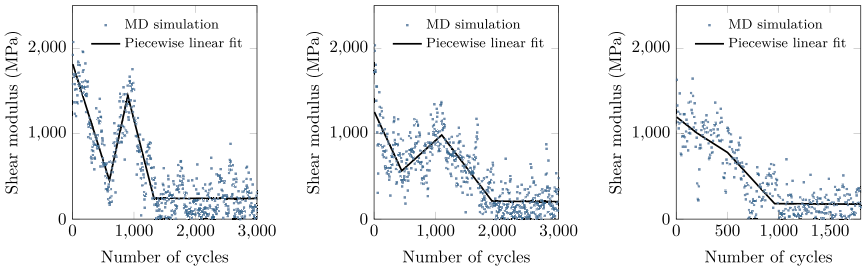

Fig. 16. Shear modulus against the number of loading/unloading cycles ($\sigma_x = \sigma_y = \sigma_z = \pm 200$ MPa) at room temperature ($\Theta = 296$ K), with an initial shear strain of 0.01.

parameter set, the euclidean norm of the difference between the yield stress obtained by MD simulation and the prediction of the Argon model was minimised. The parameters derived are: $\dot{\epsilon}_0 = 9.7746 \times 10^{11}$ 1/s, $\sigma_0 = 215.824$ MPa and $\Delta H = 1.9761 \times 10^{-19}$ J. The strain rate as a function of the deviatoric yield stress of the Argon model (see Eq. (11)) is shown in Fig. 15, with the identified parameter set used. The identified parameters are in good agreement with existing values in literature for the same epoxy system [29,30] and similar polymeric materials [40,66]. For a discussion of viscoelastic theories and an experimental validation of the Argon model, the reader is referred to Unger et al. [38].

4.3.3. Molecular shear simulations

Shear simulations following the procedure presented in Section 3.2.3 were performed to derive the rate-independent material response under shear loading, represented by the variable μ_{he}. Based on the assumption that both temperature scaling parameters are identical, only the value $\mu_{he,\mathrm{ref}}$ at the reference temperature needs to be derived. Three representative results for the variation of the shear modulus with respect to the number of cyclic stress perturbations are presented in Fig. 16. The artificial relaxation procedure leads to different trends in the shear modulus over the stress perturbation cycles as each system overcomes individual energy minima until convergence. A piecewise linear spline with three optimised knots is used to fit the simulation data and to identify a converged value. The shear modulus at the reference temperature converges on a value of $\mu_{he,\mathrm{ref}} = 205$ MPa with a standard deviation of 30 MPa.

4.3.4. Identification of remaining parameters using experimental data

The identification of the remaining parameters follows the same procedure presented in Section 4.2.1 for the first case. A single-objective genetic algorithm of an in-house optimisation framework is used. Since the number of unknown parameters is reduced from ten to four (compared to Section 4.2.1 and Table 4), the size of the starting population was chosen to be 300. For the identification, the complete stress–strain curve is used, but in contrast to the first case, only three experiments are needed. The stress–strain response at three different temperatures with the default strain rate was used (see Table 5). Several optimisation runs were performed, of which all converged on the same (global) minimum. Table 6 shows the final set of parameters obtained for the linear elastic spring element ($\mu_{e,\mathrm{ref}}$, $\lambda_{e,\mathrm{ref}}$ and α_e) together with the damage parameter (A). The reproduced stress–strain responses for the three different temperature configurations are shown in Fig. 17. Generally, a fair agreement with the experimental data is achieved, with two deviating phenomena identifiable. The strain at which the yield point is predicted is underestimated for the lowest temperature, which is similar to the prediction of the first case (compare with Fig. 10(a)). Also, the initial stiffness is slightly underestimated for the configurations with $\Theta = 296$ K and $\Theta = 326$ K.

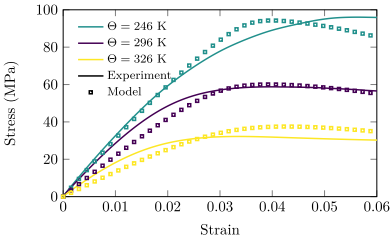

Fig. 17. Comparison of experimental stress–strain response and prediction for the experiments used within the parameter identification with a variation of the temperature.

4.3.5. Experimental validation

Fig. 18 shows the predictions for both remaining experimental configurations that were not used in the parameter identification. The stress–strain responses for varying strain rates are presented in Fig. 18(a). The same underestimation of the initial stiffness shown in Fig. 17 is identifiable, since the initial stiffness is not affected by the strain rate. However, the yield stress and the non-linear post-yield behaviour are in fair agreement with the experimental data. The yield stress for the standardised strain rate is in very good agreement, whereas the largest underestimation is observable for the slowest strain rate, with a deviation of ≈ 6 MPa (12%). Fig. 18 shows the prediction for the test configurations of nanocomposite materials with a nanoparticle fraction of 5, 10 and 15 weight percent. The yield stress for the material containing the largest fraction of nanoparticles is underestimated by ≈ 7 MPa (10%), which is a slightly larger deviation compared to the results of the first case (see Fig. 11). The parameter identification with both numerical and experimental data lead to a fair prediction without a significant loss of accuracy compared to the first case. The underestimation of initial stiffness can be seen as the strongest deviation compares to the first case, whereas the overall characteristic of the stress–strain response is very similar. This experimental validation shows that the predictive capabilities of the proposed constitutive model are not significantly compromised by using numerical data for the parameter identification. The following Section 4.4 provides a detailed summary and discussion of all results.

4.4. Summary and discussion

Comparing the experimental data with the results of both investigated cases allows the assessment of the capabilities of the constitutive

Table 6
Identified parameters using MD simulation data and three individual experimental stress–strain curves (Case 2 - Parameter identification using experimental and numerical data). The reference temperature was chosen to be $\Theta_{ref} = 296$K.

	Parameter		Value	Derived from
Hyperelastic spring	$\mu_{he,ref}$	(MPa)	205	Molecular shear simulation
	α_{he}		0.01093	$\alpha_{he} = \alpha_e$
	N		2.44	Molecular curing simulation
Linear spring	$\mu_{e,ref}$	(MPa)	605.79	Experimental tensile test
	$\lambda_{e,ref}$	(MPa)	2423.17	Experimental tensile test
	α_e		0.01093	Experimental tensile test
Non-linear dashpot	$\dot{\varepsilon}_0$	(1/s)	9.7746×10^{11}	Molecular tensile simulation
	σ_0	(MPa)	215.82	Molecular tensile simulation
	ΔH	(J)	1.9761×10^{-19}	Molecular tensile simulation
Damage	A		278.65	Experimental tensile test

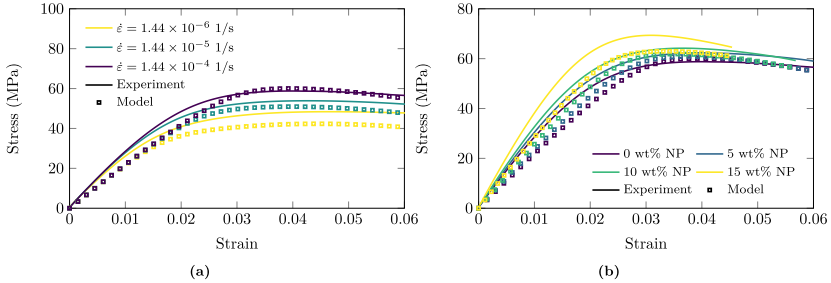

Fig. 18. Experimental validation by prediction of stress–strain response for the independent experiments: (a) variation of strain rates and (b) with nanoparticle weight fractions between 5% and 15%.

model and the proposed approach of using numerical data for parameter identification. In general, the material model is able to represent the material behaviour in good agreement with the experimental results, although two identifiable deviations stand out. Firstly, the strain at which yielding occurs is underestimated for the lowest temperature of 246 K (see Fig. 10), although the predicted yield stress is in very good agreement with the experimental results for all investigated temperatures. Secondly, the stress–strain response for the nanocomposite with 15 weight percent of nanoparticles shows the largest deviation from experimental results, with an underestimation of the yield stress (see Fig. 11). However, the prediction for the lower weight fractions of 5 and 10 percent agree well over the whole stress–strain response curve. These results suggest that the phenomenological Guth–Gold model, accounting for the strain amplification due to the nanoparticles, may not be able to capture the underlying mechanism occurring for weight fractions larger than 10 percent. For instance, the assumption of well-dispersed particles may not hold true due to increased agglomeration with increasing BNP weight fraction. The taurine modification of the Boehmite nanoparticles allows for chemical links between matrix and particle that may have a disproportionately increasing effect at higher weight fractions. To enhance the representation of the matrix particle interaction, further experimental insights are desirable to identify optimised parameters for the Guth–Gold model. Beside this aspect, it is worth noting that the proposed modified Kitagawa model (see Eqs. (14)–(16)) generally allows a good representation of the underlying temperature-dependent phenomena.

The second investigated case reveals that experiments can be replaced by numerical data without a significant reduction in accuracy. To provide a clear summary, the identified parameters using both approaches are presented for comparison in Table 7. The assumption of equal temperature scaling parameters (i.e., $\alpha_e = \alpha_{he}$) leads to a fair agreement with experimental results. Nevertheless, the difference in the identified values of both temperature-related parameters (α_e, α_{he}) in the first case (see Table 7) gives evidence that different underlying mechanisms are acting. Also, the underestimation of the initial stiffness in the stress prediction of the second case can be related to the assumption of equal temperature scaling parameters (see Figs. 17 and 18). To eliminate this, it would be desirable to identify the hyperelastic temperature dependency α_{he} based on shear simulations at different temperatures in future studies. In the final analysis, the agreement between prediction and experimental data is fair and suffers from the same two main deviations that were already observed in the first case. The additional underestimation of the yield stress for the case of the smallest strain rate (see Fig. 18) can be explained by the Argon model, which leads to an underestimation at very low strain rates, as shown by Unger et al. [38]. However, the identified values for the Argon model (non-linear dashpot) are very similar in both cases (see Table 7), highlighting that molecular tensile simulations are very well suited for replacing experimental tests. Beside the discussed difference in the temperature scaling parameters, the parameter N shows distinctly different values for both cases, which can be explained by its small influence on the governing equations for values of N larger than 1 (see Eqs. (3) and (4)). The value of the damage parameter A is comparable in the two cases and even the elastic properties (Lamé moduli $\mu_{e,ref}$ and $\lambda_{e,ref}$) are very similar, as the experimental data was used to identify both these parameters.

A criterion that can be used to quantify the accuracy of the calibrated material model for both cases is the stored strain energy defined by $U_\varepsilon = \int_0^{\varepsilon_{max}} \sigma(\varepsilon) d\varepsilon$. The strain energy in units of energy per unit volume is presented in Table 8 for all investigated test configurations. For the first studied case, the error is very small (< 2%) for all test configurations used for the parameter identification, emphasising that the general material behaviour is well represented. The largest error of 7.941% is observed for the highest BNP weight fraction, caused by the underestimation of the yield stress, as discussed above. For the second investigated case, the errors in the strain energy of the independent

Table 7
Comparison of identified parameters of Case 1 (identification using purely experimental data) and Case 2 (identification using both experimental and numerical data).

	Parameter		Value	
			Case 1	Case 2
Hyperelastic spring	$\mu_{he,\mathrm{ref}}$	(MPa)	353.67	205
	α_{he}		0.0159	0.01093
	N		12.67	2.44
Linear spring	$\mu_{e,\mathrm{ref}}$	(MPa)	623.42	605.79
	$\lambda_{e,\mathrm{ref}}$	(MPa)	2493.70	2423.17
	α_e		1.709×10^{-6}	0.01093
Non-linear dashpot	$\dot{\varepsilon}_0$	(1/s)	8.9207×10^{11}	9.7746×10^{11}
	σ_0	(MPa)	140.65	215.82
	ΔH	(J)	2.0324×10^{-19}	1.9761×10^{-19}
Damage	A		336.58	278.65

test configurations (variation of strain rate and BNP weight fraction) range between 7.489% and 13.233%, being in fair agreement with the experimental results. The comparison of the stored strain energy shows that the parameter identification using experimental and numerical data leads to a prediction of the material response without a significant loss in accuracy. It is worth noting that the lowest strain energy for all investigated nanocomposites is observed for the highest weight fraction of 15%, due to the earlier failure (i.e., more brittle behaviour).

The present constitutive model is limited to the glassy regime due to the temperature-dependent formulation of the elastic and hyperelastic springs. Only the sudden drop in modulus close to the transition, but not the glass transition to rubbery plateau, is captured. An extension to temperatures above the glass-transition temperature requires major modifications that were out of the scope of the present study. Promising results advancing in this direction were published by Richeton et al. [41] and Richeton et al. [67], with a complex formulation for the elastic modulus that captures the behaviour in both the glassy and rubbery regimes. Furthermore, an extended Cooperative model was used that represents the viscoelasticity for temperatures above the glass-transition temperature [68]. However, these approaches lead to a significantly increased number of parameters, and the parameters of the cooperative model cannot be identified using molecular simulation [38].

The originally formulated constitutive model was successfully applied to model the four-point bending test for a range of nanoparticle weight fractions up to 20 percent by Arash et al. [29]. A validation of the present constitutive model for cyclic loading conditions at different strain rates and temperatures would be important to further assess the capabilities with respect to complex load cases, as shown by Tang et al. [69] and Li et al. [70]. Future studies may also consider the effect of thermal expansion, which can be included by a decomposition of the deformation gradient, as shown by Lu and Pister [71] and implemented by Nguyen et al. [72] and Nguyen et al. [10]. This would allow further incorporation of numerical methods, as thermal properties (coefficient of thermal expansion and glass-transition temperature) can be calculated by MD simulation [25,73] In general, the proposed constitutive model can be extended towards a variety of physical and chemical phenomena that affect the mechanical material response, such as water absorption [74–76], thermal degradation [77] or physical ageing mechanisms [78].

5. Conclusions

A unique extension to finite temperatures for a physically based constitutive model is proposed and this captures the characteristic temperature-dependent viscoelastic damage behaviour of nanoparticle/epoxy nanocomposites. The model adopts the Argon model to take into account the effects of strain rate and temperature on the viscoelasticity. The individual temperature dependency of the initial linear response and the non-linear hyperelasticity are incorporated using a modified Kitagawa model. A saturation-type evolution rule is used to model the softening behaviour.

Two cases for the parameter identification of the proposed constitutive model are investigated. Firstly, purely experimental data from tensile tests at different strain rates and temperatures are used to identify all parameters. The objective of the first case is to investigate the general capabilities of the material model by evaluating how accurately the characteristic material behaviour is reproduced. A comparison of the predicted material response with experimental data at different strain rates and temperatures confirms the predictive capabilities of the proposed model. Furthermore, the model adequately represents the material behaviour of nanoparticle/epoxy nanocomposites, as shown by a validation using independent experimental results. Secondly, a combination of experimental and numerical data is used for the parameter identification. The objective of the second case is to demonstrate that experiments can partly be replaced by numerical simulations without a significant loss in accuracy. Therefore, the viscoelastic material parameters ($\dot{\varepsilon}_0$, σ_0 and ΔH) required for the Argon model together with the hyperelastic material parameters ($\mu_{he,\mathrm{ref}}$, N), are derived from MD simulation data. An experimental validation is provided by showing that the material response is in fair agreement with experimental data for different variations of strain rate, temperature and nanoparticle weight fractions. Finally, a quantitative assessment of the accuracy of both studied cases for the parameter identification is provided by using the stored strain energy as a criterion.

The capabilities and limitations of the present constitutive model are clearly stated. Therefore, a better understanding of the thermoviscoelastic behaviour of nanoparticle/epoxy nanocomposites is achieved and the associated challenges of modelling these materials are discussed. Furthermore, the present study underlines the fact that advanced numerical methods can be used to derive material parameters in the context of physically constitutive modelling and multi-scale approaches. The proposed simulation-based framework allows a significant reduction in the number of experimental tests required to identify material parameters. In future studies, experimental data obtained from cyclic loading conditions is desirable to investigate the prediction of

Table 8
Comparison of the predicted strain energy per unit volume of Case 1 and Case 2 with experimental data. The first row shows the values and respective errors in percent for the reference configuration followed by the variations of temperature, strain rate and BNP weight fraction.

Temperature Θ (K)	Strain rate $\dot{\varepsilon}$ (1/s)	BNP weight fraction (%)	Experiment (10^9 J/m^3)	Case 1 (10^9 J/m^3)	Error (%)	Case 2 (10^9 J/m^3)	Error (%)
296	1.44×10^{-4}	0	2.822	2.822	0.015	2.683	4.913
246	1.44×10^{-4}	0	4.048	4.030	0.439	4.059	0.279
326	1.44×10^{-4}	0	1.588	1.610	1.416	1.657	4.381
296	1.44×10^{-5}	0	2.621	2.593	1.050	2.393	8.700
296	1.44×10^{-6}	0	2.365	2.348	0.712	2.052	13.233
296	1.44×10^{-4}	5	2.990	2.913	2.593	2.766	7.489
296	1.44×10^{-4}	10	2.900	2.832	2.341	2.683	7.499
296	1.44×10^{-4}	15	2.432	2.239	7.941	2.115	13.045

the hysteresis behaviour in order to obtain a more comprehensive model. The incorporation of coarse-graining methods would reduce the computational cost and allow molecular simulations to be conducted at significantly larger time and length scales.

Data availability

The raw/processed data required to reproduce these findings cannot be shared at this time, as the data also forms part of an ongoing study.

Declaration of competing interest

The authors declare that they have no known competing financial interests or personal relationships that could have appeared to influence the work reported in this paper.

CRediT authorship contribution statement

Robin Unger: Conceptualization, Methodology, Software, Validation, Formal analysis, Investigation, Data curation, Writing - original draft, Writing - review & editing, Visualization. **Behrouz Arash:** Conceptualization, Investigation, Data curation, Writing - review & editing, Supervision. **Wibke Exner:** Investigation, Data curation, Writing - review & editing. **Raimund Rolfes:** Resources, Writing - review & editing, Supervision, Funding acquisition.

Acknowledgements

We would like to thank Ricarda Berger and Benedikt Hofmeister for their expertise and support with respect to the parameter identification/optimisation process. The authors acknowledge the support of the LUIS scientific computing cluster, which is funded by Leibniz Universität Hannover, the Lower Saxony Ministry of Science and Culture (MWK) and the DFG.

Funding

This work originates from two research projects: (1) “Hybrid laminates and nanoparticle-reinforced materials for improved rotor blade structures” (“LENAH - Lebensdauererhöhung und Leichtbauoptimierung durch nanomodifizierte und hybride Werkstoffsysteme im Rotorblatt”), funded by the Federal Ministry of Education and Research of Germany, and (2) “Challenges of industrial application of nanomodified and hybrid material systems in lightweight rotor blade construction” (“HANNAH - Herausforderungen der industriellen Anwendung von nanomodifizierten und hybriden Werkstoffsystemen im Rotorblattleichtbau”), funded by the Federal Ministry for Economic Affairs and Energy. The authors wish to express their gratitude for the financial support.

References

[1] B. Arash, Q. Wang, V.K. Varadan, Mechanical properties of carbon nanotube/polymer composites, Sci. Rep. 4 (1) (2015) http://dx.doi.org/10.1038/srep06479.

[2] Behrouz Arash, Harold S. Park, Timon Rabczuk, Coarse-grained model of the J-integral of carbon nanotube reinforced polymer composites, Carbon 96 (2016) 1084–1092, http://dx.doi.org/10.1016/j.carbon.2015.10.058.

[3] M. Jux, J. Fankhänel, B. Daum, T. Mahrholz, M. Sinapius, R. Rolfes, Mechanical properties of epoxy/boehmite nanocomposites in dependency of mass fraction and surface modification - an experimental and numerical approach, Polymer 141 (2018) 34–45, http://dx.doi.org/10.1016/j.polymer.2018.02.059.

[4] J. Fankhänel, D. Silbernagl, M. Ghasem Zadeh Khorasani, B. Daum, A. Kempe, H. Sturm, R. Rolfes, Mechanical properties of boehmite evaluated by atomic force microscopy experiments and molecular dynamic finite element simulations, J. Nanomater. 2016 (2016) 1–13, http://dx.doi.org/10.1155/2016/5017213.

[5] J. Fankhänel, B. Arash, R. Rolfes, Elastic interphase properties of nanoparticle/epoxy nanocomposites: a molecular dynamics study, Composites B 176 (2019) 107211, http://dx.doi.org/10.1016/j.compositesb.2019.107211.

[6] Naureen Shahid, Richard G. Villate, Andrew R. Barron, Chemically functionalized alumina nanoparticle effect on carbon fiber/epoxy composites, Compos. Sci. Technol. 65 (14) (2005) 2250–2258, http://dx.doi.org/10.1016/j.compscitech.2005.04.001.

[7] C. Miehe, Superimposed finite elastic–viscoelastic–plastoelastic stress response with damage in filled rubbery polymers. experiments, modelling and algorithmic implementation, J. Mech. Phys. Solids 48 (2) (2000) 323–365, http://dx.doi.org/10.1016/S0022-5096(99)00017-4.

[8] Lorenzo Bardella, A phenomenological constitutive law for the nonlinear viscoelastic behaviour of epoxy resins in the glassy state, Eur. J. Mech. A Solids 20 (6) (2001) 907–924.

[9] X. Poulain, A.A. Benzerga, R.K. Goldberg, Finite-strain elasto-viscoplastic behavior of an epoxy resin: experiments and modeling in the glassy regime, Int. J. Plast. 62 (2014) 138–161, http://dx.doi.org/10.1016/j.ijplas.2014.07.002.

[10] V.-D. Nguyen, F. Lani, T. Pardoen, X.P. Morelle, L. Noels, A large strain hyperelastic viscoelastic-viscoplastic-damage constitutive model based on a multi-mechanism non-local damage continuum for amorphous glassy polymers, Int. J. Solids Struct. 96 (2016) 192–216, http://dx.doi.org/10.1016/j.ijsolstr.2016.06.008.

[11] M. Vogler, R. Rolfes, P.P. Camanho, Modeling the inelastic deformation and fracture of polymer composites part I: plasticity model, Mech. Mater. 59 (2013) 50–64, http://dx.doi.org/10.1016/j.mechmat.2012.12.002.

[12] A. Dean, S. Sahraee, K. Özenc, J. Reinoso, R. Rolfes, M. Kaliske, A thermodynamically consistent framework to couple damage and plasticity microplane-based formulations for fracture modeling: development and algorithmic treatment, Int. J. Fract. 203 (1–2) (2017) 115–134, http://dx.doi.org/10.1007/s10704-016-0131-9.

[13] A.D. Drozdov, A. Dorfmann, The effect of temperature on the viscoelastic response of rubbery polymers at finite strains, Acta Mech. 154 (1–4) (2002) 189–214, http://dx.doi.org/10.1007/BF01170707.

[14] Ellen M. Arruda, Mary C. Boyce, A three-dimensional constitutive model for the large stretch behavior of rubber elastic materials, J. Mech. Phys. Solids 41 (2) (1993) 389–412.

[15] E. Kontou, Viscoplastic deformation of an epoxy resin at elevated temperatures, J. Appl. Polym. Sci. 101 (3) (2006) 2027–2033, http://dx.doi.org/10.1002/app.23768.

[16] S.W. Park, R.A. Schapery, A viscoelastic constitutive model for particulate composites with growing damage, Int. J. Solids Struct. 34 (8) (1997) 931–947, http://dx.doi.org/10.1016/S0020-7683(96)00066-2.

[17] I.B.C.M. Rocha, F.P. van der Meer, S. Raijmaekers, F. Lahuerta, R.P.L. Nijssen, L.J. Sluys, Numerical/experimental study of the monotonic and cyclic viscoelastic/viscoplastic/fracture behavior of an epoxy resin, Int. J. Solids Struct. 168 (2019) 153–165, http://dx.doi.org/10.1016/j.ijsolstr.2019.03.018.

[18] A.R. Melro, P.P. Camanho, F.M. Andrade Pires, S.T. Pinho, Micromechanical analysis of polymer composites reinforced by unidirectional fibres: part I — constitutive modelling, Int. J. Solids Struct. 50 (11–12) (2013) 1897–1905, http://dx.doi.org/10.1016/j.ijsolstr.2013.02.009.

[19] H.J. Qi, M.C. Boyce, Stress–strain behavior of thermoplastic polyurethanes, Mech. Mater. 37 (8) (2005) 817–839, http://dx.doi.org/10.1016/j.mechmat.2004.08.001.

[20] H. Qi, Constitutive model for stretch-induced softening of the stress?stretch behavior of elastomeric materials, J. Mech. Phys. Solids 52 (10) (2004) 2187–2205, http://dx.doi.org/10.1016/j.jmps.2004.04.008.

[21] J Vandommelen, D Parks, M Boyce, W Brekelmans, F Baaijens, Micromechanical modeling of the elasto-viscoplastic behavior of semi-crystalline polymers, J. Mech. Phys. Solids 51 (3) (2003) 519–541, http://dx.doi.org/10.1016/S0022-5096(02)00063-7.

[22] S. Ahzi, A. Makradi, R.V. Gregory, D.D. Edie, Modeling of deformation behavior and strain-induced crystallization in poly(ethylene terephthalate) above the glass transition temperature, Mech. Mater. 35 (12) (2003) 1139–1148, http://dx.doi.org/10.1016/S0167-6636(03)00004-8.

[23] G. Ayoub, F. Zaïri, M. Naït-Abdelaziz, J.M. Gloaguen, Modelling large deformation behaviour under loading–unloading of semicrystalline polymers: application to a high density polyethylene, Int. J. Plast. 26 (3) (2010) 329–347, http://dx.doi.org/10.1016/j.ijplas.2009.07.005.

[24] Hyungbum Park, Joonmyung Choi, Byungjo Kim, Seunghwa Yang, Hyunseong Shin, Maenghyo Cho, Toward the constitutive modeling of epoxy matrix: temperature-accelerated quasi-static molecular simulations consistent with the experimental test, Composites B 142 (2018) 131–141, http://dx.doi.org/10.1016/j.compositesb.2018.01.018.

[25] Chunyu Li, Alejandro Strachan, Molecular scale simulations on thermoset polymers: a review, J. Polym. Sci. B 53 (2) (2015) 103–122, http://dx.doi.org/10.1002/polb.23489.

[26] Suyoung Yu, Seunghwa Yang, Maenghyo Cho, Multi-scale modeling of cross-linked epoxy nanocomposites, Polymer 50 (3) (2009) 945–952, http://dx.doi.org/10.1016/j.polymer.2008.11.054.

[27] Ying Li, Shan Tang, Brendan C. Abberton, Martin Krger, Craig Burkhart, Bing Jiang, George J. Papakonstantopoulos, Mike Poldneff, Wing Kam Liu, A predictive multiscale computational framework for viscoelastic properties of linear polymers, Polymer 53 (25) (2012) 5935–5952, http://dx.doi.org/10.1016/j.polymer.2012.09.055.

[28] N. Vu-Bac, M.A. Bessa, Timon Rabczuk, Wing Kam Liu, A multiscale model for the quasi-static thermo-plastic behavior of highly cross-linked glassy polymers, Macromolecules 48 (18) (2015) 6713–6723, http://dx.doi.org/10.1021/acs.macromol.5b01236.

[29] Behrouz Arash, Wibke Exner, Raimund Rolfes, A viscoelastic damage model for nanoparticle/epoxy nanocomposites at finite strain: a multiscale approach, J. Mech. Phys. Solids 128 (2019) 162–180, http://dx.doi.org/10.1016/j.jmps.2019.04.004.

[30] Behrouz Arash, Wibke Exner, Raimund Rolfes, Viscoelastic damage behavior of fiber reinforced nanoparticle-filled epoxy nanocomposites: multiscale modeling and experimental validation, Composites B 174 (2019) 107005, http://dx.doi.org/10.1016/j.compositesb.2019.107005.

[31] Jörgen S. Bergström, Mary C. Boyce, Mechanical behavior of particle filled elastomers, Rubber Chem. Technol. 72 (4) (1999) 633–656, http://dx.doi.org/10.5254/1.3538823.

[32] Eugene Guth, On the hydrodynamical theory of the viscosity of suspensions, Phys. Rev. 53 (1938).

[33] Eugene Guth, Theory of filler reinforcement, Rubber Chem. Technol. 18 (3) (1945) 596–604, http://dx.doi.org/10.5254/1.3546754.

[34] David L. Henann, Lallit Anand, A large strain isotropic elasticity model based on molecular dynamics simulations of a metallic glass, J. Elasticity 104 (1–2) (2011) 281–302, http://dx.doi.org/10.1007/s10659-010-9297-y.

[35] H. Xiao, L.S. Chen, Hencky's elasticity model and linear stress-strain relations in isotropic finite hyperelasticity, Acta Mech. 157 (1–4) (2002) 51–60, http://dx.doi.org/10.1007/BF01182154.

[36] L. Anand, Moderate deformations in extension-torsion of incompressible isotropic elastic materials, J. Mech. Phys. Solids 34 (3) (1986) 293–304, http://dx.doi.org/10.1016/0022-5096(86)90021-9.

[37] L. Anand, On h. hencky's approximate strain-energy function for moderate deformations, J. Appl. Mech. 46 (1) (1979) 78–82, http://dx.doi.org/10.1115/1.3424532.

[38] Robin Unger, Wibke Exner, Behrouz Arash, Raimund Rolfes, Non-linear viscoelasticity of epoxy resins: molecular simulation-based prediction and experimental validation, Polymer (2019) 121722, http://dx.doi.org/10.1016/j.polymer.2019.121722.

[39] L.H. Sperling, Introduction to physical polymer science, p. 878.

[40] Wayne D. Cook, Anthony E. Mayr, Graham H. Edward, Yielding behaviour in model epoxy thermosets–II. temperature dependence, Polymer 39 (16) (1998) 3725–3733.

[41] J. Richeton, G. Schlatter, K.S. Vecchio, Y. Rémond, S. Ahzi, A unified model for stiffness modulus of amorphous polymers across transition temperatures and strain rates, Polymer 46 (19) (2005) 8194–8201, http://dx.doi.org/10.1016/j.polymer.2005.06.103.

[42] M. Kitagawa, Power law relationship between yield stress and shear modulus for glassy polymers, J. Polym. Sci. 15 (9) (1977) 1601–1611.

[43] Olin Epoxy AIRSTONE 886H Hardener, Material Safety Data Sheet, UPPC GmbH, Schemmenberger Str. 39, 88487 Mietingen-Baltringen, Germany, Apr. 2011.

[44] Olin Epoxy AIRSTONE 880E Epoxy Resin, Material Safety Data Sheet, UPPC GmbH, Schemmenberger Str 39, 88487 Mietingen-Baltringen, Germany, Apr. 2011.

[45] Media Ghasem Zadeh Khorasani, Dorothee Silbernagl, Paulina Szymoniak, Vasile-Dan Hodoroaba, Heinz Sturm, The effect of boehmite nanoparticles on nanomechanical and thermomechanical properties correlated to crosslinking density of epoxy, Polymer 164 (2019) 174–182, http://dx.doi.org/10.1016/j.polymer.2018.12.054.

[46] Media Ghasem Zadeh Khorasani, Dorothee Silbernagl, Daniel Platz, Heinz Sturm, Insights into nano-scale physical and mechanical properties of epoxy/boehmite nanocomposite using different afm modes, Polymers 11 (2) (2019) 235, http://dx.doi.org/10.3390/polym11020235.

[47] Media Ghasem Zadeh Khorasani, Anna-Maria Elert, Vasile-Dan Hodoroaba, Leonardo Agudo Jácome, Korinna Altmann, Dorothee Silbernagl, Heinz Sturm, Short- and long-range mechanical and chemical interphases caused by interaction of boehmite with anhydride-cured epoxy resins, Nanomaterials 9 (6) (2019) 853, http://dx.doi.org/10.3390/nano9060853.

[48] Christine Arlt, Wibke Exner, Ulrich Riedel, Heinz Sturm, Michael Sinapius, Nanoscaled boehmites' modes of action in a polymer and its carbon fiber reinforced plastic, in: Martin Wiedemann, Michael Sinapius (Eds.), Adaptive, Tolerant and Efficient Composite Structures, Springer Berlin Heidelberg, Berlin, Heidelberg, 2013, pp. 49–58, http://dx.doi.org/10.1007/978-3-642-29190-6_4.

[49] X. Bokhimi, J.A. Toledo-Antonio, M.L. Guzmán-Castillo, F. Hernández-Beltrán, Relationship between crystallite size and bond lengths in boehmite, J. Solid State Chem. 159 (1) (2001) 32–40, http://dx.doi.org/10.1006/jssc.2001.9124.

[50] Lutz Nasdala, Andreas Kempe, Raimund Rolfes, Are finite elements appropriate for use in molecular dynamic simulations?, Compos. Sci. Technol. 72 (9) (2012) 989–1000, http://dx.doi.org/10.1016/j.compscitech.2012.03.008.

[51] Lutz Nasdala, Andreas Kempe, Raimund Rolfes, The molecular dynamic finite element method (MDFEM), Comput. Mater. Con. 19 (1) (2010) 57.

[52] Lutz Nasdala, Andreas Kempe, Raimund Rolfes, Molecular dynamic finite element method (MDFEM), in: Computational Finite Element Methods in Nanotechnology, CRC Press, 2013, pp. 331–372.

[53] Steve Plimpton, Fast parallel algorithms for short-range molecular dynamics, J. Comput. Phys. 117 (1) (1995) 1–19, http://dx.doi.org/10.1006/jcph.1995.1039.

[54] Stephen L. Mayo, Barry D. Olafson, William A. Goddard, DREIDING: a generic force field for molecular simulations, J. Phys. Chem. 94 (26) (1990) 8897–8909.

[55] Chaofu Wu, Weijian Xu, Atomistic molecular simulations of structure and dynamics of crosslinked epoxy resin, Polymer 48 (19) (2007) 5802–5812, http://dx.doi.org/10.1016/j.polymer.2007.07.019.

[56] Carla E. Estridge, The effects of competitive primary and secondary amine reactivity on the structural evolution and properties of an epoxy thermoset resin during cure: a molecular dynamics study, Polymer 141 (2018) 12–20, http://dx.doi.org/10.1016/j.polymer.2018.02.062.

[57] Chunyu Li, Alejandro Strachan, Molecular simulations of crosslinking process of thermosetting polymers, Polymer 51 (25) (2010) 6058–6070, http://dx.doi.org/10.1016/j.polymer.2010.10.033.

[58] Vikas Varshney, Soumya S. Patnaik, Ajit K. Roy, Barry L. Farmer, A molecular dynamics study of epoxy-based networks: cross-linking procedure and prediction of molecular and material properties, Macromolecules 41 (18) (2008) 6837–6842, http://dx.doi.org/10.1021/ma801153e.

[59] Robin Unger, Ulrike Braun, Johannes Fankhänel, Benedikt Daum, Behrouz Arash, Raimund Rolfes, Molecular modelling of epoxy resin crosslinking experimentally validated by near-infrared spectroscopy, Comput. Mater. Sci. 161 (2019) 223–235, http://dx.doi.org/10.1016/j.commatsci.2019.01.054.

[60] L. Martínez, R. Andrade, E.G. Birgin, J.M. Martínez, PACKMOL: a package for building initial configurations for molecular dynamics simulations, J. Comput. Chem. 30 (13) (2009) 2157–2164, http://dx.doi.org/10.1002/jcc.21224.

[61] The Open Babel Package, version 2.3.1 http://openbabel.org.

[62] Simone Melchionna, Giovanni Ciccotti, Brad Lee Holian, Hoover *npt* dynamics for systems varying in shape and size, Mol. Phys. 78 (3) (1993) 533–544, http://dx.doi.org/10.1080/00268979300100371.

[63] Yingtian Yu, Mengyi Wang, Dawei Zhang, Bu Wang, Gaurav Sant, Mathieu Bauchy, Stretched exponential relaxation of glasses at low temperature, Phys. Rev. Lett. 115 (16) (2015) http://dx.doi.org/10.1103/PhysRevLett.115.165901.

[64] David E. Goldberg, Genetic Algorithms in Search, Optimization, and Machine Learning, Addison-Wesley Pub. Co, Reading, Mass, 1989.

[65] I.M. Ward, J. Sweeney, Mechanical Properties of Solid Polymers, third ed., Wiley, Chichester, West Sussex, United Kingdom, 2013.

[66] J. Richeton, S. Ahzi, L. Daridon, Thermodynamic investigation of yield-stress models for amorphous polymers, Phil. Mag. 87 (24) (2007) 3629–3643, http://dx.doi.org/10.1080/14786430701381162.

[67] J. Richeton, S. Ahzi, K.S. Vecchio, F.C. Jiang, A. Makradi, Modeling and validation of the large deformation inelastic response of amorphous polymers over a wide range of temperatures and strain rates, Int. J. Solids Struct. 44 (24) (2007) 7938–7954, http://dx.doi.org/10.1016/j.ijsolstr.2007.05.018.

[68] J. Richeton, S. Ahzi, L. Daridon, Y. Rémond, A formulation of the cooperative model for the yield stress of amorphous polymers for a wide range of strain rates and temperatures, Polymer 46 (16) (2005) 6035–6043, http://dx.doi.org/10.1016/j.polymer.2005.05.079.

[69] Shan Tang, M. Steven Greene, Wing Kam Liu, Two-scale mechanism-based theory of nonlinear viscoelasticity, J. Mech. Phys. Solids 60 (2) (2012) 199–226, http://dx.doi.org/10.1016/j.jmps.2011.11.003.

[70] Ying Li, Shan Tang, Martin Kröger, Wing Kam Liu, Molecular simulation guided constitutive modeling on finite strain viscoelasticity of elastomers, J. Mech. Phys. Solids 88 (2016) 204–226, http://dx.doi.org/10.1016/j.jmps.2015.12.007.

[71] S.C.H. Lu, K.S. Pister, Decomposition of deformation and representation of the free energy function for isotropic thermoelastic solids, Int. J. Solids Struct. 11 (7–8) (1975) 927–934, http://dx.doi.org/10.1016/0020-7683(75)90015-3.

[72] T. Nguyen, H. Jerryqi, F. Castro, K. Long, A thermoviscoelastic model for amorphous shape memory polymers: incorporating structural and stress relaxation, J. Mech. Phys. Solids 56 (9) (2008) 2792–2814, http://dx.doi.org/10.1016/j.jmps.2008.04.007.

[73] Chunyu Li, Alejandro Strachan, Molecular dynamics predictions of thermal and mechanical properties of thermoset polymer epon862/detda, Polymer 52 (13) (2011) 2920–2928, http://dx.doi.org/10.1016/j.polymer.2011.04.041.

[74] Meredith N. Silberstein, Mary C. Boyce, Constitutive modeling of the rate, temperature, and hydration dependent deformation response of nafion to monotonic and cyclic loading, J. Power Sources 195 (17) (2010) 5692–5706, http://dx.doi.org/10.1016/j.jpowsour.2010.03.047.

[75] Chao Yu, Guozheng Kang, Kaijuan Chen, A hygro-thermo-mechanical coupled cyclic constitutive model for polymers with considering glass transition, Int. J. Plast. 89 (2017) 29–65, http://dx.doi.org/10.1016/j.ijplas.2016.11.001.

[76] Nathan Sharp, Chunyu Li, Alejandro Strachan, Douglas Adams, R. Byron Pipes, Effects of water on epoxy cure kinetics and glass transition temperature utilizing molecular dynamics simulations, J. Polym. Sci. B 55 (15) (2017) 1150–1159, http://dx.doi.org/10.1002/polb.24357.

[77] R. Polanský, V. Mentlík, P. Prosr, J. Sušír, Influence of thermal treatment on the glass transition temperature of thermosetting epoxy laminate, Polym. Test. 28 (4) (2009) 428–436, http://dx.doi.org/10.1016/j.polymertesting.2009.03.004.

[78] G.M. Odegard, A. Bandyopadhyay, Physical aging of epoxy polymers and their composites, J. Polym. Sci. B 49 (24) (2011) 1695–1716, http://dx.doi.org/10.1002/polb.22384.

Chapter 6

Summary and Outlook

6.1 Summary

The engineering progress that continuously changes the world is an accumulation of individual improvements arising from a broad basis of fundamental research. The present thesis is a contribution to the field of fundamental research of computational material science and provides connecting points to applied research and engineering applications to underline its importance. In this thesis, molecular simulation-based methods for the multi-scale constitutive modelling of nanoparticle/epoxy nanocomposites are developed and successfully validated. Each publication is a contribution to current challenges and open questions in the field of computational material science.
A reliable characterisation and prediction of material properties using molecular simulations already starts with the initial model generation. Although it is generally agreed that an accurate representation of the curing mechanism is crucial to obtain realistic simulation models, a comprehensive experimental validation of current approaches was pending in the literature. The first publication addresses this aspect with the development of a molecular curing simulation concerning efficiency and accuracy. The trade-off between these contradicting aspects is investigated with a parameter study. Based on this study, the cut-off distance was chosen to the largest value, leading to an increased efficiency without a loss in accuracy. The main innovation of the first publication is a systematic framework to evaluate the capabilities of simulation-based methods to predict the network topology of epoxy systems and to validate the simulation results of the curing mechanism with experimental data. For the first time, the evolution of all reactive groups during the curing process is predicted in good agreement with experimental near-infrared spectroscopy data. Furthermore, the experimentally validated method allows studying the curing mechanism of other thermosetting polymers.
Following up on the realistic model generation is was possible to dedicate the second publication to one of the superior challenges of molecular simulations, namely bridging the significantly different timescales between the atomistic level and experiments. It was shown that the proposed simulation-based method can be efficiently used to calibrate viscoelastic models. The provided experimental validation emphasises that a successful prediction of viscoelastic properties at experimental timescales is possible by using data obtained purely from molecu-

lar simulations. A study of three theories provides a clear picture of the abilities and limitations of their application for the prediction of viscoelasticity. It can be concluded that the Argon model is able to predict the viscoelasticity over a huge range of strain rates and a broad range of temperatures in the glassy regime in good agreement with experimental results. Furthermore, the results underline that the fundamental physical phenomena on the molecular level are covered by the conducted molecular simulations. This publication points out how advanced molecular methods can be exploited to significantly reduce the amount of experimental testing required for fundamental material characterisation.
Both previous substantial achievements are the premises on which the third publication is based. Here, the major innovation is the proposal of a physically-based constitutive model for nanoparticle/epoxy nanocomposites at finite temperatures in the glassy regime. One crucial aspect is the description of the temperature-dependent elastic properties, for which an approach was presented based on the Kitagawa model. A comparison to experimental results validates the predictive capabilities of the developed model that is able to capture the main characteristics of the material response including the non-linear hyperelasticity, softening behaviour and the effect of temperature. A consistent framework is provided that utilises molecular simulation-based methods to identify required parameters. With the proposed framework, it is possible to considerably reduce the number of experimental tests required for the identification of material parameters without a significant loss of accuracy in the material response prediction.
The molecular simulation-based methods developed in this thesis, effectively contribute to the fundamental research on polymer material science for engineering applications. The developed methods, consistently experimentally validated, provide specific approaches for some of the open questions in the current state of the art. The proposed framework guides the way to a virtual material development to improve existing and design new thermosetting polymers and related nanocomposites. The capabilities and limitations are clearly stated and the framework allows to be extended towards various specific challenges in the future. Finally, it can be concluded that the implementation of advanced of molecular simulations offers significant advantages for a faster and more efficient material development by replacing some experiments required and allowing to investigate physical effects at the nano-scale.

6.2 Limitations and outlook

The present work can be understood as a fundamental framework, which in its current form is not available as a ready-to-use software application. The framework address some of the major open questions in the state of the art and generally allows for extensions in several directions.
There is great potential for improvement in the identification of elastic material parameters from molecular simulations. However, this aspect is rather challenging as no physically-based theory is available that describes the elasticity as a

function of temperature and strain rate. With the proposed modified Kitagawa model a start was made that leads to good agreement with experimental results for the effect of temperature. In future studies, the effect of the strain rate on the elastic properties is worth to be investigated as the current formulation does not consider this aspect, but strong evidence can be found that the significant difference between MD and experimental timescales affects the Young's modulus [26, 58, 76]. However, no effect of the strain rate on the initial stiffness is identifiable in the experimental strain rate range (see Figure 1.3 (b) on page 7). A more comprehensive model that includes the effect of both, temperature and strain rate, is desirable and would allow describing the elasticity based on molecular simulation. This would lead to a further reduction of required experimental tests, as only the damage mechanism would be left for experimentally-based parameter identification in the proposed constitutive model.

The present multi-scale framework provides methods for a consistent transfer of information from the nano-scale (molecular simulations) to the micro-scale (constitutive model). The current work can be extended to a more comprehensive multi-scale model by including the phenomena of chemical shrinkage. Using the molecular curing simulation at the nano-scale, the chemical shrinkage can directly be derived as a function of the epoxy conversion. At the next higher micro-scale, a decomposition of the deformation gradient is required to incorporate the chemical shrinkage. By implementing an additional decomposition of the deformation gradient also the effect of thermal expansion can be considered, for which the required parameter (coefficient of thermal expansion) can also be obtained by molecular simulations. With such an extended constitutive model, the manufacturing induced eigenstresses that arise from the curing (i.e., chemical shrinkage) and the following cool down (i.e., thermal expansion) can be studied without any additional experiments required.

The proposed framework can also be used to investigate the effect of humidity on the curing mechanism and mechanical behaviour. Therefore, water molecules need to be added to the uncured simulation model and the proposed procedure is evaluated again without any further changes required.

The current approach is limited to an indirect representation of nanoparticles in terms of the Guth-Gold model that provides a formulation to account for the amplified chain stretch due to nanoparticles. The available computational power is used for molecular tensile simulations at very small strain rates that are required to identify reliable parameters for the Argon model. An explicit representation of nanoparticles was out of scope due to the significantly increased computational cost that arises from the required larger box sizes. However, the results of the third publication indicate that the implementation of the Guth-Gold model leads to material behaviour in good agreement with experimental data for weight fractions up to ten per cent. For higher weight fractions, either the nanoparticle-polymer interaction may play a significant role or agglomerations may occur, both are not considered. To study the particle-polymer interaction, molecular simulations with an explicit representation of the particle

are desirable and would allow identifying optimised parameters for the Guth-Gold model. This can be achieved by using coarse-graining methods that reduce the computational cost, making larger time and length scales feasible. An even more comprehensive framework can be achieved with the implementation of the proposed constitutive model in a multi-scale framework that explicitly describes nanoparticle agglomeration, as recently presented by Fankhänel et al. [26]. The combination of agglomeration effects and the complex viscoelastic material behaviour has a great potential for studying and understanding the underlying mechanism occurring from nanoparticle interactions.
In its current form, the framework is limited to the transfer of information from the nano-scale to the micro-scale at which the present validation only considers a uniaxial stress state. To analyse the general capabilities of the proposed model more accurately, a comparison to three-dimensional stress states is desirable for future works. A more comprehensive model can be obtained by using experimental data obtained from cyclic loading conditions to investigate the prediction of hysteresis behaviour. To simulate complex geometries and provide validation in terms of structural response, implementation into a FEM framework is necessary. Furthermore, this would allow simulating micromechanical models of fibre-reinforced composites, as illustrated in Figure 1.5 on page 11, and thus allow the homogenisation of the material behaviour for the macro-scale.
Beside previous aspects, the developed molecular simulation-based methods are only validated for one amine-cured epoxy resin. A validation using different thermosetting polymers is important to underline that the methods are generally valid and universally applicable for thermosetting polymers.

Bibliography

[1] M. P. Allen and D. J. Tildesley, *Computer simulation of liquids*, Second edition, Oxford, United Kingdom: Oxford University Press, 2017.

[2] Amin Aramoon, Timothy D. Breitzman, Christopher Woodward, and Jaafar A. El-Awady, "Coarse-Grained Molecular Dynamics Study of the Curing and Properties of Highly Cross-Linked Epoxy Polymers", en, in: *The Journal of Physical Chemistry B* Vol. 120 (2016), pp. 9495–9505, DOI: 10.1021/acs.jpcb.6b03809.

[3] Behrouz Arash, Wibke Exner, and Raimund Rolfes, "A viscoelastic damage model for nanoparticle/epoxy nanocomposites at finite strain: A multiscale approach", en, in: *Journal of the Mechanics and Physics of Solids* Vol. 128 (2019), pp. 162–180, DOI: 10.1016/j.jmps.2019.04.004.

[4] Behrouz Arash, Wibke Exner, and Raimund Rolfes, "Viscoelastic damage behavior of fiber reinforced nanoparticle-filled epoxy nanocomposites: Multiscale modeling and experimental validation", en, in: *Composites Part B: Engineering* Vol. 174 (2019), p. 107005, DOI: 10.1016/j.compositesb.2019.107005.

[5] A. S. Argon, "A theory for the low-temperature plastic deformation of glassy polymers", en, in: *Philosophical Magazine* Vol. 28 (1973), pp. 839–865, DOI: 10.1080/14786437308220987.

[6] A. S. Argon and M. I. Bessonov, "Plastic deformation in polyimides, with new implications on the theory of plastic deformation of glassy polymers", en, in: *Philosophical Magazine* Vol. 35 (1977), pp. 917–933, DOI: 10.1080/14786437708232634.

[7] Ali S. Argon and M. I. Bessonov, "Plastic flow in glassy polymers", in: *Polymer Engineering & Science* Vol. 17 (1977), pp. 174–182.

[8] Christine Arlt, Wibke Exner, Ulrich Riedel, Heinz Sturm, and Michael Sinapius, "Nanoscaled Boehmites' Modes of Action in a Polymer and its Carbon Fiber Reinforced Plastic", in: *Adaptive, tolerant and efficient composite structures*, ed. by Martin Wiedemann and Michael Sinapius, Berlin, Heidelberg: Springer Berlin Heidelberg, 2013, pp. 49–58, DOI: 10.1007/978-3-642-29190-6_4.

[9] N. Attig, K. Binder, H. Grubmüller, and K. D. Kremer, *Computational soft matter: from synthetic polymers to proteins; Winter School, 29 February - 6 March 2004, Gustav-Stresemann-Institut, Bonn, Germany. 2: Lecture notes*, en, NIC series 23, OCLC: 253989746, Jülich: NIC, 2004.

[10] N. Vu-Bac, M. A. Bessa, Timon Rabczuk, and Wing Kam Liu, "A Multi-scale Model for the Quasi-Static Thermo-Plastic Behavior of Highly Cross-Linked Glassy Polymers", en, in: *Macromolecules* Vol. 48 (2015), pp. 6713–6723, DOI: 10.1021/acs.macromol.5b01236.

[11] Ananyo Bandyopadhyay, Pavan K. Valavala, Thomas C. Clancy, Kristopher E. Wise, and Gregory M. Odegard, "Molecular modeling of crosslinked epoxy polymers: The effect of crosslink density on thermomechanical properties", en, in: *Polymer* Vol. 52 (2011), pp. 2445–2452, DOI: 10.1016/j.polymer.2011.03.052.

[12] John M. Barton, A.S. Deazle, I. Hamerton, B.J. Howlin, and J.R. Jones, "The application of molecular simulation to the rational design of new materials: 2. Prediction of the physico-mechanical properties of linear epoxy systems", en, in: *Polymer* Vol. 38 (1997), pp. 4305–4310, DOI: 10.1016/S0032-3861(96)01018-X.

[13] C. Bauwens-Crowet, J. C. Bauwens, and G. Homes, "Tensile yield-stress behavior of glassy polymers", in: *Journal of Polymer Science Part A-2: Polymer Physics* Vol. 7 (1969), pp. 735–742.

[14] C. Bauwens-Crowet, J.-C. Bauwens, and Georges Homes, "The temperature dependence of yield of polycarbonate in uniaxial compression and tensile tests", in: *Journal of Materials Science* Vol. 7 (1972), pp. 176–183.

[15] J. C. Bauwens, C. Bauwens-Crowet, and G. Homes, "Tensile yield-stress behavior of poly (vinyl chloride) and polycarbonate in the glass transition region", in: *Journal of Polymer Science Part A-2: Polymer Physics* Vol. 7 (1969), pp. 1745–1754.

[16] P. Bultinck, W. Langenaeker, P. Lahorte, F. De Proft, P. Geerlings, C. Van Alsenoy, and J. P. Tollenaere, "The Electronegativity Equalization Method II: Applicability of Different Atomic Charge Schemes", en, in: *The Journal of Physical Chemistry A* Vol. 106 (2002), pp. 7895–7901, DOI: 10.1021/jp020547v.

[17] Patrick Bultinck, Wilfried Langenaeker, Ramon Carbó-Dorca, and Jan P. Tollenaere, "Fast Calculation of Quantum Chemical Molecular Descriptors from the Electronegativity Equalization Method", en, in: *Journal of Chemical Information and Computer Sciences* Vol. 43 (2003), pp. 422–428, DOI: 10.1021/ci0255883.

[18] Wayne D. Cook, Anthony E. Mayr, and Graham H. Edward, "Yielding behaviour in model epoxy thermosets—II. Temperature dependence", in: *Polymer* Vol. 39 (1998), pp. 3725–3733.

[19] D. C. Doherty, B. N. Holmes, P. Leung, and R. B. Ross, "Polymerization molecular dynamics simulations. I. Cross-linked atomistic models for poly (methacrylate) networks", in: *Computational and Theoretical Polymer Science* Vol. 8 (1998), pp. 169–178.

[20] Masao Doi and Samuel F. Edwards, *The theory of polymer dynamics*, eng, Reprinted, International series of monographs on physics 73, OCLC: 845169495, Oxford: Clarendon Press, 2007.

[21] E. Duemichen, M. Javdanitehran, M. Erdmann, V. Trappe, H. Sturm, U. Braun, and G. Ziegmann, "Analyzing the network formation and curing kinetics of epoxy resins by in situ near-infrared measurements with variable heating rates", en, in: *Thermochimica Acta* Vol. 616 (2015), pp. 49–60, DOI: 10.1016/j.tca.2015.08.008.

[22] Maren Erdmann, Volker Trappe, Heinz Sturm, Ulrike Braun, and Erik Duemichen, "Cure conversion of structural epoxies by cure state analysis and in situ cure kinetics using nondestructive NIR spectroscopy", en, in: *Thermochimica Acta* Vol. 650 (2017), pp. 8–17, DOI: 10.1016/j.tca.2017.01.010.

[23] Carla E. Estridge, "The effects of competitive primary and secondary amine reactivity on the structural evolution and properties of an epoxy thermoset resin during cure: A molecular dynamics study", en, in: *Polymer* Vol. 141 (2018), pp. 12–20, DOI: 10.1016/j.polymer.2018.02.062.

[24] Henry Eyring, "The Activated Complex in Chemical Reactions", en, in: *The Journal of Chemical Physics* Vol. 3 (1935), pp. 107–115, DOI: 10.1063/1.1749604.

[25] Henry Eyring, "Viscosity, Plasticity, and Diffusion as Examples of Absolute Reaction Rates", en, in: *The Journal of Chemical Physics* Vol. 4 (1936), pp. 283–291, DOI: 10.1063/1.1749836.

[26] J. Fankhänel, B. Arash, and R. Rolfes, "Elastic interphase properties of nanoparticle/epoxy nanocomposites: A molecular dynamics study", en, in: *Composites Part B: Engineering* Vol. 176 (2019), p. 107211, DOI: 10.1016/j.compositesb.2019.107211.

[27] J. Fankhänel, D. Silbernagl, M. Ghasem Zadeh Khorasani, B. Daum, A. Kempe, H. Sturm, and R. Rolfes, "Mechanical Properties of Boehmite Evaluated by Atomic Force Microscopy Experiments and Molecular Dynamic Finite Element Simulations", en, in: *Journal of Nanomaterials* Vol. 2016 (2016), pp. 1–13, DOI: 10.1155/2016/5017213.

[28] Abdolhossein Fereidoon, Shahram Aleaghaee, and Iman Taraghi, "Mechanical properties of hybrid graphene/TiO2 (rutile) nanocomposite: A molecular dynamics simulation", en, in: *Computational Materials Science* Vol. 102 (2015), pp. 220–227, DOI: 10.1016/j.commatsci.2015.02.044.

[29] *Förderbekanntmachung Angewandte nichtnukleare Forschungsförderung im 7. Energie-forschungsprogramm „Innovationen für die Energiewende"*, Bekanntmachung, Bundesministerium für Wirtschaft und Energie (BMWi) Öffentlichkeitsarbeit 11019 Berlin, 2018.

[30] D. G. Fotheringham and B. W. Cherry, "The role of recovery forces in the deformation of linear polyethylene", en, in: *Journal of Materials Science* Vol. 13 (1978), pp. 951–964, DOI: 10.1007/BF00544690.

[31] D. G. Fotheringham, B. W. Cherry, and C. Bauwens-Crowet, "Comment on "the compression yield behaviour of polymethyl methacrylate over a wide range of temperatures and strain-rates"", in: *Journal of Materials Science* Vol. 11 (1976), pp. 1368–1371.

[32] Johann Gasteiger and Mario Marsili, "A new model for calculating atomic charges in molecules", en, in: *Tetrahedron Letters* Vol. 19 (1978), pp. 3181–3184, DOI: 10.1016/S0040-4039(01)94977-9.

[33] David R. Heine, Gary S. Grest, Christian D. Lorenz, Mesfin Tsige, and Mark J. Stevens, "Atomistic Simulations of End-Linked Poly(dimethylsiloxane) Networks: Structure and Relaxation", en, in: *Macromolecules* Vol. 37 (2004), pp. 3857–3864, DOI: 10.1021/ma035760j.

[34] J. H. Hodgkin, G. P. Simon, and R. J. Varley, "Thermoplastic toughening of epoxy resins: a critical review", en, in: *Polymers for Advanced Technologies* Vol. 9 (1998), pp. 3–10, DOI: 10.1002/(SICI)1099-1581(199801)9:1<3::AID-PAT727>3.0.CO;2-I.

[35] *Innovationen für die Energiewende, 7. Energieforschungsprogramm der Bundesregier-ung*, de, Bekanntmachung, Bundesministerium für Wirtschaft und Energie (BMWi) Öffentlichkeitsarbeit 11019 Berlin, 2018.

[36] Atsushi Izumi, Toshio Nakao, and Mitsuhiro Shibayama, "Atomistic molecular dynamics study of cross-linked phenolic resins", en, in: *Soft Matter* Vol. 8 (2012), p. 5283, DOI: 10.1039/c2sm25067e.

[37] Jeffrey Jordan, Karl I. Jacob, Rina Tannenbaum, Mohammed A. Sharaf, and Iwona Jasiuk, "Experimental trends in polymer nanocomposites—a review", en, in: *Materials Science and Engineering: A* Vol. 393 (2005), pp. 1–11, DOI: 10.1016/j.msea.2004.09.044.

[38] M. Kitagawa, "Power law relationship between yield stress and shear modulus for glassy polymers", in: *Journal of Polymer Science: Polymer Physics Edition* Vol. 15 (1977), pp. 1601–1611.

[39] Chang Lyoul Kong, "Combining rules for intermolecular potential parameters. II. Rules for the Lennard-Jones (12–6) potential and the Morse potential", en, in: *The Journal of Chemical Physics* Vol. 59 (1973), pp. 2464–2467, DOI: 10.1063/1.1680358.

[40] Oleksandr G. Kravchenko, Chunyu Li, Alejandro Strachan, Sergii G. Kravchenko, and R. Byron Pipes, "Prediction of the chemical and thermal shrinkage in a thermoset polymer", en, in: *Composites Part A: Applied Science and Manufacturing* Vol. 66 (2014), pp. 35–43, DOI: 10.1016/j.compositesa.2014.07.002.

[41] G. A. M. van Kuik et al., "Long-term research challenges in wind energy – a research agenda by the European Academy of Wind Energy", en, in: *Wind Energy Science* Vol. 1 (2016), pp. 1–39, DOI: 10.5194/wes-1-1-2016.

[42] Fabrice Lapique and Keith Redford, "Curing effects on viscosity and mechanical properties of a commercial epoxy resin adhesive", en, in: *International Journal of Adhesion and Adhesives* Vol. 22 (2002), pp. 337–346, DOI: 10.1016/S0143-7496(02)00013-1.

[43] Chunyu Li and Alejandro Strachan, "Molecular dynamics predictions of thermal and mechanical properties of thermoset polymer EPON862/DETDA", en, in: *Polymer* Vol. 52 (2011), pp. 2920–2928, DOI: 10.1016/j.polymer.2011.04.041.

[44] Chunyu Li and Alejandro Strachan, "Molecular scale simulations on thermoset polymers: A review", en, in: *Journal of Polymer Science Part B: Polymer Physics* Vol. 53 (2015), pp. 103–122, DOI: 10.1002/polb.23489.

[45] Chunyu Li and Alejandro Strachan, "Molecular simulations of crosslinking process of thermosetting polymers", en, in: *Polymer* Vol. 51 (2010), pp. 6058–6070, DOI: 10.1016/j.polymer.2010.10.033.

[46] Ying Li et al., "A predictive multiscale computational framework for viscoelastic properties of linear polymers", en, in: *Polymer* Vol. 53 (2012), pp. 5935–5952, DOI: 10.1016/j.polymer.2012.09.055.

[47] Teik-Cheng Lim, "The Relationship between Lennard-Jones (12-6) and Morse Potential Functions", en, in: *Zeitschrift für Naturforschung A* Vol. 58 (2003), DOI: 10.1515/zna-2003-1104.

[48] George Marsh, "Airbus A350 XWB update", en, in: *Reinforced Plastics* Vol. 54 (2010), pp. 20–24, DOI: 10.1016/S0034-3617(10)70212-5.

[49] George Marsh, "Airbus takes on Boeing with reinforced plastic A350 XWB", en, in: *Reinforced Plastics* Vol. 51 (2007), pp. 26–29, DOI: 10.1016/S0034-3617(07)70383-1.

[50] Stephen L. Mayo, Barry D. Olafson, and William A. Goddard, "DREIDING: a generic force field for molecular simulations", in: *Journal of Physical chemistry* Vol. 94 (1990), pp. 8897–8909.

[51] Anthony E. Mayr, Wayne D. Cook, and Graham H. Edward, "Yielding behaviour in model epoxy thermosets—I. Effect of strain rate and composition", in: *Polymer* Vol. 39 (1998), pp. 3719–3724.

[52] Wilfried J. Mortier, Swapan K. Ghosh, and S. Shankar, "Electronegativity-equalization method for the calculation of atomic charges in molecules", en, in: *Journal of the American Chemical Society* Vol. 108 (1986), pp. 4315–4320, DOI: 10.1021/ja00275a013.

[53] Wilfried J. Mortier, Karin Van Genechten, and Johann Gasteiger, "Electronegativity equalization: application and parametrization", en, in: *Journal of the American Chemical Society* Vol. 107 (1985), pp. 829–835, DOI: 10.1021/ja00290a017.

[54] Lutz Nasdala, Andreas Kempe, and Raimund Rolfes, "Are finite elements appropriate for use in molecular dynamic simulations?", en, in: *Composites Science and Technology* Vol. 72 (2012), pp. 989–1000, DOI: 10.1016/j.compscitech.2012.03.008.

[55] Lutz Nasdala, Andreas Kempe, and Raimund Rolfes, "Molecular Dynamic Finite Element Method (MDFEM)", English, in: *Computational Finite Element Methods in Nanotechnology*, CRC Press, 2013, pp. 331–372.

[56] Lutz Nasdala, Andreas Kempe, and Raimund Rolfes, "The molecular dynamic finite element method (MDFEM)", in: *Computers Materials and Continua* Vol. 19 (2010), p. 57.

[57] G. M. Odegard and A. Bandyopadhyay, "Physical aging of epoxy polymers and their composites", en, in: *Journal of Polymer Science Part B: Polymer Physics* Vol. 49 (2011), pp. 1695–1716, DOI: 10.1002/polb.22384.

[58] Gregory M. Odegard, Benjamin D. Jensen, S. Gowtham, Jianyang Wu, Jianying He, and Zhiliang Zhang, "Predicting mechanical response of crosslinked epoxy using ReaxFF", en, in: *Chemical Physics Letters* Vol. 591 (2014), pp. 175–178, DOI: 10.1016/j.cplett.2013.11.036.

[59] Tomonaga Okabe, Yutaka Oya, Koichi Tanabe, Gota Kikugawa, and Kenichi Yoshioka, "Molecular dynamics simulation of crosslinked epoxy resins: Curing and mechanical properties", en, in: *European Polymer Journal* Vol. 80 (2016), pp. 78–88, DOI: 10.1016/j.eurpolymj.2016.04.019.

[60] Tomonaga Okabe, Tomohiro Takehara, Keisuke Inose, Noriyuki Hirano, Masaaki Ni-shikawa, and Takuya Uehara, "Curing reaction of epoxy resin composed of mixed base resin and curing agent: Experiments and molecular simulation", en, in: *Polymer* Vol. 54 (2013), pp. 4660–4668, DOI: 10.1016/j.polymer.2013.06.026.

[61] Surya D. Pandita, Liwei Wang, Ramani S. Mahendran, Venkata R. Machavaram, Muhammad S. Irfan, Dee Harris, and Gerard F. Fernando, "Simultaneous DSC-FTIR spectroscopy: Comparison of cross-linking kinetics of an epoxy/amine resin system", en, in: *Thermochimica Acta* Vol. 543 (2012), pp. 9–17, DOI: 10.1016/j.tca.2012.04.024.

[62] Hyungbum Park, Joonmyung Choi, Byungjo Kim, Seunghwa Yang, Hyunseong Shin, and Maenghyo Cho, "Toward the constitutive modeling of epoxy matrix: Temperature-accelerated quasi-static molecular simulations consistent with the experimental test", en, in: *Composites Part B: Engineering* Vol. 142 (2018), pp. 131–141, DOI: 10.1016/j.compositesb.2018.01.018.

[63] Steve Plimpton, "Fast Parallel Algorithms for Short-Range Molecular Dynamics", en, in: *Journal of Computational Physics* Vol. 117 (1995), pp. 1–19, DOI: 10.1006/jcph.1995.1039.

[64] R. Polanský, V. Mentlík, P. Prosr, and J. Sušír, "Influence of thermal treatment on the glass transition temperature of thermosetting epoxy laminate", en, in: *Polymer Testing* Vol. 28 (2009), pp. 428–436, DOI: 10.1016/j.polymertesting.2009.03.004.

[65] X. Poulain, A.A. Benzerga, and R.K. Goldberg, "Finite-strain elasto-viscoplastic behavior of an epoxy resin: Experiments and modeling in the glassy regime", en, in: *International Journal of Plasticity* Vol. 62 (2014), pp. 138–161, DOI: 10.1016/j.ijplas.2014.07.002.

[66] Matthew S. Radue, Benjamin D. Jensen, S. Gowtham, Danielle R. Klimek-McDonald, Julia A. King, and Gregory M. Odegard, "Comparing the mechanical response of di-, tri-, and tetra-functional resin epoxies with reactive molecular dynamics", en, in: *Journal of Polymer Science Part B: Polymer Physics* Vol. 56 (2018), pp. 255–264, DOI: 10.1002/polb.24539.

[67] Taikyue Ree and Henry Eyring, "THE RELAXATION THEORY OF TRANSPORT PHENOMENA", en, in: *Rheology*, Elsevier, 1958, pp. 83–144, DOI: 10.1016/B978-0-12-395695-8.50008-2.

[68] Taikyue Ree and Henry Eyring, "Theory of Non-Newtonian Flow. I. Solid Plastic System", en, in: *Journal of Applied Physics* Vol. 26 (1955), pp. 793–800, DOI: 10.1063/1.1722098.

[69] Taikyue Ree and Henry Eyring, "Theory of Non-Newtonian Flow. II. Solution System of High Polymers", en, in: *Journal of Applied Physics* Vol. 26 (1955), pp. 800–809, DOI: 10.1063/1.1722099.

[70] J. Richeton, S. Ahzi, L. Daridon, and Y. Rémond, "A formulation of the cooperative model for the yield stress of amorphous polymers for a wide range of strain rates and temperatures", en, in: *Polymer* Vol. 46 (2005), pp. 6035–6043, DOI: 10.1016/j.polymer.2005.05.079.

[71] J. Richeton, S. Ahzi, K.S. Vecchio, F.C. Jiang, and A. Makradi, "Modeling and validation of the large deformation inelastic response of amorphous polymers over a wide range of temperatures and strain rates", en, in: *International Journal of Solids and Structures* Vol. 44 (2007), pp. 7938–7954, DOI: 10.1016/j.ijsolstr.2007.05.018.

[72] Richard E. Robertson, "Theory for the Plasticity of Glassy Polymers", en, in: *The Journal of Chemical Physics* Vol. 44 (1966), pp. 3950–3956, DOI: 10.1063/1.1726558.

[73] Nathan Sharp, Chunyu Li, Alejandro Strachan, Douglas Adams, and R. Byron Pipes, "Effects of water on epoxy cure kinetics and glass transition temperature utilizing molecular dynamics simulations", en, in: *Journal of Polymer Science Part B: Polymer Physics* Vol. 55 (2017), pp. 1150–1159, DOI: 10.1002/polb.24357.

[74] Meredith N. Silberstein and Mary C. Boyce, "Constitutive modeling of the rate, temperature, and hydration dependent deformation response of Nafion to monotonic and cyclic loading", en, in: *Journal of Power Sources* Vol. 195 (2010), pp. 5692–5706, DOI: 10.1016/j.jpowsour.2010.03.047.

[75] J. W. Sinclair, "Effects of Cure Temperature on Epoxy Resin Properties", en, in: *The Journal of Adhesion* Vol. 38 (1992), pp. 219–234, DOI: 10.1080/00218469208030456.

[76] Timothy W. Sirk, Ketan S. Khare, Mir Karim, Joseph L. Lenhart, Jan W. Andzelm, Gregory B. McKenna, and Rajesh Khare, "High strain rate mechanical properties of a cross-linked epoxy across the glass transition", en, in: *Polymer* Vol. 54 (2013), pp. 7048–7057, DOI: 10.1016/j.polymer.2013.10.051.

[77] Ellad B. Tadmor and Ronald E. Miller, *Modeling Materials: Continuum, Atomistic and Multiscale Techniques*, Cambridge: Cambridge University Press, 2011, DOI: 10.1017/CBO9781139003582.

[78] *The new SG 10.0-193 DD (Siemens Gamesa product brochure)*, Product Brochure, Siemens Gamesa Renewable Energy, S.A. Parque Tecnológico de Bizkaia, edificio 222 48170, Zamudio, Vizcaya, Spain, 2019.

[79] D. A. Tilbrook, G. J. Pearson, M. Braden, and P. V. Coveney, "Prediction of polymerization shrinkage using molecular modeling", in: *Journal of Polymer Science Part B: Polymer Physics* Vol. 41 (2003), pp. 528–548.

[80] Vikas Varshney, Soumya S. Patnaik, Ajit K. Roy, and Barry L. Farmer, "A Molecular Dynamics Study of Epoxy-Based Networks: Cross-Linking Procedure and Prediction of Molecular and Material Properties", en, in: *Macromolecules* Vol. 41 (2008), pp. 6837–6842, DOI: 10.1021/ma801153e.

[81] Georgios G. Vogiatzis and Doros N. Theodorou, "Multiscale Molecular Simulations of Polymer-Matrix Nanocomposites: or What Molecular Simulations Have Taught us About the Fascinating Nanoworld", en, in: *Archives of Computational Methods in Engineering* Vol. 25 (2018), pp. 591–645, DOI: 10.1007/s11831-016-9207-y.

[82] Chaofu Wu and Weijian Xu, "Atomistic molecular modelling of crosslinked epoxy resin", en, in: *Polymer* Vol. 47 (2006), pp. 6004–6009, DOI: 10.1016/j.polymer.2006.06.025.

[83] Chaofu Wu and Weijian Xu, "Atomistic molecular simulations of structure and dynamics of crosslinked epoxy resin", en, in: *Polymer* Vol. 48 (2007), pp. 5802–5812, DOI: 10.1016/j.polymer.2007.07.019.

[84] Shaorui Yang and Jianmin Qu, "Computing thermomechanical properties of crosslinked epoxy by molecular dynamic simulations", en, in: *Polymer* Vol. 53 (2012), pp. 4806–4817, DOI: 10.1016/j.polymer.2012.08.045.

[85] Irene Yarovsky and Evan Evans, "Computer simulation of structure and properties of crosslinked polymers: application to epoxy resins", in: *Polymer* Vol. 43 (2002), pp. 963–969.

[86] Chao Yu, Guozheng Kang, and Kaijuan Chen, "A hygro-thermo-mechanical coupled cyclic constitutive model for polymers with considering glass transition", en, in: *International Journal of Plasticity* Vol. 89 (2017), pp. 29–65, DOI: 10.1016/j.ijplas.2016.11.001.

[87] Suyoung Yu, Seunghwa Yang, and Maenghyo Cho, "Multi-scale modeling of cross-linked epoxy nanocomposites", en, in: *Polymer* Vol. 50 (2009), pp. 945–952, DOI: 10.1016/j.polymer.2008.11.054.